

Politecnico di Torino
Dipartimento di Scienza dei Materiali ed Ingegneria Chimica
Dottorato di ricerca in Ingegneria Chimica
XXIV cycle (2009-2011)

Thesis

**Polymeric nanocapsules for
pharmaceutical applications**

PhD Student
Ilaria Valente

Supervisors
Prof. Antonello A. Barresi
Prof. Daniele L. Marchisio

Second Referee
Prof. Davide Manca

Coordinator
Prof. Vito Specchia

Acknowledgments

This thesis is dedicated to my parents and my brother.

I would like to thank my supervisors, Prof. Antonello Barresi and Prof. Daniele Marchisio for having given me the chance of working on this topic. I am grateful of the opportunity I have had of working in the academic field.

Secondly, my gratitude is for Prof. Jordi Puiggali, from the Universitat Politècnica de Catalunya who welcomed me in his group. I thank him and all the staff there: Prof. Luis Javier Del Valle Mendoza, Dr. Alfonso Galan Rodriguez, Dr. Maria Teresa Casas and Dr. Lourdes Franco.

I thank also Prof. Franco Dosio and Dr. Barbara Stella for the important collaboration we had during all the PhD time.

I also thank Dr. Edvige Celasco for her support in the XPS analysis.

Finally I would like to thank all the young researchers and PhD students I had the opportunity to know and to spend time together. They made everyday life and research less hard and difficult.

Contents

Introduction	5
1. Theoretical background and state of the art	7
1.1. <i>Pharmaceutical nanocarriers</i>	7
1.1.1. Nanospheres	9
1.1.2. Nanocapsules	9
1.2. <i>Polymers</i>	10
1.2.1. Cyanoacrylates	11
1.2.2. P(MePEGCA-co-HDCA)	12
1.3. <i>Production processes</i>	13
1.3.1. Micromixers	14
1.4. <i>References</i>	17
2. Characterization of the polymer	19
2.1. <i>Introduction</i>	19
2.2. <i>Synthesis</i>	19
2.2.1. Materials	20
2.2.2. Preparation of the monomers.....	20
2.2.3. Condensation/Polymerization of the monomers.....	21
2.3. <i>Physicochemical characterization</i>	23
2.3.1. Measurements	23
2.3.2. Solubility.....	24
2.3.3. Thermal characterization	25
2.3.4. Spherulitic morphologies	27
2.3.5. X-rays.....	29
2.4. <i>Degradation</i>	31
2.4.1. Measurements	31
2.4.2. Degradation experiments.....	31
2.4.3. Results	31
2.5. <i>References</i>	37

3. Production of PEGylated nanocapsules through solvent-displacement in confined impinging jets mixers	39
3.1. Introduction	39
3.2. Theoretical background	41
3.3. Materials and methods.....	43
3.4. Results and discussion.....	49
3.5. Conclusions	61
3.6. References.....	62
4. Production of nanospheres and nanocapsules for pharmaceutical use: process design and scale up	65
4.1. Introduction	65
4.2. Materials and methods.....	68
4.2.1. Materials	68
4.2.2. Mixers.....	68
4.2.3. Nanoparticle preparation.....	70
4.3. Results and discussion.....	71
4.3.1. Nanospheres (MR=0) in CIJMs	71
4.3.2. Nanocapsules in CIJMs	79
4.3.3. Characterization	81
4.3.4. Relationships for particle size and scale up.....	85
4.3.5. Vortex mixers	93
4.4. Conclusions	94
4.5. References.....	96
5. Nanoparticle advanced characterization	100
5.1. Introduction	100
5.2. Materials and methods.....	101
5.2.1. Materials and operating conditions	101
5.2.2. Preparation for XPS analysis.....	101
5.2.3. Preparation for TEM analysis	102
5.2.4. Characterization	103
5.3. XPS results.....	104
5.4. TEM results	114
5.4.1. Nanosphere photos.....	117

5.5.	<i>Discussion</i>	119
5.6.	<i>References</i>	122
6.	Drug loading and drug release	123
6.1.	<i>Introduction</i>	123
6.2.	<i>Materials and method</i>	124
6.2.1.	Materials	124
6.2.2.	Preparation of loaded nanoparticles.....	125
6.2.3.	Drug release	126
6.2.4.	Antibacterial activity	127
6.3.	<i>Results</i>	128
6.3.1.	Size	128
6.3.2.	Drug incorporation	129
6.3.3.	Antibacterial activity	135
6.4.	<i>References</i>	138
7.	Conclusions	139
	Lists of Figures	142

Introduction

Nanotechnology is a promising research area in many fields, as for example energy, environmental applications as well as medicine. In pharmaceutical research the use of nanotechnology is of great interest for the possibilities it offers to control drug delivery and to vehicle poor water-soluble drugs or macromolecules, like proteins, peptides or nucleic acids.

Historically, the development of nanoparticles of different kind (liposomes, polymeric nanoparticles, etc.) in drug therapy was initiated in order to improve drug efficacy as much as possible. Drug activity mainly depends on its concentration at the active site, as well as many side effects depend on its concentration in healthy organs or tissues. In turn, drug distribution in the body depends on the physicochemical properties of the drug, so that the drug might have no affinity with the diseased area; the use of a nanocarrier to vehicle the drug can overcome this problem. The carrier can, in fact, accumulate selectively at the target tissue (passive targeting). The carrier can also be bound with a specific molecule (usually an antibody) which has high selectivity for the target cell (active targeting).

The use of a carrier can also modify the time of release of the drug, allowing to obtain a continue release of the drug which guarantees therapeutic concentration of the drug in the target site for an extended period of time.

The size of these particulate carriers is fundamental because it determines the route of administration of the drug. If too big (usually $> 1 \mu\text{m}$) they cannot be administered by the traditional route (intravenous for example) because capillaries would be blocked and the carrier should be implanted near the target tissue. For this and other reasons it is important that the size of these systems is in the range of nanometers.

Nanocarriers are typically liposomes or nanoparticles, but new carriers are being developed both for treatment and diagnostic scope. The formulation of polymers suitable for pharmaceutical applications (which have to be biodegradable and biocompatible) is another important field of exploration, together with the development of new and more efficient ways to produce these carriers

The aim of this work is to characterize two particular classes of carriers, nanocapsules and nanospheres obtained from an amphiphilic copolymer of the cyanoacrylates family, in continuous micromixers. The work comprises the characterization of the polymer, the investigation of the different process parameters, processes design and scale up and final particle characterization.

This thesis is organized as follows.

Firstly, in Chapter 2, the characterization of the polymer is shown. The polymer was characterized in terms of its physicochemical characteristics and degradation time.

Then nanocapsules production in CIJMs is discussed (Chapter 3).

In Chapter 4 the effect of the main parameters involved in the production process are studied and scale up criteria are suggested.

Advanced characterization through X-ray Photon Electron Spectroscopy (XPS) and Transmission Electron Microscopy (TEM) on nanocapsules and nanospheres is shown in Chapter 5.

Results related to loaded nanocapsules and nanospheres with a model drug are reported in Chapter 6. Results include release and anti-bacterial tests.

Conclusions about the system studied and the collected results are summarized in Chapter 7.

1. Theoretical background and state of the art

1.1. Pharmaceutical nanocarriers

Pharmaceutical carriers refer to any systems capable to act as a vehicle for active compounds in therapy. In recent years carriers with size in the nanometers range have attracted the interest of researchers and of the pharma industry thanks to their ability to be injected through the general routes of administration without the risk of blocking the blood stream in the capillaries. Carriers in the nanometers range are usually referred to as nanoparticles. Nanoparticles are colloidal systems with particle diameters between 1 and 1000 nm where the drug can be encapsulated, adsorbed or dispersed in them. A wide range of materials have been studied in drug delivery, including lipids, polymers and inorganic materials. The growing interest towards these systems is due to their ability to modify drug delivery. As already mentioned, the nano-size range allows to inject them directly in the blood stream; moreover it was seen that smaller dimensions reduce the opsonization phenomenon and the subsequent phagocytosis by macrophages as well as it reduces the rate of clearance (the rate the kidney has to purify the blood from external components). At the same time circulation time can be increased by binding to the surface hydrophilic molecules such as polyethylene glycol (PEG), because it creates an aqueous shell around the particles which avoids the adhesion of the opsonins on particle surface. Small size and enhanced circulation time lead to

an increased accumulation of the particles (and obviously of the entrapped drug) in tissues with increased vascular permeability and lymphatic drainage such as tumours and inflamed tissues. This phenomenon, named as enhanced permeability and retention (EPR) effect, is exploited as a way of passive targeting (Figure 1.1.1).

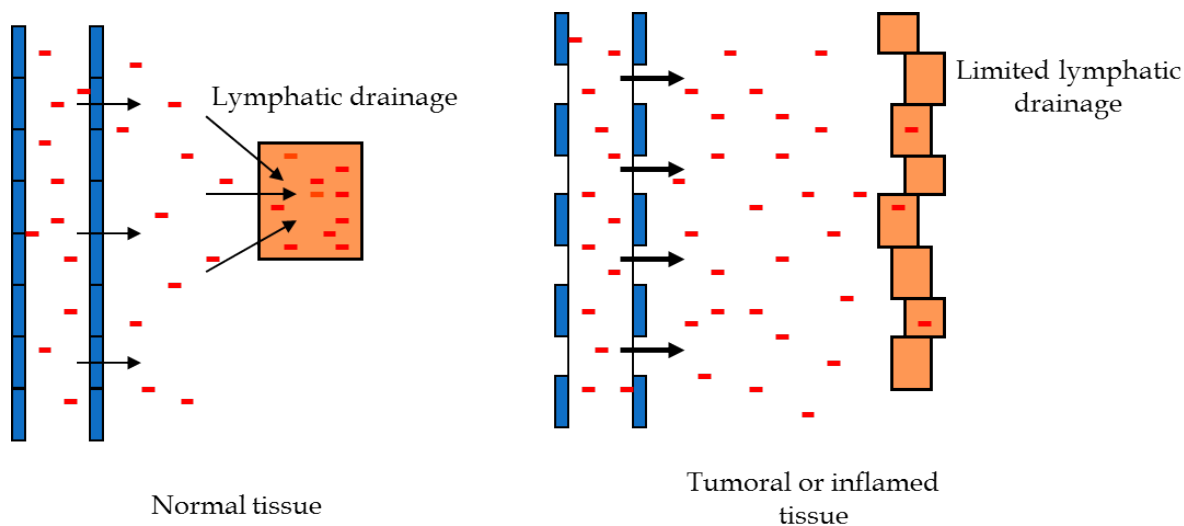


Figure 1.1. Blood vessels and lymphatic drainage in a normal tissue and in a diseased tissue: red squares represent the particles, which accumulate more in the diseased tissue.

In the last 30 years nanotechnology has been studied in particular for the treatment of complex diseases, such cancer, infections, metabolic diseases, autoimmune diseases and inflammation. Today some of these systems are already marketed and widely used (Caelyx®, Ambisome®, which are both liposomes) and others are in clinical trials. It has to be noted that liposomes are made of phospholipids, the natural component of cell membrane, whereas nanoparticles are made of polymers.

Nanoparticles composed of biocompatible polymers have been widely investigated in order to use them as drug delivery systems. They offer the advantage they can be used to vehicle hydrophobic drugs via solubilization in the hydrophobic core of the particles. Polymeric nanoparticles can be distinguished in nanospheres and nanocapsules. Nanospheres and nanocapsules can be prepared by

polymerization *in situ* or from a preformed polymer. The second type of preparation offers some advantages: polymer physicochemical characteristics are well defined and there are not residual monomers in the medium.

1.1.1. Nanospheres

Nanospheres are constituted by the polymer which forms a solid matrix usually defined as a monolithic system (homogeneous). In this system the polymer chains arrange in a “frozen” state phase-separated from the bulk solution. In case the polymer is an amphiphilic copolymer, hydrophobic chains should form the inner part of the particle, whereas the hydrophilic part goes on the surface of the particle.

Drugs can be dissolved, entrapped, encapsulated, chemically bound or adsorbed to the constituent polymer matrix.

Nanospheres can be prepared by polymerization *in situ* or from a preformed polymer. In the first case nanospheres can be obtained by emulsion polymerization or by interfacial polymerization. For preformed polymers, nanospheres preparation can be achieved by emulsification/solvent evaporation, emulsification/solvent diffusion and salting out techniques, but the most common one is solvent displacement, also called nanoprecipitation. In this method the polymer is dissolved in an organic water-soluble solvent, which is then added to an anti-solvent, usually water, which can contain or not a surfactant and other additives. The solvent immediately diffuses in the aqueous phase leading to the polymer precipitation and nanosphere formation.

1.1.2. Nanocapsules

Nanocapsules are colloidal-sized, vesicular system (heterogeneous) in which the drug is confined to a reservoir surrounded by the polymer. The core is a lipophilic liquid surrounded by a single layer of polymer. Nanocapsules are useful to vehicle hydrophobic drugs, since drugs are dissolved in the liquid core and can

be loaded in high quantity. Nanocapsules have some advantages over nanospheres, because they require a lower amount of polymer for each particle and as consequence drug loading as percentage of polymer content is higher. Moreover, drug solubility can be greatly increased varying the inner liquid.

Nanocapsules, like nanospheres, can be either obtained following an interfacial polymerization of monomers or from preformed polymers. In the former case, the molecular weight of the final polymer will depend on the preparation conditions and also on the drug used, while in the latter polymer characteristics are well defined. They are usually produced by nanoprecipitation, where drug, polymer and oil are dissolved in the solvent and then added to the aqueous phase. They can be produced also by emulsion-diffusion method and emulsion-coacervation method.

In Figure 1.2 a graphic representation of nanosphere and nanocapsule by an amphiphilic copolymer, with hydrophilic chains stretched out is shown.

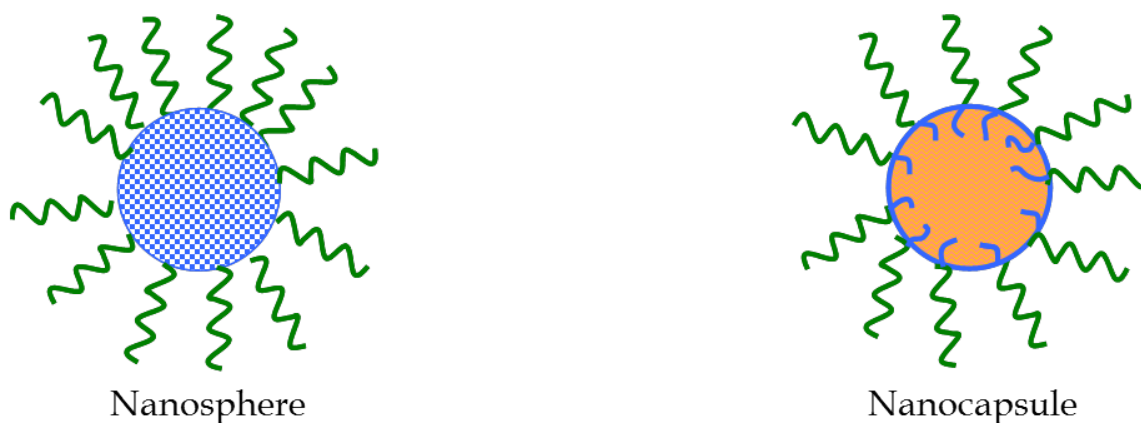


Figure 1.2. Representation of a nanospheres and of a nanocapsules made of an amphiphilic copolymer: blue part is the hydrophobic part, green part is the hydrophilic one.

1.2. Polymers

Polymers are widely used in drug delivery thanks to some specific qualities they have. They can be manipulated in many ways, by increasing their chain length through cross-linking or by hydrophobising or hydrophilizing them with polymers

and other groups, yielding a wealth of materials with a wide spectrum of possible applications. The resulting materials are capable of a variety of drug-enhancing functions:

- to prolong drug availability;
- to favorably alter biodistribution if formulated into dense nanoparticles;
- to enable hydrophobic drug administration if formulated as micelles;
- to transport a drug to its usually inaccessible site of action if formulated as gene medicines;
- to make drugs available in response to stimuli.

Great attention is given to the biodegradability and biocompatibility of the polymers. It is important that polymers used in medicine are not dangerous for tissue and that they can be eliminated by the human body without producing dangerous molecules.

1.2.1. Cyanoacrylates

The use of poly(alkylcyanoacrylates) (PACAs) started in the early 80s, even if the monomers have been used since the 60s thanks to their adhesive properties. They were used as tissue adhesive, as surgical glue and embolitic material for endovascular surgery. In 80s, together with the rise of drug nanoparticulate carriers, PACAs particles started to be investigated. As said before, monomers were firstly employed in biomedical field, mainly for skin wound closure. Early cyanoacrylates, as methylcyanoacrylate, are not in use anymore, except for some cases, and were replaced by longer-chains alkylcyanoacrylates such as N-butylcyanoacrylate and octylcyanoacrylate.

PACAs were widely used in the production of nanoparticles for drug delivery. Polyisobutylcyanoacrylates and poly(isohexylcyanoacrylate) are two of the most commonly used. PACAs were bound and modified with different molecules, such as polyethylene glycol (PEG), polysaccharides (Chauvierrea et al., 2010) and folic acid (Stella et al., 2007). Modifying polymer molecules with PEG chains is very common in pharmaceutical applications to obtain “stealth” nanoparticles, because

long PEG chains create an aqueous shell around the particles, avoiding nanoparticles to be recognized and rapidly eliminated from blood circulation by the Reticulo Endothelial System (RES). They are bioerodible polymers: the main path of degradation is the hydrolysis of the ester bond of the alkyl side chain of the polymer.

1.2.2. P(MePEGCA-co-HDCA)

P(methoxypolyethyleneglycol cyanoacrylate-co-hexadecyl cyanoacrylate) is an amphiphilic block co-polymer which was synthesized for the first time by Peracchia et al. (1997). It was studied to provide the characteristics of long-chains cyanoacrylates and the advantages of PEG chains to give amphiphilic properties and increase blood lifetime of nanoparticles. This copolymer was synthesized by a single-step condensation of cyanoacetate monomers with formaldehyde, as described in details in Chapter 2. The copolymer was produced at different hexadecyl/PEG chains ratio in order to investigate the effect of the different hydrophilic level on polymer characteristics. The more suitable for pharmaceutical application in nanoparticles preparation resulted to be the one with a hexadecyl/PEG ratio of 4:1. In this ratio it has a good balance between hydrophility and lipophilicity, so that it is not miscible in water, but at the same time is miscible in water-miscible solvents.

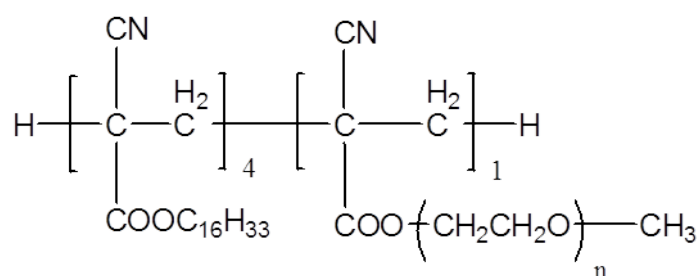


Figure 1.3. Poly(methoxypolyethyleneglycole cyanoacrylate-co-hexadecyl cyanoacrylate) formula.

Several studies (see for example Peracchia et al. 1998) show that PEG-coating reduces cytotoxicity towards mouse peritoneal macrophage and increases degradability of the polymer in presence of calf serum.

The molecular weight of the copolymer synthesized with a ratio 4:1 was measured to be 3.5 kDa. Since the molecular weight of PEG chains used in the synthesis is of 2000 D, it is reasonable to think that the macromolecules within this range are oligomers. As highlighted in Brigger et al. (2000) the final ratio 4:1 is only a mean value of different molecular species: in each copolymer batch more lipophilic oligomers (with a higher hexadecyl chains content) or more hydrophilic oligomers (with a higher MePEG chains) might be present.

1.3.Production processes

Polymer nanospheres and nanocapsules can be prepared both by polymerization methods (Bouchemal et al., 2006, Pitaksuteepong et al., 2002) and from a preformed polymer, by different mechanisms such as solvent-displacement (Peracchia et al., 1998), emulsion-diffusion (Moinard-Checot et al., 2008), double-emulsification (Garti, 1997). The different processes and the characteristics of the nanocapsules produced have been recently compared (Mora-Huertas et al., 2010). In the first way (polymerization method) particle formation follows immediately the polymerization of the monomers. This method is now less used because it presents some limitations: polymer characteristics are not well defined and it is possible to have residual monomers in the solution. For this reason the synthesis of nanoparticles from a preformed polymer is now preferred and widely used.

The most common route for nanosphere and nanocapsule production are solvent-displacement, also called nanoprecipitation, emulsification-solvent diffusion method and emulsification-solvent evaporation method, as said before. The right method for a specific preparation depends on the type of solvent used. Rieger et Horn (2001) give the following guidelines:

1. Emulsion-evaporation method is used with lipophilic solvents and particle formation occurs through an emulsion step. Polymeric particles are formed inside the organic drops (o/w emulsion) and the solvent is separated by evaporation.
2. Emulsion-diffusion method is used with amphiphilic solvents and the emulsion is transient and then transforms into a nanodispersion.
3. Solvent-displacement method is used with hydrophilic solvents and particle formation occurs by nanoprecipitation through either nucleation and growth steps or through spinodal decomposition.

In this thesis, solvent-displacement is used. It will be described in details in Chapter 3.

1.3.1. Micromixers

Microdevices refer to systems with characteristic length-scales from the micrometer to the millimeter range. These devices allow to control the process conditions and are characterized by good and fast homogenization of the feed streams, short mean residence time and narrow residence time distribution.

Two different principles can be followed to produce mixing at the microscale. Firstly, by using an energy input from the exterior (active mixing). Ultrasound, acoustic, bubble-induced vibrations, periodic variations of flow rate, magneto-hydrodynamic action, etc. can be used as external energy sources.

Otherwise, the flow energy, generated by pump action or hydrostatic potential, is used to restructure a flow in a way which results in faster mixing: this second means is named passive mixing.

In passive mixing, Y- and T-flow geometries are the main examples. There are other ways to produce mixing in a microdevice. Confined impinging jets mixers (CIJMs) consist of two high velocity jets which collide in a small chamber, providing good and fast mixing. Chamber size and inlet jets diameters affect mixing efficiency. Their use in nanoprecipitation for pharmaceutical application is interesting since they allow to control final particle size modifying some parameters, such as the inlet

jet velocity or geometrical details, such as the ratio between chamber diameter and inlet jet (Δ).

CIJMs were highly studied in nanoprecipitation processes because they result in mixing times shorter than the characteristic process time for nanoprecipitation. Rapid mixing is measured in CIJMs for two reasons (Johnson and Prud'homme, 2003): they produce a region of high turbulent energy dissipation and ensure that the process streams flow through the high intensity region without bypassing.

A different geometry is the multi inlet vortex mixer (MIVM), where a variable number of inlet jets (usually from 2 to 4) are fed tangentially in a cylindrical mixing chamber. Differently from CIJMs, in MIVMs it is not necessary that the inlet streams have the same momenta in order to provide good mixing. Thanks to this, MIVMs offer more possibilities, because different inlet streams can be fed at different flow rates without affecting mixing performance.

These geometries are reported in Figure 1.4.

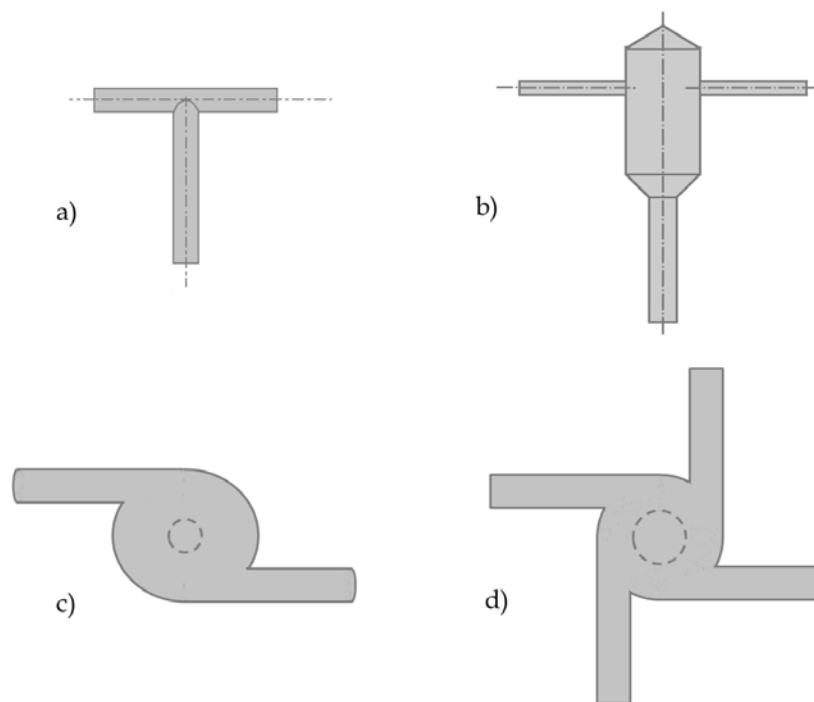


Figure 1.4. Section view of some kind of passive mixing devices used in this thesis: a) T-mixer, b)CIJM (front view), c) MIVM with 2 inlet jets (above view) and d) MIVM with 4 inlet jets (above view).

The work is focused on the use of CIJMs of different size and geometry (Chapter 3). Some experiments are performed in vortex mixers, while in Chapter 4 some data from previous work in CIJMs and Tee-mixers are used to discuss on design and scale up criteria of micromixers.

1.4.References

Bouchemal K., Briancon S., Fessi H., Chevalier Y., Bonnet I., Perrier E., 2006, Simultaneous emulsification and interfacial polycondensation for the preparation of colloidal suspensions of nanocapsules, *Materials Science & Engineering C-Biomimetic and Supramolecular Systems* 26, 472-480.

Chauvierrea C., Manchandab R., Labarrec D., Vauthier C., Mardena M.C., Leclerc L., 2010, Artificial oxygen carrier based on polysaccharides-poly(alkylcyanoacrylates) nanoparticle templates. *Biomaterials* 31 (23), 6069-6074.

Garti N., 1997, Double emulsions - Scope, limitations and new achievements. *Colloids and Surfaces A-Physicochemical and Engineering Aspects* 123, 233-246.

Horn D., Rieger J., 2001, Organic nanoparticles in the aqueous phase: theory, experiment and use. *Angewandte Chemie International Editions* 40, 4330-4361.

Johnson B.K., Prud'homme R.K., 2003, Chemical processing and micromixing in confined impinging jets. *AIChE Journal* 49, 2264-2282.

Moinard-Checot D., Chevalier Y., Briancon S., Beney L., Fessi H., 2008, Mechanism of nanocapsules formation by the emulsion-diffusion process. *Journal of Colloid and Interface Science* 317, 458-468.

Mora-Huertas C.E., Fessi H., Elaissari A., 2010, Polymer-based nanocapsules for drug delivery. *International Journal of Pharmaceutics* 385, 113-142.

Peracchia M.T., Desmaele D., Couvreur P., d'Angelo J., 1997, Synthesis of a novel poly(MePEG cyanoacrylate-co-alkyl cyanoacrylate) amphiphilic copolymer for nanoparticle technology. *Macromolecules* 30, 846-851.

Peracchia M.T., Vauthier C., Desmaele D., Gulik A., Dedieu J.C., Demoy M., d'Angelo J., Couvreur P., 1998, Pegylated nanoparticles from a novel methoxypolyethylene glycol cyanoacrylate hexadecyl cyanoacrylate amphiphilic copolymer. *Pharmaceutical Research* 15, 550-556.

Pitaksuteepong T., Davies N.M., Tucker I.G., Rades T., 2002, Factors influencing the entrapment of hydrophilic compounds in nanocapsules prepared by interfacial polymerisation of water-in-oil microemulsions. *European Journal of Pharmaceutics and Biopharmaceutics* 53, 335-342.

Stella B., Arpicco S., Rocco F., Marsaud V., Renoir J.M., Cattel L., Couvreur P., 2007, Encapsulation of gemcitabine lipophilic derivatives into polycyanoacrylate nanospheres and nanocapsules. *International Journal of Pharmaceutics* 344, 71-77.

2. Characterization of the polymer

2.1. Introduction

Several works have been focused on the preparation of nanoparticles from poly(MePEGCA-co-HDCA) with a hydrophilic/hydrophobic ratio of one to four by nanoprecipitation and by emulsion/solvent evaporation methods (Peracchia et al., 1997, Peracchia et al., 1998). In general, unimodal size distributions were obtained with the mean diameter ranging between 98 and 199 nm and varying in function of the polymer concentration and the applied method. It was also demonstrated that nanoparticles had an adequate density of MePEG chains on their surface to provide enhanced stability in the blood stream and to ensure long circulating times (Peracchia et al., 1999, Brigger et al., 2000).

This chapter is focused on physicochemical characterization of the polymer, with respect to thermal, morphological and crystalline aspects and degradability.

2.2. Synthesis

In this work the amphiphilic poly(methoxy-polyethylene glycol)-co-hexadecylcyanoacrylate (P(MePEGCA-co-HDCA)) was used for the preparation of stealth nanoparticles for pharmaceutical applications. It was synthesized, following the procedure of Peracchia et al. (1997) with some minor changes. The standard

synthesis proposes the use of a base-catalyzed condensation of MePEG cyanoacetate (MePEGCA) and cyanoacetic acid with formaldehyde. This kind of condensation/polymerization involve a Michael addition as the step-growth mechanism, where the steric hindrance determines the chain lengths. The use of cyanoacetate monomers allows better control of the polymerization process in comparison to the use of the cyanoacrylate monomers, which react very fast in presence of bases and other nucleophilic agents.

2.2.1. Materials

Poly(ethylen-glycol) methyl ether (MePEG), with average molecular weight 2000 D, was purchased from Sigma Aldrich, whereas 1-hexadecanol and cyanoacetic acid (CA) from Fluka Chemika. All other reagents were of analytical grade from Sigma-Aldrich but the solvents from Carlo Erba.

2.2.2. Preparation of the monomers

The two monomers were prepared by esterification of the cyanoacetic acid with the corresponding alcohol (polyethylenglycole-methyl ether and hexadecanol) following the methodology reported by Peracchia et al. (1997).

MePEG cyanoacetate (MePEGCA) was synthesized by esterification of MePEG (22 g, 11 mmol) and cyanoacetic acid (ACA, 1.87 g, 22 mmol) in the presence of N-(3-dimethylaminopropyl)-N'-ethylcarbodiimide hydrochloride (EDC) and (dymethylamino)pyridine (DMAP) as catalyst. The two reagents were dissolved in dichloromethan (DCM, molar ratio acid/MePEG 2:1) and then EDC (4.22 g, 11 mmol) and DMAP (0.134 g) were added. The reaction was carried at room temperature in nitrogen atmosphere, stirring for 24 hours. After this time it was washed with six 25 ml portions of water. The organic phase was collected and dried over magnesium sulphate (MgSO₄). Then it was filtered and concentrated under reduced pressure to leave a viscous oil which solidified on standing.

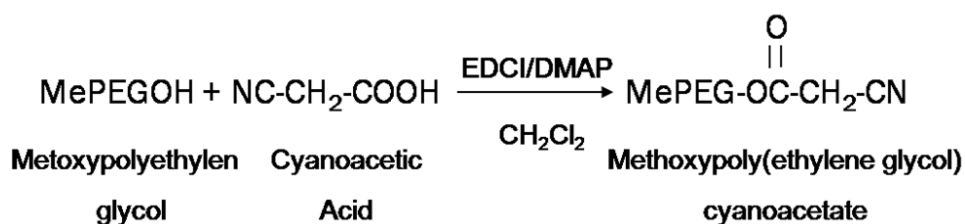


Figure 2.1. Synthesis of MePEGCA.

n-Hexadecylcyanoacetate (HDCA) was synthesized by esterification of *n*-hexadecanol (10 g, 41,2 mmol) and cyanoacetic acid (3.87 g, 45.4 mmol). Hexadecanol was dissolved in 100 ml DCM, while ACA was dissolved in the necessary volume of ethyl acetate and then added to the solution of hexadecanol in DCM. DMAP was dissolved in DCM and added. 1,3-dicyclohexylcarbodiimide (DCC, 9.35 g) was dissolved in DCM and added by dropping to the reaction mixture. The reaction was stirred at room temperature at nitrogen atmosphere for 2 hours.

Hexane is added to the mixture and the white solid that formed was filtered off. The mixture was then purified by flash chromatography (silica gel 60, 230-400 mesh) using hexane/ethyl acetate (90:10) as eluting phase. The product was collected and concentrated under reduced pressure.

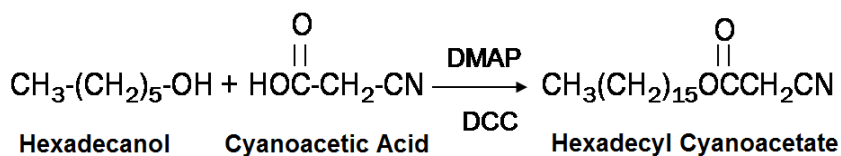


Figure 2.2. Synthesis of HDCA.

2.2.3. Condensation/Polymerization of the monomers

The two monomers were condensed using formaldehyde as polymerization agent, in a respective molar ratio 1:4 for MePEGCA and HDCA.

MePEGCA (10.34 g, 5 mmol) and HDCA (6.18 20 mmol) were previously dissolved separately in 50 ml of DCM. Then they were mixed together and 50 ml ethanol were added. Then formaldehyde 37% was added in excess (6.08 ml, 75 mmol) in order to guarantee 100% of polymerization. Finally dymethylamine (DMA, 8,44 ml) was added and the reaction was left on stirring in nitrogen atmosphere until complete consumption of the two monomers (seen through thin layer cromathography, TLC).

The mixture was washed firstly with 30 ml chloridric acid 1 N and then 2 times with 30 ml water. The organic phase was collected and dried over MgSO₄. Then it was filtered and concentrated under reduced pressure to give the final product.

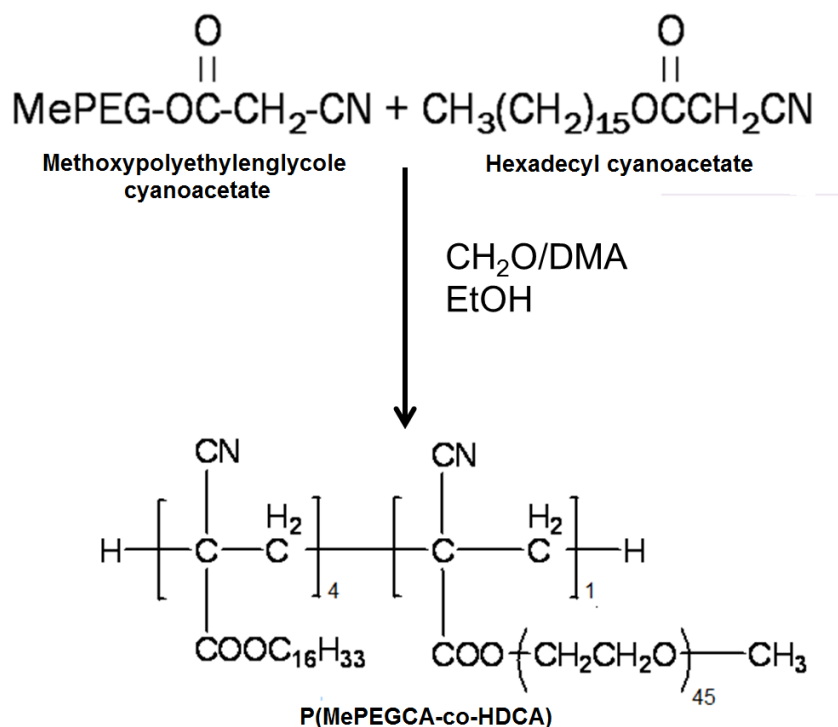


Figure 2.3. Polymerization reaction.

2.3. Physicochemical characterization

2.3.1. Measurements

Solubility evaluation of the as-synthesized polymer in the different solvents are present in literature (Peracchia et al., 1997). In this work the solubility of the polymer was studied in the water/acetone mixture. The experiments were performed at 30 °C and the solubility was measured by evaluating the turbidity of copolymer solution, after addition of controlled amounts of water to the acetone polymer solution. The water fraction investigated were 50%, 66% and 90%. As it will be explained in Chapter 3, 50% fraction and 66% fraction correspond to the solvent-antisolvent mixture obtained when working without quenching and with quenching, respectively. Many acetone solutions at different concentrations were diluted with water at the three value indicated before. Final concentration of the polymer was then recalculated. In this way the first concentration dissolving in the mixture without giving any turbidity is considered the polymer solubility in the fraction water/acetone under investigation.

Calorimetric data were obtained by differential scanning calorimetry (DSC) with a TA Instruments Q100 series equipped with a refrigerated cooling system (RCS) operating from -90 °C to 550 °C. Experiments were conducted under a flow of dry nitrogen with a sample weight of approximately 10 mg while calibration was performed with indium. Heating and cooling runs were performed at rates of 20 °C/min and 10 °C/min, respectively.

Wide angle X-ray diffraction patterns were obtained using a PANalytical X'Pert diffractometer, Cu K α radiation ($\lambda = 0.1542$ nm) and a silicium monocrystal sample holder.

Spherulitic morphologies were studied using a Zeiss Axioskop 40 Pol light polarizing microscope equipped with a Linkam temperature control system configured by a THMS 600 heating and freezing stage connected to a LNP 94 liquid nitrogen cooling system. Micrographs were taken with a Zeiss AxiosCam MRC5

digital camera. A first-order red tint plate was employed to determine the sign of spherulite birefringence under crossed polarizers.

2.3.2. Solubility

The as-synthesized polymer is an amphiphilic polymer, with a hydrophilic (PEG cyanoacrylate) and a lipophilic (hexadecyl cyanoacrylate) monomer. According to the results reported by Peracchia et al. (1997), the solubility of the polymer changes with the relative ratio between the two monomers. The ratio used in the synthesis here performed is one to four, meaning that the final polymer has one PEG monomer each four hexadecyl cyanoacrylate monomers. The as-synthesized polymer shows a good balance between hydrophilic and lipophilic monomers, being soluble in most of the organic solvents. As it will become clearer later on, this is an advantage when the scope is to produce nanoparticles with solvent-displacement.

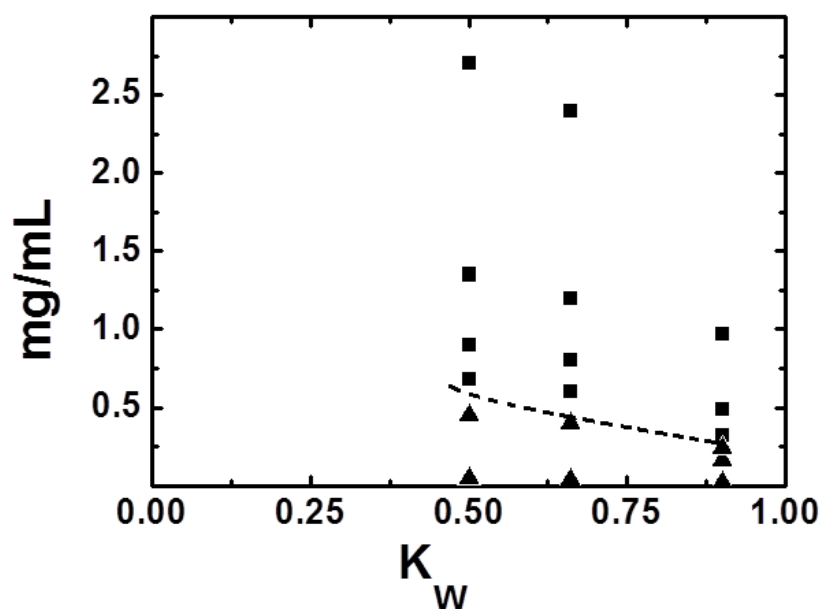


Figure 2.4. Precipitation texts of the polymer at different water fraction (K_w): ■ polymer precipitates, ▲ polymer is soluble. Dashed lines indicates solubility curve.

Residual solubility at 30 °C in three different water/acetone mixture has been evaluated. Results are shown in Figure 2.4 and numerical values of the residual solubility are reported in Table 2.1. The residual solubility in the mixture at 0.5 and 0.66 is quite high and it decreases only at higher water fraction (0.9). This can be due to the different molecules of polymer which can be present in a batch: in fact, in the chemical synthesis it is not possible to control monomers distribution in a molecule, so that more lipophilic molecules precipitate when water amount increase, but the hydrophilic ones remain in solution.

Table 2.1. Residual polymer solubility (g/l) in the water/acetone mixture at three different water fraction.

polymer solubility			
water fraction	0.5	0.66	0.9
g/l	0.45	0.4	0.243

2.3.3. Thermal characterization

Poly(MePEGCA-co-HDCA) has a semicrystalline character as demonstrated by the DSC scans shown in Figure 2.4a. Thus, the as-synthesized sample has a predominant peak at 53 °C and a minor one close to 33-34 °C, which should correspond to the melting of crystalline domains of PEG and the HD alkyl groups, respectively. The sample easily crystallized from the melt giving rise to a complex exothermic peak where the crystallization of the two indicated domains could not be well differentiated. It is interesting to note that the crystallinity of the as-synthesized sample, which came from evaporation of a dichloromethane solution, could be increased by the hot crystallization process as a consequence of a better rearrangement of the HDCA domains. Hence, the increase on the global melting enthalpy (i.e. from 123 to 138 J/g) is mainly a consequence of the peak associated to

the melt of HDCA domains which increased and became sharper after hot crystallization. The DSC heating run of a quenched sample does not reveal significant changes and demonstrated that the sample easily crystallized even at the high cooling rates. Notice that the glass transition temperature could not be well observed due to high crystallinity of the sample. Two points are noticeable from the thermal analysis: a) the sample experiences a partial fusion around 34 °C which is a temperature slightly lower to the human body temperature at which the potential drug delivery systems should be applied; b) despite the complexity of the sample, its crystallinity remains high indeed at the temperature of 37 °C at which samples are expected to be employed.

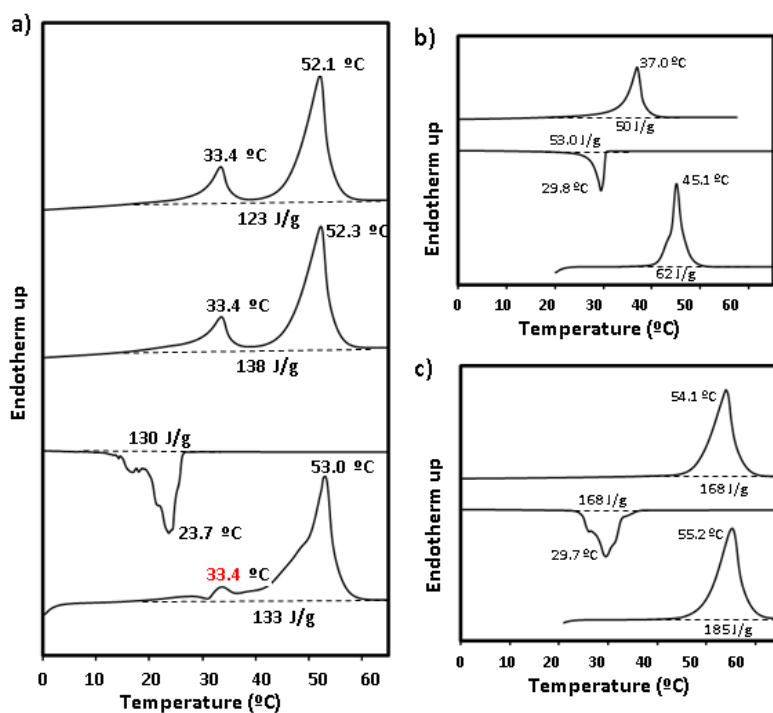


Figure 2.5. DSC scans performed on poly(MePEGCA-co-HDCA) (a), poly(HDCA) (b) and PEG samples (c). Scans, from bottom to top, correspond to the heating run of the as-synthesized (a,c) or the commercial sample (c), the cooling run from the melt state (a, b, c), the heating run of a hot crystallized sample (a, b, c) and the heating run of a sample quenched from the melt state (a).

For the sake of completeness, in Figure 2.5b and Figure 2.5c DSC scans performed with Poly(hexadecylcyanoacrylate) (PHDCA) homopolymer and the PEG are reported. These traces clearly confirm the previous assignation given for the melting peaks of poly(MePEGCA-co-HDCA) and the similar crystallization temperature of both samples. Results also demonstrated that poly(MePEGCA-co-HDCA) has an intermediate melting enthalpy between those of the crystals constituted by the two types of lateral chains. Basically, enthalpies associated to each peak (e.g. 18 and 120 J/g for the hot crystallized sample) fit reasonably well with the expected values (18 and 118 J/g) assuming a weight percentage of PEG close to 64%. Finally, it should be pointed out the complexity of the crystallization exothermic peak of PEG which extends over an interval of approximately 15 °C and on the contrary the sharp appearance of the peak associated to the PHDCA. This, in addition, suggests an almost instantaneous primary crystallization that could be a consequence of a high nucleation density.

2.3.4. Spherulitic morphologies

Crystallization from the melt gave spherulites with a fibrillar texture that corresponded to the crystallization of the PEG lateral chains, although domains constituted by HDCA units could also be envisaged. Figure 2.6a shows a typical crystallization performed at 4 °C (i.e. at a low degree of supercooling) where well developed spherulites could be observed together with zones with a different texture (indicated by arrows in Figure 2.6d) that seems to be constituted by smaller microcrystals. These zones melted when the sample was heated up to the melting temperature associated to the HDCA domains (Figure 2.6b) and recrystallized giving textures similar to those initially observed, when the temperature was subsequently decreased down to room temperature (Figure 2.6c). Experiments clearly demonstrated the complex crystallization process of samples constituted by blocks able to crystallize independently (i.e. those constituted by the PEG lateral groups and HDCA units) and furthermore with a similar crystallization temperature. Phase separation and crystalline morphology studies of block

copolymers are nowadays receiving great attention (Muthukumar et al., 1998, Zhue et al., 1999, Ryan et al., 1995, Schäffer et al., 2000, Kawai et al., 2007) and even microstructures that can be formed from the melt, from solution and for both thin and bulk samples have been extensively reviewed (Müller et al., 2007, Nandan et al., 2006).

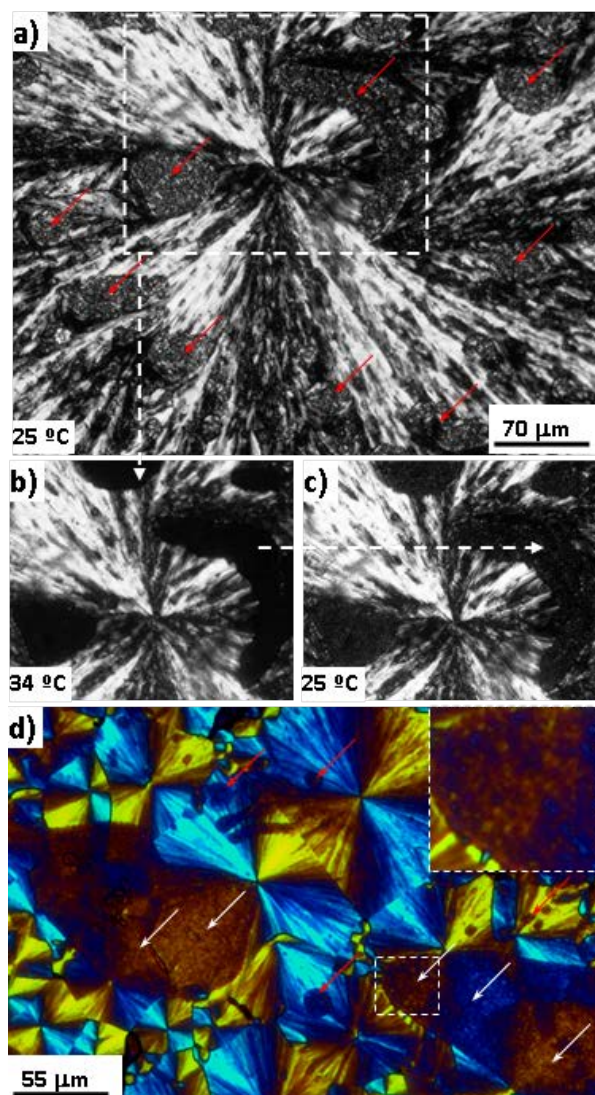


Figure 2.6. Polarizing optical micrographs of poly(MePEGCA-co-HDCA) isothermally crystallized at 4 °C (a, b, c) and -24 °C (d). Micrographs were taken at room temperature (a, d), at 34 °C (b) and at room temperature after heating the crystallized sample to 34 °C. A first-order red tint plate was used for micrograph d). The inset of d) shows a magnification of the dashed area where small and flat microcrystals could be envisaged. Arrows points out crystalline microdomains constituted by poly(HDCA).

Nucleation density obviously increased when the crystallization temperature decreased and consequently smaller spherulites were observed at the end of the crystallization process as shown in Figure 2.6d for isothermal experiments performed at -24 °C. In all cases, a negative birefringence was characteristic of the PEG spherulites, whereas a more confusing sign was observed for the alkyl chain crystals due to their smaller size. In fact, primary nucleation was much higher for these crystals as suggested also by the DSC data. Optical micrographs reveal that the alkyl chain microcrystals had a flat appearance and usually appeared aggregated in such a way that the birefringence sign of the PEG spherulite was kept (see white and red arrows in Figure 2.6d). In some cases, these microcrystals gave rise to spherulite arms with a speckle appearance (white arrows).

2.3.5. X-rays

X-ray powder diffraction patterns (Figure 2.7) of poly(MePEGCA-co-HDCA) revealed the presence of reflections characteristic of polyethylene glycol as well as additional peaks which should be assigned to a crystalline structure associated to the packing of the hexadecyl lateral groups. The structure of polyethylene glycol is defined by a $P21/a$ space group and a unit cell with parameters $a = 0.805$ nm, $b = 1.304$ nm, c (fiber axis) = 1.948 nm and $\beta = 125.4^\circ$ that contains four $7/2$ helices based on TTG sequences (Figure 2.6c). The corresponding X-ray diffraction pattern (Figure 2.6c) is characterized by strong peaks at 0.462 nm (120 reflection) and 0.386-0.277 nm (112, 032, 13-2 and 21-2 reflections) and weak peaks at 0.603 nm and 0.586 nm which are indexed as the 021 and 110 reflections. All of these reflections can be well observed in the X-ray diffraction profile of poly(MePEGCA-co-HDCA) together with peaks at 2.988, 1.494 and 0.416 nm of remarkable intensity. These peaks are also detected in the diffractogram of poly(hexadecylcyanoacrylate) and suggests a hexagonal unit cell with parameters $a = 0.479$ nm, $b = 0.479$ nm, c (fiber axis) = 2.988 nm. Thus, the stronger peak (100 reflection) corresponds to the hexagonal packing of the polymethylene segments whereas the higher spacing peaks can be indexed as the 001 and 002 reflections. Note that the c parameter is larger than the

expected length of a hexadecylacrylate lateral group with an extended conformation (i.e. ca. 1.62 nm). Hence, the *c* axis of the crystalline structure should correspond to two lateral groups as presumable if hexadecylacrylate groups in the main chain have a syndiotactic arrangement. Note that an isotactic arrangement should lead to a high steric hindrances since the spacing between polymethylene sequence should be close to only 0.25 nm.

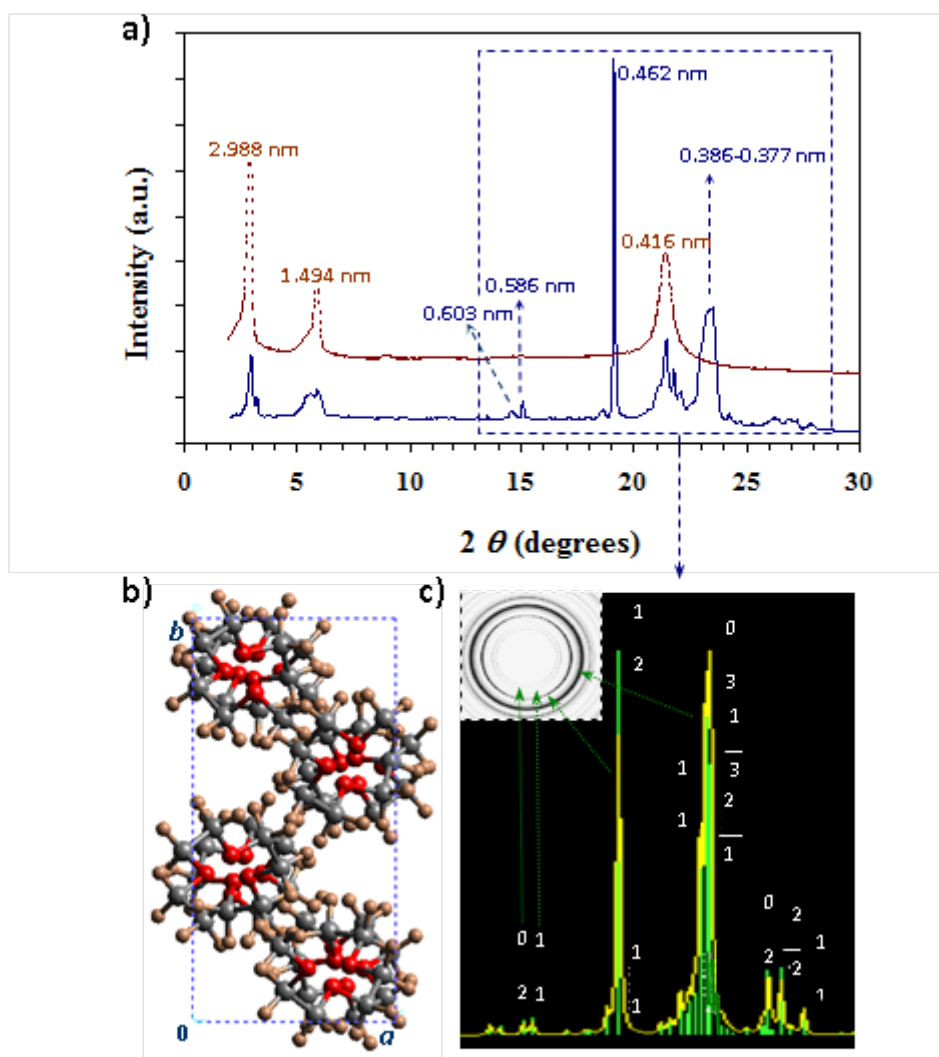


Figure 2.7. a) Powder X-ray diffraction profiles of poly(MePEGCA-co-HDCA) (blue) and poly(cyano hexadecylacrylate) (brown). b) Down the chain axis projection of the PEG structure showing the packing arrangement of the four $7/2$ helices. c) Simulated powder X-ray diffraction profile of PEG and corresponding diffraction pattern (inset).

2.4.Degradation

2.4.1. Measurements

¹H-NMR spectra were acquired with a Bruker AMX-300 spectrometer operating at 300.1 MHz. Chemical shifts were calibrated using tetramethylsilane as an internal standard. Dried dimethyl sulfoxide-d₆ (DMSO) was used as the solvent.

2.4.2. Degradation experiments

Little polymer tablets were prepared by weighing 150 mg. After preparation every tablet was weighed by analytic balance, put in 15 ml of milliQ water and left at fixed temperature. Two different conditions were investigated: 4 °C and 18 °C. At scheduled time a tablet was taken out the water, well dried and weighed, in order to calculate the weight loss. Some of the samples were then analysed by ¹H-NMR in order to study the polymer chemical degradation.

2.4.3. Results

Degradation of poly(MePEGCA-co-HDCA) in milliQ water at temperatures of 18 and 4 °C was characterized by a quick process that took place over a maximum period of 8 and 24 h and that caused a weight loss of approximately 61% (Figure 2.8). After that, the copolymer was not sensitive to the hydrolytic attack and the sample weight remained practically constant, at least over an exposure time of 300 hours (12 days).

¹H-NMR spectra were taken after different incubation times and results as peak areas are shown in Table 2.2. NMR spectra were performed on the dried polymer, except for the analysis performed at 8 hours on water medium. In this case, water of the degradation experiments was evaporated and the solute, corresponding to the fraction which was dissolved by water, was analysed at ¹H-NMR. In NMR analysis chemical shift of hydrogen is measured in respect to a reference (threemethyl silane) and this chemical shift is indicated as ppm, considering that threemethyl silane correspond to 0 ppm.

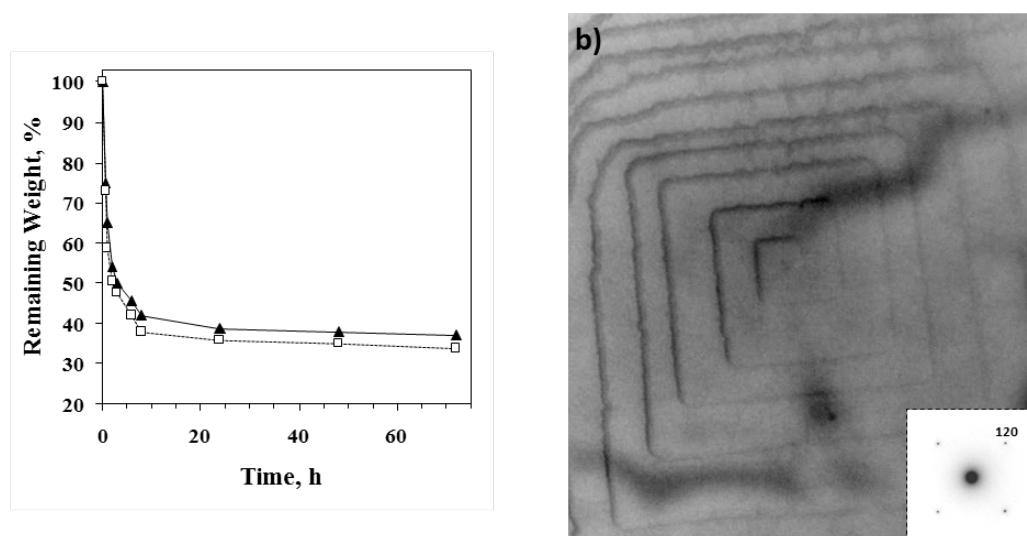


Figure 2.8. a) Plot of the remaining weight of a poly(MePEGCA-co-HDCA) disk sample versus exposure time in distilled water at 18 °C (▲) and 4 °C (□). b) Electron micrograph of PEG lamellar crystals recovered from the release medium. The inset shows the corresponding electron diffraction pattern.

By comparing the area peak of different hydrogen of the molecule it is evident the loss in PEG chains as well in polymerization methyl (peak at 2.30-2.60). PEG chain loss is confirmed by the spectra performed on water medium, where PEG signal is very high, confirming that most of PEG remains in water.

Table 2.2. Area of the ^1H NMR peaks for each signal in the samples after degradation in water. pattern.

ppm	1.26	1.73	0.88	2.30-2.60	4.25	3.64	3.38
homopolymer	100	7.04	11.49	5.39	7.01	--	--
copolymer	100	5.62	11.04	13.50	5.85	148.07	3.78
t=8h, 18°C	100	5.71	11.38	4.77	4.84	7.79	0.10
t=8h, water medium, 18°C	100	--	8.38	183.0	--	6801.3	144.34
t=8h, 4°C	100	5.95	11.44	5.78	5.75	12.33	0.33
t=24h, 18°C	100	5.50	11.87	4.79	6.19	3.75	0.09
t=24h, 4°C	100	5.61	11.75	5.76	5.78	5.96	0.21
t=48h, 18°C	100	4.98	11.83	4.46	4.80	5.16	0.03
t=48h, 4°C	100	5.36	11.92	6.29	5.94	6.81	0.21
t=72h, 18°C	100	5.77	11.74	4.70	5.95	4.94	0.14
t=72h, 4°C	100	5.71	11.08	5.40	6.22	5.27	0.15

Figure 2.9a and c compare the $^1\text{H-NMR}$ spectra of the as-synthesized sample and that degraded up to a weight loss of 61%. The initial sample was characterized by a molar ratio of one to four between pegylated and hexadecyl (HD) lateral chains as deduced from the areas of the signals at 3.37 and 0.88 ppm assigned to the methyl groups belonging to the two ester moieties (Peracchia et al., 1997). Methylene groups of the main chain and the lateral hexadecyl and PEG groups appeared also well differentiated at 2.60-2.30, 1.25 and 3.64 ppm, respectively, and consequently could also be considered to follow the degradation process. Spectra of samples exposed to water clearly shows as the signal at 3.64 ppm practically disappeared while the ratio between the areas of signals at 0.88 and 2.60-2.30 ppm remained practically constant. According to the composition determined from $^1\text{H-NMR}$ spectra, the MePEG lateral groups represented a 55 wt-% of the copolymer and consequently the observed degradation could be well justified by the ester group cleavage involving only the pegylated chains.

Spectra of the residue extracted from the hydrolytic degradation medium after 8 hours of incubation basically corresponded, as expected, to the PEG lateral groups (Figure 2.9b), although a minor amount of hexadecyl groups could also be detected as well as signals corresponding to the methylene groups of the main chain. In fact, water soluble poly(cyanocrylic acid) is produced by hydrolysis of all ester groups (Lenaerts et al., 1984).

The hexadecyl groups detected in the aqueous medium were originated by hydrolysis of some ester groups initially accessible to the solvent which could exist in the solid sample and even in small polymer fractions that could be solubilized at the beginning of incubation. It is clear that the one to four ratio between MePEG and the alkyl HD lateral chains in the as-synthesized sample is an average value and that molecules with different compositions and solubilities must be present. Thus, a 10 wt-% of the sample was solubilized by extraction with trichloromethane/water in a period of time at which degradation was practically negligible (i.e. less than 5% for 30 min of exposure) .

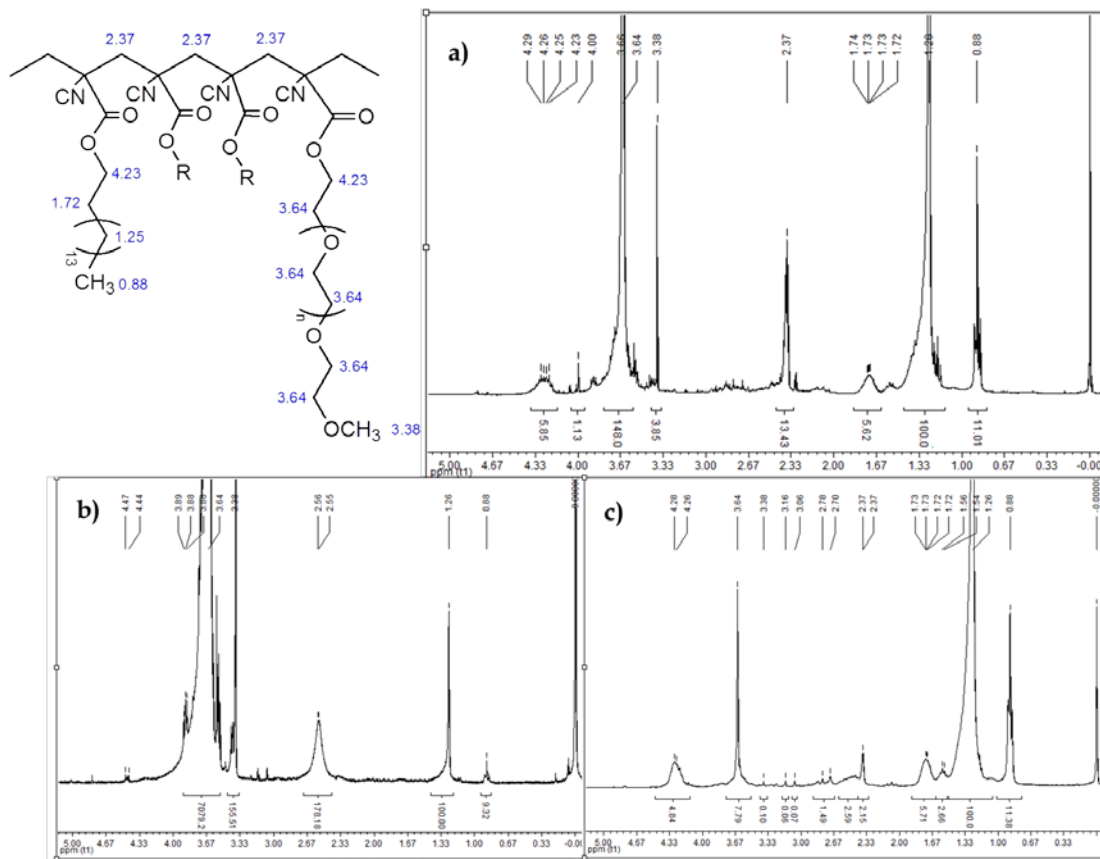


Figure 2.9. a) $^1\text{H-NMR}$ spectra of the as-synthesized poly(MePEGCA-co-HDCA) sample and chemical scheme showing the assignment of signals (inset). b) $^1\text{H-NMR}$ spectra of the solubilized fraction of a poly(MePEGCA-co-HDCA) sample after 8 h of exposure to water at 18 °C. c) $^1\text{H-NMR}$ spectra of a poly(MePEGCA-co-HDCA) sample after 8 h of exposure to water at 18 °C.

The $^1\text{H-NMR}$ spectra (see Figure 2.10) of this fraction indicated a 1:1 ratio between MePEG and HD lateral chains and demonstrated the existence of molecules with high hydrophilicity in the initial sample.

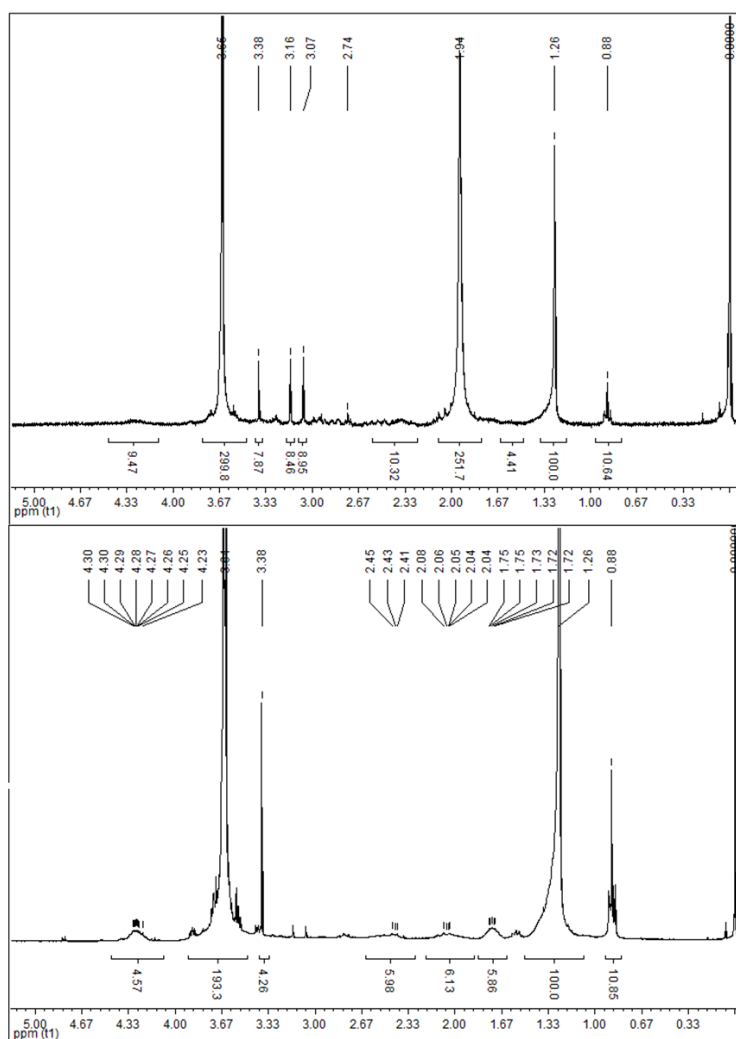


Figure 2.10. $^1\text{H-NMR}$ spectra of polymer after extraction: polymer solubilized in water (top) and polymer solubilized in trichloromethane.

In summary, $^1\text{H-NMR}$ spectra clearly demonstrated that degradation took place mainly through the ester bond cleavage of the hydrophilic PEGylated chains whereas the cyanoacrylic backbone and even the hydrophobic hexadecyl side chains remained practically unaltered. It is interesting to note that the ester bond of the hydrophobic moiety was not highly susceptible to hydrolysis since probably it was not well exposed to the degradation medium. These results are in full agreement with preliminary studies performed on fetal calf-serum which indicates that the hexadecyl homopolymer was not degraded during the first 3 hours of incubation

whereas the studied copolymer showed a linear dependence of degradation with the exposure time, being attained a 30% after only 3 hours of exposure (Peracchia et al., 1998). However, in this case the action of esterases present in the serum medium could not be differentiated from a simple hydrolytic attack. It has to be also pointed out that the rapid loss of PEG chains can be due also to the solubilization in water of more hydrophilic polymer molecules. Since the synthesis does not allow to control monomers distribution in the polymer molecules, it can be possible that molecules with an higher ratio in PEG monomers dissolve in water, so that this phenomena cannot be distinguished from the hydrolysis of esters bonds.

2.5.References

Kawai T., Rahman N., Matsuba G., Nishida K., Kanaya T., Nakano M., Okamoto H., Kawada J., Usuki A., Honma N., Nakajima K., Matsuda M., 2007, Crystallization and melting behavior of poly(L-lactic acid). *Macromolecules* 40, 9463-9469.

Lenaerts V., Couvreur P., Christiaens-Leyh D., Joiris E., Roland M., 1984, Degradation of poly (isobutyl cyanoacrylate) nanoparticles. *Biomaterials* 5, 65-68.

Müller, A. J., Balsamo, V., Arnal, M. L., 2007, Crystallization in block copolymers with more than one crystallizable block. In: Reiter G, Strobl G, editors. *Lecture Notes in Physics: Progress in Understanding of Polymer Crystallization*. Berlin: Springer.

Muthukumar M., Ober C.K., Thomas E.L., 1997, Competing interactions and levels of ordering in self-organizing polymeric materials. *Science* 277, 1225-1232.

Nandan B., Hsu J.Y., Chen H.L., 2006, Crystallization Behavior of Crystalline-Amorphous Diblock Copolymers Consisting of a Rubbery Amorphous Block. *Polymer Review* 46:143-172.

Peracchia M.T., Desmaële D., Couvreur P., d'Angelo J., 1997, Synthesis of a novel poly(MePEG cyanoacrylate-co-alkyl cyanoacrylate) amphiphilic copolymer for nanoparticle technology. *Macromolecules* 30, 846-851.

Peracchia M.T., Vauthier C., Desmaële, Gulk A., Dedieu J.C., Demoy M., d'Angelo J., Couvreur P., 1998, Pegylated nanoparticles from a novel methoxypolyethylene glycol cyanoacrylate hexadecyl cyanoacrylate amphiphilic copolymer. *Pharmaceutical Research* 15, 550-556.

Peracchia M.T., Fattal E., Desmaële D., Besnard M., Noël J.P., Gomis J.M., Appel M., d'Angelo J., Couvreur P., 1999, Stealth® PEGylated polycyanoacrylate nanoparticles for intravenous administration and splenic targeting. *Journal of Controlled Release* 60, 121-128.

Ryan A.J., Hamley I.W., Bras W., Bates F.S., 1995, Structure development in semicrystalline diblock copolymers crystallizing from the ordered melt. *Macromolecules* 28, 3860-3868.

Schäffer E., Thurn-Albrecht T., Russell T.P., Steiner U., 2000, Electrically induced structure formation and pattern transfer. *Nature* 403, 874-877.

Zhu L, Chen Y., Zhang A., Calhoun B.H., Chun M., Quirk R.P., Cheng S.Z.D., Hsiao BS, Yeh F., Hashimoto T. 1999, Phase structures and morphologies determined by competitions among self-organization, crystallization, and vitrification in a disordered poly(ethylene oxide)-*b*-polystyrene diblock copolymer. *Physical Reviews B* 60, 10022-10031.

3. Production of PEGylated nanocapsules through solvent-displacement in confined impinging jets mixers

3.1. Introduction

Polymer nanoparticles include polymeric nanospheres and polymeric nanocapsules. In nanospheres the drug is dispersed in the polymeric matrix, whereas polymeric nanocapsules have an inner liquid core surrounded by a polymeric layer, so that different drugs can be dissolved in the inner core, according to their solubility. The drug molecules inside the nanospheres are dispersed in the polymer matrix in a sort of solid solution, whereas in nanocapsules they are dissolved in the liquid core; as a consequence, drug release occurs according to different mechanisms in nanospheres and nanocapsules.

This chapter is focused on polymeric nanocapsules for pharmaceutical applications, but also nanosphere are produced for comparison.

Nanospheres and nanocapsules are produced by solvent-displacement (also called interfacial deposition or flash nanoprecipitation) which has some advantages respect to other preparation method (see Chapter 1). In fact, solvent-displacement allows to use polymers with controlled molecular weight, avoids the presence of residual monomers in solution, it is simpler, gives more reproducible results and it

is easier to scale up. Solvent-displacement consists in mixing a water miscible organic phase, containing the polymer, the oil and generally the drug, with an aqueous phase. The organic phase is referred to as solvent, whereas water is the anti-solvent. When the two phases are mixed together, the organic phase diffuses rapidly into the water, where it is soluble and where, on the contrary the polymer, the oil and the drug are insoluble. The rapid diffusion of the solvent in the anti-solvent is the driving force in nanocapsule formation, inducing oily drops formation and the interfacial deposition of the polymer around the oily drops.

Being the overall process very rapid it is influenced by mixing and in order to obtain good mixing conditions, special micro-mixers must be used. Confined impinging jets mixers (CIJMs) provide optimum mixing conditions. Their use in nanosphere formation was extensively studied (Marchisio et al., 2006, Gavi et al., 2008, 2010) and they were found to be very useful in controlling the final particle size (Lince et al., 2008). CIJMs consist of two high velocity linear jets of fluid that collide inside a small chamber, whose size affects the overall mixing rate.

Mixing mechanism and nanoparticle formation in CIJMs, similar to the ones studied in this work, were analysed in previous papers through computational fluid dynamics (CFD) simulations (Lince et al., 2009, Gavi et al., 2007). CFD simulations allow to quantify the mixing dynamics of the two inlet streams inside the mixing chamber. Three types of mixing are generally present: macro-mixing at the mixer scale, meso-mixing at the scale of the largest turbulent eddies and micro-mixing at the molecular scale. Each step controls the next one and can be rate limiting. CIJMs limit the meso-mixing time and ensure fast homogenization (i.e., short macro-mixing time) of the two fluids. Characteristic global mixing times in these equipments were calculated by CFD and are in the order of magnitude of milliseconds (Lince et al. 2010, Lince et al., 2011a).

The use of the CIJMs for the production of polymer nanocapsules suitable for pharmaceutical applications is investigated for the first time. Since the mechanisms of nanocapsule formation are likely different from those of nanospheres, we are particularly interested in investigating the interplay between mixing and

nanocapsules formation, with the precise scope of highlighting similarities and differences. Attention is played to the control of nanocapsule size distribution. In fact, different applications translate into different requirements. For example, in the case of intravenous administration, nanocapsules have to be smaller than 300 nm. For other applications, such as cosmetic (Alvarez-Roman et al., 2001) or food (Zambrano-Zaragoza et al., 2011) size limitations are different; therefore the development of strategies to control the final nanocapsule size turns out to be very useful.

It should be highlighted that no drug loading has been considered in this chapter. Although in the case of nanospheres the absence or the presence of the drug can significantly alter the results, especially in terms of stability (as shown for example for doxorubicin loaded nanospheres, Lince et al., 2001b), in the case of nanocapsules the situation seems to be very different. In fact, the oil separates from the initial single-phase system through spinodal decomposition: no energetic barrier has to be overcome (as dictated by the Cahn-Hilliard equation) and molecular diffusion is the bottleneck. In addition being the drug generally hydrophobic and in low concentration (in comparison with the oil), drug molecules will likely move rapidly inside the oily drops. Indeed a successive study with a drug is required to prove this last point and this simpler oil-polymer system will be used as reference.

3.2.Theoretical background

The formation of nanocapsules and nanospheres during solvent-displacement is a complex process and many theories and interpretations have been presented in the literature. Knowledge of what happens at the molecular level is of primary importance for manipulating and controlling the overall process. Classical precipitation theory explains particle formation in three steps: nucleation, molecular growth and particle aggregation (Horn and Rieger, 2001). Super-saturation is the driving force for particle formation and in solvent-displacement is built up by mixing of the solvent and the anti-solvent. Since in this work we are interested in

both nanospheres and nanocapsules, it is necessary to review and briefly discuss the theory presented in the literature for these two systems.

In the case of nanospheres, the copolymer and organic compound are dissolved in the solvent and when mixed with the anti-solvent particles are formed. Johnson and Prud'homme (2003) describe nanosphere formation as the competition of two simultaneous phenomena: nucleation of drug particles and copolymer self-assembly. The two phenomena are characterized by different time-scales and in order to allow the copolymer molecules to interact with (and to deposit on) the growing particles, the two time-scales have to match one another. Typical operating conditions, used in the production of most of the organic-drug particles, are characterized by extremely high super-saturation, resulting in very small nucleus size, practically instantaneous nucleation, with very little energy barrier. It is also important to compare these time-scales with the mixing time-scale. It was in fact observed that faster mixing generally results in smaller drug particles with higher functionalization by the copolymer, however once a certain limit is reached no significant change in nanoparticle properties is observed. This is probably related to the development of a spatially independent self-similar state caused by the achievement of fully turbulent flow.

In the case of nanocapsules the inner core of the particle consists instead of a lipophilic liquid (usually oil) which is insoluble in the mixture of solvent and anti-solvent. Thus in nanocapsule formation two phenomena are involved: oily drop formation and polymer deposition around the oily drop. Oily drop formation takes place through spinodal decomposition (as dictated by the Cahn-Hilliard equation). Therefore, although due to the high super-saturation the nucleation process involved in nanosphere formation generates a very small energy barrier, some differences between nanospheres and nanocapsules, where on the contrary spinodal decomposition occurs spontaneously without any energy barrier, might be observed.

In addition, when solvent and anti-solvent are mixed together, the oil dissolved in the solvent separates resulting in drops which tend to coalesce. This

can be prevented by the deposition of the copolymer around the drops, however in the case of nanocapsules polymer reorientation on the interface might play a different role. In any case, also for nanocapsules mixing efficiency is expected to be fundamental in order to have homogeneous and optimal conditions for the formation of very small drops and an even distribution of copolymer molecules around drops.

Some authors (Fessi et al., 1989, Quintanar-Guerrero et al., 1998) have acknowledged the important contribution of the Gibbs-Marangoni effect on the formation of nanocapsules, in which the driving force is the difference in the interfacial tension between the solvent and the anti-solvent. This effect is not considered in this work since it is important when nanocapsules are produced with the classical method, adding slowly the solvent to the aqueous phase. Using micro-mixers, such as CIJMs, under very intense turbulent mixing conditions this effect is probably less important.

3.3. Materials and methods

The poly(methoxypolyethyleneglycol cyanoacrylate-co-hexadecyl cyanoacrylate) (poly(MePEGCA-co-HDCA) in what follows) copolymer was synthesized by the author as reported in Chapter 2. The ratio between MePEG cyanoacetate/hexadecyl cyanoacetate was one to four.

In all experiments Miglyol® 812N was used as liquid core (courtesy of Sasol Italy S.p.A). This oil is a mixture of capryc and caprylic triglyceride with a density of 0.94-0.95 g/cm³. The solvent is Acetone Chromasolv (HPLC grade), purchased by Sigma-Aldrich. Milli-Q RG system by Millipore® was used to produce the ultrapure water employed in all the experiments.

Nanocapsules and nanospheres were prepared by solvent-displacement. In nanocapsule precipitation the copolymer together with Miglyol was dissolved in acetone and then mixed with pure water, whereas in nanospheres only the copolymer was dissolved in the solvent. Apart from this, the two preparations were

identical. After mixing with water the particulate system was immediately formed. As already mentioned, since the process is strongly influenced by mixing, CIJMs were used, that ensure high turbulence levels and short mixing times. Precipitation was carried out with and without quenching, in order to highlight the possible influence of aggregation; to this purpose the outlet of the mixer (8 ml containing equal volumes of acetone and water) was collected in a beaker containing 4 ml of water. Tests have been carried out in order to identify the best quenching volume ratio. The 4 ml of water (corresponding to a 1:2 acetone:water final ratio in the mixture) was found to be a good trade off, since quenching with larger volumes did not results in significantly different data.

In the laboratory set up, solvent solution and anti-solvent were loaded into two different plastic syringes of 100 ml of volume and fed into the mixers by using a syringe pump (KDS200, KD Scientific). The pump was calibrated in order to make sure that the imposed flow rate was actually delivered. Then, the solvent was removed by a rotating low pressure evaporative device (Stuart® Rotary Evaporators). The possible azeotrope for the acetone-water mixture is in the acetone rich region, therefore complete removal of acetone is possible (since the starting point is an already water rich solution). The effect of acetone removal on nanocapsules was quantified and found to be within the range of experimental uncertainty. Stability of the nanocapsule size after solvent removal was monitored by storing samples at 4°C for several weeks and measuring the nanocapsule size at regular time interval. No significant size changes were detected.

Four different CIJMs were used in this work. Three of them are scaled by a factor of two and one has bigger inlet diameter, in order to study the effect of a different inlet jet in the same mixing chamber. A sketch is reported in Figure 3.1 whereas the quotes are reported in Table 3.1. They are labelled in what follows as scale down, CIJM-d1, scale up (corresponding to three CIJMs exactly scaled by a geometric factor equal to two) and CIJM-d2 (corresponding to the same chamber size of CIJM-d1 but with bigger inlet pipe). The comparison of the results obtained

with these four mixers allows to evidence scale up and scale down effects, as well as the effect of the chamber and inlet pipe size on the final size distribution.

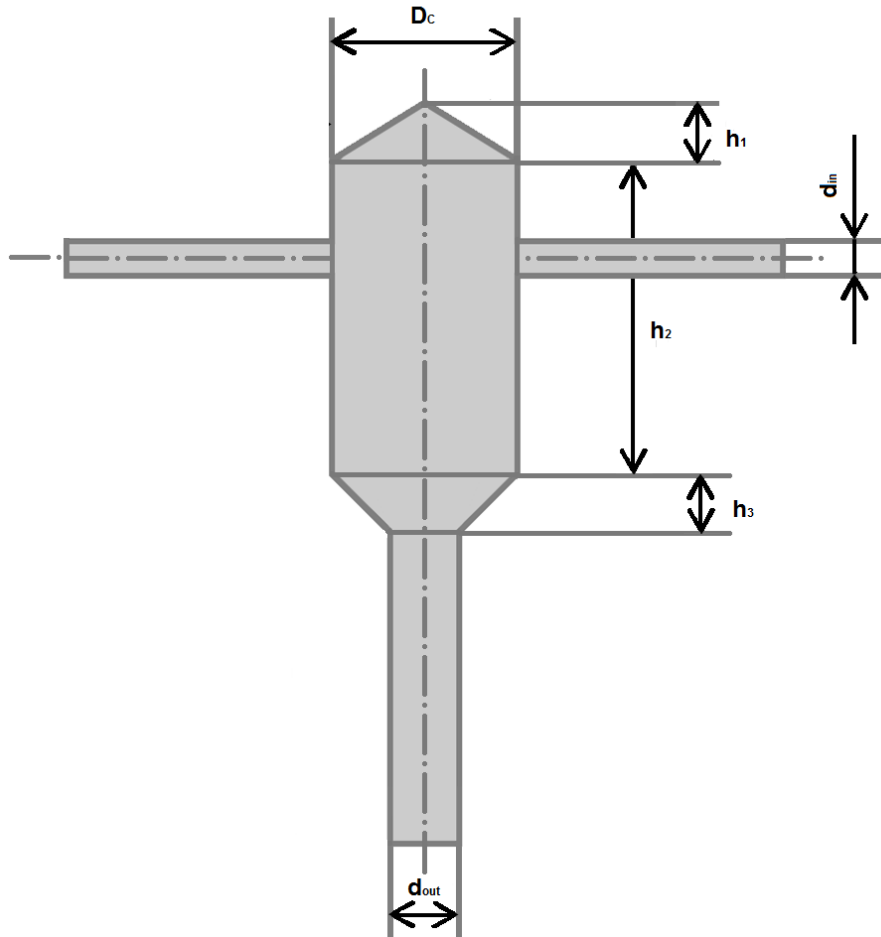


Figure 3.1. Sketch of the CIJMs used in this work.

Table 3.1. Geometrical details of the CIJMs used for the experiments.

Mixer	d_{in} (mm)	d_{out} (mm)	D_c (mm)	h (mm)			Volume (mm^3)
				h_1	h_2	h_3	
scale down	0.5	1	2.4	0.5	4.5	0.6	22.5
CIJM-d1	1	2	4.8	1	9	1.2	180.3
scale up	2	4	9.8	2.3	17	3	1288.3
CIJM-d2	2	2	4.8	1	9	1.2	180.3

Nanocapsules and nanospheres were characterized in terms of their size distribution and zeta potential. The Z-average size of nanocapsules was determined by Dynamic Light Scattering (DLS, Zetasizer Nanoseries ZS90, Malvern Instrument) that measures accurately in the size range from 2 nm to 3 μm . Zetasizer Nanoseries ZS90 does not use a movable detector, but uses classical fixed detection arrangement at 90° to the laser and the centre of the cell area. This arrangement reduces the detectable size range and requires low concentration samples. In DLS measurements, the intensity size distribution is converted by using the Mie theory to a volume size distribution. In order to obtain the volume size distribution it is necessary to provide the instrument the refractive index of the material (which does not significantly influence the final result of the measurement) and of the dispersant. Before measuring, the sample was diluted of 1:100 in order to reduce the solid concentration. In DLS it is important to have a sample with appropriate particle concentration, in fact, it has not to be too concentrated, because each single photon should be scattered only once before reaching the detector, but it has to be concentrated enough to result in sufficient statistics. The parameters which assure the quality of the measurements (i.e., poly-dispersion index, correlation function parameter) were controlled for each single sample and measurements were repeated when the quality criteria were not reached. Each sample was measured three times and the average value is reported in the figures.

The surface charge of nanoparticles was inferred through zeta potential measurements in water, by the same instrument, after dilution 1:10. In zeta potential measurements the instrument measures the electrophoretic mobility, which is the velocity of a particle in an electric field. The zeta potential is then calculated from the Henry equation, that makes use of the Smoluchowsky approximation, valid for particles in aqueous samples.

All the experiments were performed after dissolving the copolymer and the oil in the acetone. No stabilizing agent was added to the aqueous phase since the PEGylated polymer can act as a stabilizer due to its amphiphilic nature.

In order to investigate the interplay between mixing and nanocapsule formation experiments were carried out in a wide flow rate range up to 120 ml/min for both solutions. Results from previous work (Lince et al., 2011a) show that under these conditions the mixers work under different fluid dynamic regimes. In fact, microPIV measurements performed in CIJMs similar to ours (Gavi et al., 2010) allowed to determine the flow in the mixers: it is highly turbulent only at the highest flow rates (larger than 40 ml/min for the smallest mixers and larger than 90 ml/min for the biggest) and is instead transitional for the lowest flow rates. In all cases however, the outlet stream is well mixed, since also at relatively low flow rates good mixing performances are generally obtained (Lince et al., 2011b). The reason for investigating the performance of these devices also at low flow rates, when the flow is not fully turbulent, is to verify the possibility of using mixing as an operating parameter to control the final nanocapsule size. The Reynolds number used in the figures refer to the inlet pipe and are used as label for each operating condition (corresponding to a particular flow rate): the turbulence we are interested in is the one in the mixing chamber, and as said above, we know each operating condition corresponds to a more or less turbulent situation in the mixing chamber.

In these experiments the acetone solution contained 6 mg/ml of copolymer and 8 μ l/ml of oil (7.6 mg/ml), equivalent to an oil-to-copolymer mass ratio value of $MR = 1.26$. We performed the experiments both with and without quenching to understand the mechanism of nanocapsule formation and the main differences with respect to nanospheres. In some cases experiments were repeated three times in order to quantify the experimental variability, reported together with the data in the form of error bars.

The effect of oil concentration on nanocapsule size was studied at four different oil concentrations: zero (i.e. nanospheres), 4.8 μ l/ml (4.56 mg/ml), 8 μ l/ml (7.6 mg/ml) and 15 μ l/ml (14.25 mg/ml) with 6 mg/ml of copolymer concentration. The respective oil-to-copolymer mass ratio was 0.76, 1.26 and 2.37. These experiments were performed in all the CIJMs. Moreover, the same experiments were performed in the CIJM-d1, varying the copolymer concentration (10 mg/ml, 6

mg/ml and 3.2 mg/ml). In this case the oil concentration was kept constant at 8 $\mu\text{l/ml}$; in this way the oil-to-copolymer mass ratio was the same of the previous experiments (0.76, 1.26 and 2.37).

A further set of experiments, keeping constant the oil-to-copolymer mass ratio, was also carried out. In this case both copolymer and oil concentrations were varied in order to check if resulted in nanocapsules with similar size. The two mass ratio considered were 0.76 (with the following different concentrations: 4 mg/ml copolymer and 3.2 $\mu\text{l/ml}$ oil, 6 mg/ml copolymer and 4.8 $\mu\text{l/ml}$ oil, 10 mg/ml copolymer and 8 $\mu\text{l/ml}$ oil) and 2.37 (3.2 mg/ml copolymer and 8 $\mu\text{l/ml}$ oil, 6 mg/ml copolymer and 15 $\mu\text{l/ml}$ oil) . This set of experiments was carried out only in CIJM-d1 mixer.

Both the flow rate and the inlet diameter of the mixer were varied in the experiments resulting in different mixing regimes inside the device. Since flow rate (FR), velocity of the inlet jet (v_j) and inlet diameter (d_{in}) are related through the following relationship:

$$\pi \frac{d_{in}^2}{4} v_j = FR \quad (1)$$

at the same flow rate, the fluid velocity is different in different mixers, resulting in different mixing efficiencies. According to Johnson and Prud'homme (2003b) the overall mixing time (τ_{mix}) when the flow is fully turbulent can be calculated as follows:

$$\tau_{mix} \propto v_j^{-3/2} \quad (2)$$

and, of course different mixers, are characterized by different residence times:

$$\tau_{res} = \frac{V_M}{FR} \quad (3)$$

where τ_{res} is the residence time and V_M is the volume of the mixer.

As determined in previous investigation by means of CFD, mixing time (τ_{mix}) in CIJMs like the ones here used are in the order of milliseconds, while residence time is always above this order of time, allowing the fluid to stay in the mixer enough time.

3.4. Results and discussion

Nanocapsule formation was firstly investigated by comparing different mixers and different flow rates (with and without quenching) and subsequently by comparing different initial compositions (copolymer and oil concentration). Results for the three CIJMs geometrically similar are reported in Figure 3.2. The figure shows the zeta potential and the mean particle size for nanocapsules prepared with an acetone solution of 6 mg/ml of copolymer and 8 μ l/ml of oil (resulting in MR = 1.26) at different flow rate values, with and without quenching.

Let us first highlight the effect of the quenching water: if nanocapsules are not quenched their final mean size (after solvent evaporation) is significantly larger; this general behavior will be observed in all the cases investigated, and will be discussed in the following.

A common trend for all the mixers can be observed, and it is interesting to observe that it is the same for both the quenched and the non-quenched particles. The data seem to evidence a point after which further increases in flow rate have little effect; this is expected by previous works in similar fields and the theory explains that this should happen when the mixing time is faster than the particle formation time. The goal of using special intensive mixers (such as the ones used in this work) is to ensure that the mixing time is faster than the particle formation time so that the system can be mixed homogeneously, before further phenomena occur. It is not completely correct to specify a single break point, as in the range considered in fact the size is affected by fluid dynamics in a similar way, but this is true on a logarithmic scale. The effect of a variation of the inlet flow rate is strong at low flow rates (generally below 20 ml/min), while it is very weak at higher flow rates, generally larger than 40 ml/min.

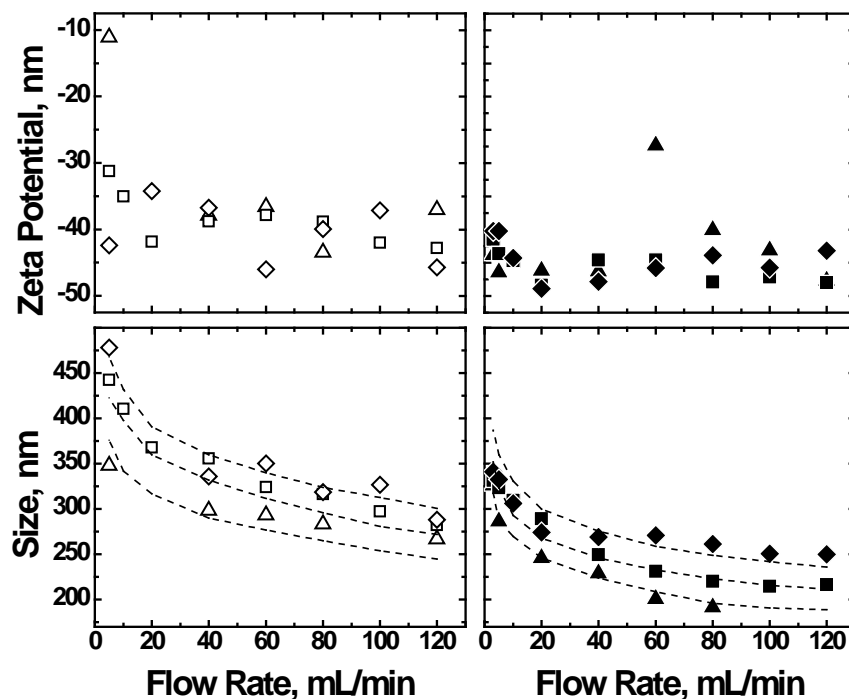


Figure 3.2. Zeta potential (top) and mean particle size (bottom) versus the flow rate for nanocapsules obtained without quenching water (left, open symbols) and with quenching water (right, filled symbols) for different mixers: scale down (Δ, \blacktriangle), CIJM-d1 (\square, \blacksquare) and scale up (\diamond, \blacklozenge). Experiments at constant polymer (6 mg/ml) and oil (8 μ L/ml) concentration (MR=1.26).

It must be said that at very low flow rate the uncertainty of the experimental data is relatively high, especially for the larger mixers, for which a lower reproducibility is observed: this may be a consequence of the fluid dynamic regime, as the inlet jets are laminar and thus the flow in the chamber is in the transitional region, with turbulence developing. In any case it seems that the size increase that is observed, even when no quench is used, is similar in the whole range investigated, included the low flow rate region, thus confirming that the mixing performances of these devices are good also in the laminar regime.

In Figure 3.2 the performances of the three mixers are compared by plotting the size of the nanocapsules obtained versus the inlet flow rate (the flow rate in each of the two inlets is considered), in order to evidence the influence of the size of the apparatus at constant throughput. The measured zeta potential is, as average,

between -30 mV and -45 mV, indicating that nanocapsules are stable from the electrochemical point of view. They reach lower values (-40 and -50 mV) if water dilution is carried out.

The scale down mixer results in the smaller nanocapsules, probably due to the fact that it gives the best mixing conditions, at fixed flow rate. Since scale down mixer inlet jet diameter is 0.5 mm, the inlet stream can reach very high velocities, and as a consequence, high turbulent energy dissipation rates and very short mixing times. But the inlet jet velocity is not the controlling variable, as shown in Figure 3.3: in fact, it can be noted that comparing the size obtained in the different mixers at the same inlet velocity, the conclusion is reversed, and the smallest nanocapsules are obtained in the scale up mixer, while the scale down mixer gives larger particles (and with higher energy costs). Only the quenched particle case is shown, but the behaviour is similar (at least for the three scaled mixers) for the non-quenched case. In these cases the ratio between the inlet jet diameter and the chamber size is maintained constant, thus it is not possible to evidence which one of these geometric parameters eventually is more important; but it may be concluded that a larger size is surely favourable, because it allows to increase throughput reducing at the same time the final particle size (or eventually to obtain the same size at reduced jet velocity, and thus with lower energy input).

It is thus evident that the size of the apparatus plays a more complex role: if the Reynolds number is used to characterize the fluid dynamics conditions, and thus mixing, it is observed that the curves corresponding to the three mixers collapse onto a single one; of course Reynolds number can take into account only fluid dynamics similarity and only for geometrically similar devices, thus the behavior described above is observed only for the three scaled mixer and for the same inlet concentrations of oil and polymer (that is for a fixed characteristic process time). As it will be widely discussed in the next chapter, Reynolds number is an important parameter to scale the apparatus. It allows to consider together factors describing the turbulence of the system, and to find a parameter which

describes all the particles obtained at the same concentration in geometrically similar mixers.

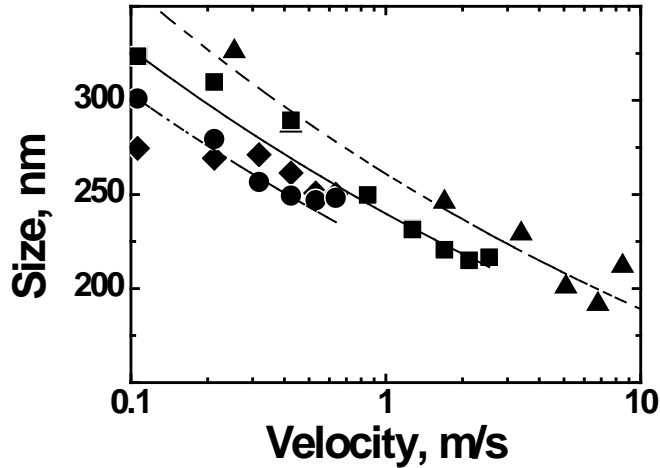


Figure 3.3. Mean particle size versus the inlet stream velocity for nanocapsules obtained with different CIJMs: scale down mixer (▲), CIJM-d1 mixer (■), scale up mixer (◆), CIJM-d2 mixer (●). Experiments at constant polymer (6 mg/ml) and oil (8 μ L/ml) concentration (MR=1.26).

More complex to explain is the behavior of the CIJM-d2, which has the same chamber of the CIJM-d1, but larger inlet pipe diameters, equal to those of the scale up device: in particular significant differences are observed with and without quench. When nanocapsules are quenched, the size of the particles obtained, at a given flow rate, is approximately the same in the CIJM-d2 and in the scale up mixer: it can be noted that in this case the inlet velocity is also the same, as the pipe diameter is equal (see also Figure 3.3); this would suggest that the jet velocity is more relevant than the chamber size to determine mixing conditions. On the other hand, at a given jet velocity, smaller particles are obtained in the CIJM-d2 than in CIJM-d1: this might indicate that, for a given chamber volume, it is favourable to have a larger interaction zone of the two streams; it can be noted anyway that operating at the same jet velocity in the two considered mixers requires larger flow rates in the one with larger pipe diameters (the CIJM-d2), and this leads to proportionally shorter residence times: thus the smaller size might be also a

consequence of the reduced time for coalescence, and connected to a lower yield of the process.

If the outlet flow is not quenched, the behavior is different: at a given flow rate the CIJM-d2 produces particles significantly larger than all the others, and in particular larger than the scale up mixer; comparing the performances at a given inlet velocity, CIJM-d2 and CIJM-d1 produce nanocapsules of similar size. The comparison with the scale up mixer evidences that in this case a larger chamber is favourable, as it allows to obtain smaller nanocapsules; as suggested by Johnson and Prud'homme (2003b), what may be relevant is the ratio between the inlet pipe diameter and a characteristic chamber dimension: this value must not be too large, to allow the mixing to be confined within the chamber. It is possible that in CIJM-d2 the particle formation process is not completed in the mixer, and this can explain the significant size increase observed in case of non-quenched nanocapsules; the CFD simulations carried out in a previous work for the same geometry confirm that the mixing process (at very low flow rates) may be not complete (Lince et al., 2011a). This fact may be also responsible for the larger experimental uncertainty that is observed in the test carried out in the CIJM-d2.

The influence on the mean nanocapsule size of the inlet pipe diameter, for mixers with the same chamber volume, is shown in Figure 3.4; in this case the data are plotted considering the inlet jet Reynolds number (for an inlet jet with average properties of the mixed liquid streams). It can be noted that in case of quenched nanocapsules a unique curve is obtained (and as discussed before, this is the same curve valid for all the mixers in these concentration conditions), while for non-quenched ones larger sizes are obtained in the CIJM-d2, as discussed before. Figure 3.4 allows also to compare the experimental uncertainty in the case of quenched and non-quenched processes: in the latter case it is significantly higher. Zeta potential measurements (not shown) result in values slightly lower than -30 mV.

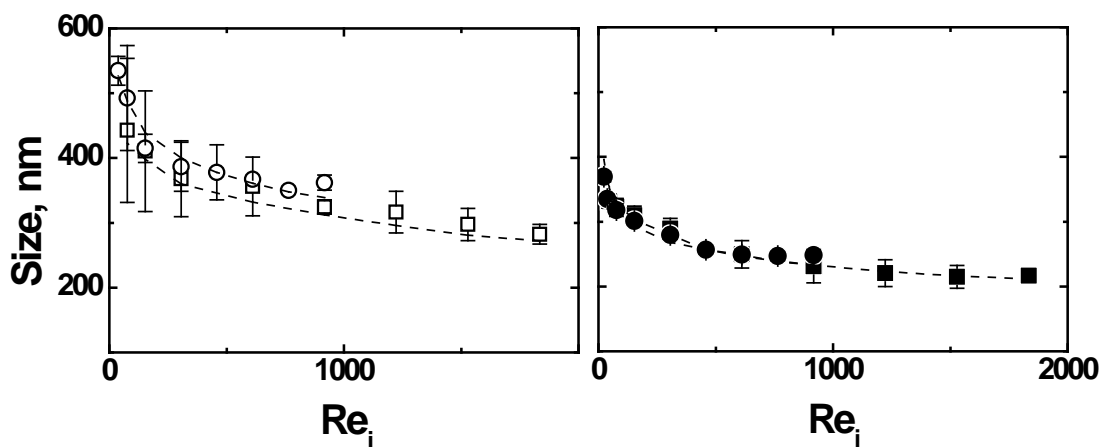


Figure 3.4. Mean particle size versus the jet Reynolds number for nanocapsules obtained without quenching water (left, open symbols) and with quenching water (right, filled symbols) for CIJMs characterized by different inlet pipes and same mixing chamber: CIJM-d1 (□,■), CIJM-d2 (○,●). Experiments at constant polymer (6 mg/ml) and oil (8 μ L/ml) concentration (MR=1.26).

These results show the feasibility of CIJMs for the production of nanocapsules and prove that fast mixing is needed in order to control nanocapsule size and in order to guarantee high reproducibility. Better mixing conditions allow the formation of smaller oily drops and a better coverage by the copolymer, resulting in smaller particles. Moreover, results show that quenching is an important factor and cannot be avoided if nanocapsules with controlled characteristics are desired. It may be also concluded that the process can be scaled using the Reynolds number, at least for geometrically similar devices; the relative size of inlet pipes and chamber has shown to affect the process, but its influence on final nanocapsule size is complex, and cannot be taken into account with a simple relationship, such as that proposed for the mixing time in literature (Johnson and Prud'homme, 2003b). Also the influence of the mixing time will be deepened in next chapter, as well Reynolds number and its correlation with particle size. The effect of oil concentration on nanocapsule formation was also investigated. At a constant copolymer concentration of 6 mg/ml, the oil concentration was varied between zero (resulting in nanospheres) and a maximum value. Data are collected in Figure 3.5, where the results obtained for four different oil-to-copolymer mass ratios are reported for each

mixer; the data are plotted versus the Reynolds number, on the basis of the results discussed in the previous parts of this work, and as the experiments were carried out in the same flow rate range for the different mixers, obviously the extension of the jet Reynolds number range is different. The results confirm that for every set of concentrations, a single curve is obtained for the different scaled mixers (in fact, the approximation curve drawn in the different graphs of the figure is this common line), while a behaviour similar to that discussed before is observed for the CIJM-d2. These conclusions are generally valid also for other polymer concentrations, but as it will be shown in the following, for very low polymer concentrations the formation of nanocapsules may be difficult.

As a general trend, it is possible to state that decreasing the oil-to-copolymer mass ratio the mean particle size decreases. That can be due to the fact that when the oil-to-copolymer mass ratio increases there is not enough copolymer to cover a larger surface area, resulting in bigger nanocapsules.

Each experiment at a given oil-to-copolymer mass ratio was repeated with and without quenching water. Quenching reduces the final nanocapsule size, but the effect is stronger at higher ratios, where there is a lower amount of copolymer. As already mentioned, the operation of quenching allows to stop nanocapsule evolution and freeze them as they are immediately after exiting the CIJM. In fact, quenching dilutes the residual polymer concentration and the particulate system decreasing the probability of nanocapsule collision and further growth. If we compare the results at different oil-to-copolymer mass ratios, it is clear that size increase is larger at high MR values, where there is less copolymer to cover the oily drops. As a matter of fact the results obtained at $MR = 0.76$ present a very small difference with or without quenching. This suggests that the copolymer coating has an important role in stabilizing the suspensions and avoiding nanocapsule aggregation and coalescence.

In Figure 3.5 also nanospheres produced under similar operating conditions are shown for comparison; the size is always much smaller than that obtained in nanocapsules, which is mainly determined by the size of the oil drops formed. The

small variation between quenched and not-quenched samples suggests that it can happen for further aggregation of copolymer molecules from the solution and not for the collision of the nanospheres.

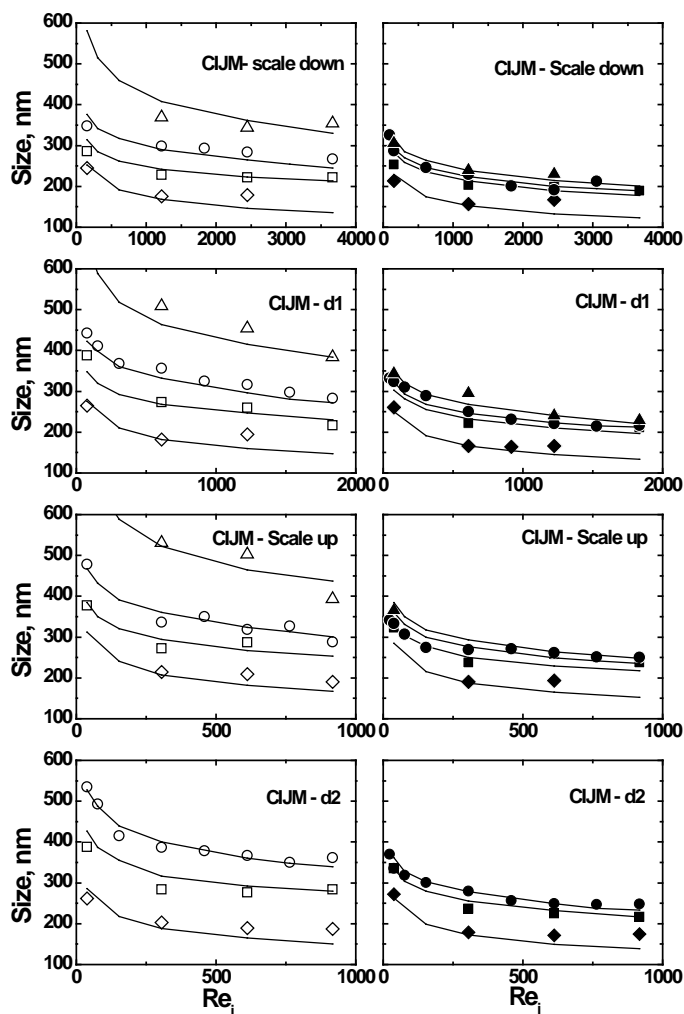


Figure 3.5. Mean particle size versus the jet Reynolds number (a) and versus flow rate (b) for nanocapsules and nanospheres obtained at four different oil-to-copolymer mass ratios, $MR = 0$ (\diamond, \blacklozenge), $MR = 0.76$ (\square, \blacksquare), $MR = 1.26$ (\circ, \bullet) and $MR = 2.37$ ($\triangle, \blacktriangle$) without quenching (left, open symbols) and with quenching (right, filled symbols) for (from top to bottom) scale down, CIJM-d1, scale up and CIJM-d2. Constant polymer concentration (6 mg/ml).

In comparison to nanospheres ($MR = 0$), where there is no oil inside, in nanocapsule the energy barrier that has to be overcome due to repulsion forces in case of aggregation seems to be lower due to the presence of the oil. Thus the

stability of the nanocapsule suspension could be related with the thickness of the copolymer wall formed. This will surely decrease if the oil-to-copolymer mass ratio is increased and in the case considered is the largest at $MR = 0.76$. Moreover, we can assume that good mixing allows more copolymer to be available for covering oily drops. In Chapter 5 the external layers of nanocapsules will be investigated by means of X-Ray photo-electron spectroscopy and some conclusions which support this hypothesis will be discussed.

In Figure 3.6 zeta potential is shown as a function of the size for nanocapsules obtained with different mixers, the flow rates and oil-to-copolymer ratios. As it is possible to see no significant differences are detectable depending on the mixers used, showing that both nanocapsules and nanospheres present the same superficial properties, in terms of Zeta potential, independently on the mixer used; small differences seem to exist between nanocapsules and nanospheres, but no significant differences are noted among nanocapsules obtained at different MR. The fact that the presence of the oil does not impact the final zeta potential value of nanocapsules could be interpreted as a proof of the fact that the oil stays inside the copolymer shell. This hypothesis is supported by preliminary experimental evidences obtained with XPS, shown in Chapter 5.

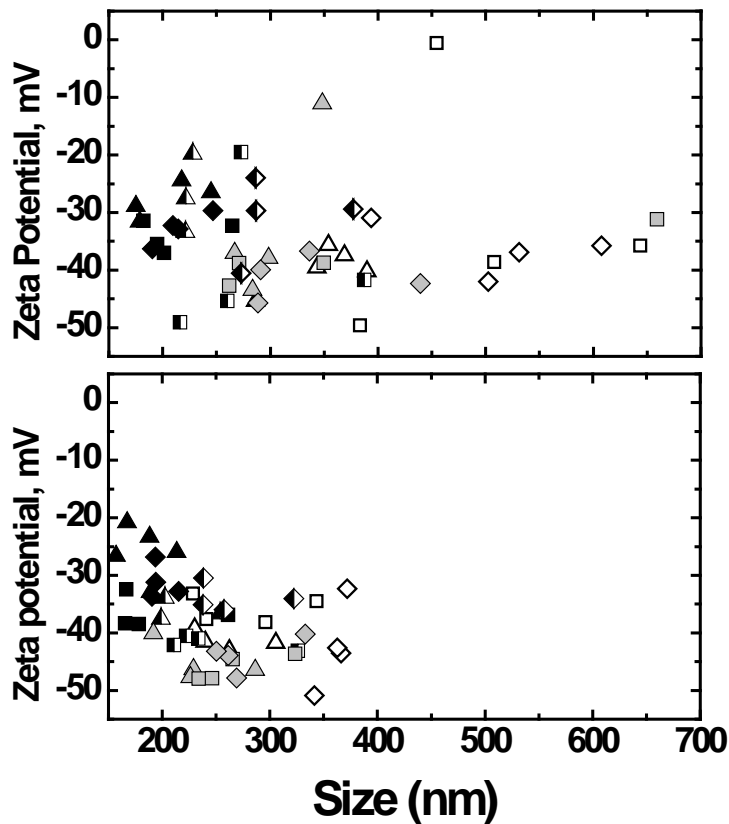


Figure 3.6. Zeta potential (mV) as a function of particle size (nm) obtained with different mixers: scale down (triangle), CIJM-d1 (square) and scale up (rhomb). Top graph: particles without quenching. Bottom graph: particles with quenching. Both nanospheres and nanocapsules are present: nanospheres (black), nanocapsules at MR = 0.76 (half black), nanocapsules at MR = 1.26 (light grey) and nanocapsules at MR = 2.37 (white).

As already reported, the copolymer concentration was also varied, keeping constant the oil concentration. Experiments were performed only in CIJM-d1 with and without quenching and all the previous trends were confirmed, as shown in Figure 3.7 where the data are plotted versus Reynolds as in previous cases. It may be noted that at low polymer concentration, the size of the nanocapsules measured becomes extremely large, and it is evident that the situation must be different from the other cases, where a proportional variation of the polymer had a relatively small effect. Probably under these conditions the polymer quantity available for the formation of the copolymer shell is too small, and the forming nanocapsules

collapse; in Table 3.2 particle size obtained at high mixing intensities are reported for each sample analysed. The sample with the lower polymer amount is oversized in comparison with the other samples, suggesting the polymer amount is not sufficient to produce nanocapsules.

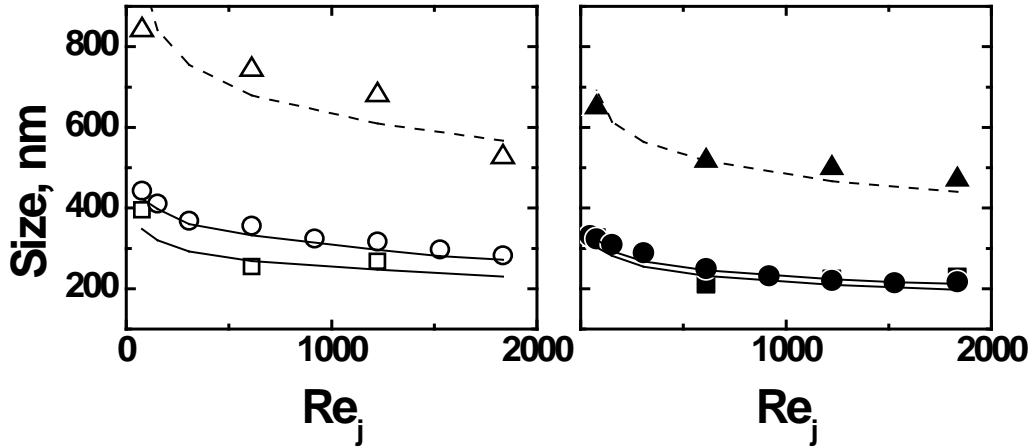


Figure 3.7. Mean particle size versus the jet Reynolds number for nanocapsules obtained at constant oil concentration (8 $\mu\text{L/ml}$) and at copolymer concentration of 10 mg/ml (MR = 0.76, \square, \blacksquare), 6 mg/ml (MR = 1.26, \circ, \bullet) and 3.2 mg/ml (MR = 2.37, \diamond, \blacklozenge) in CIJM-d1 without quenching (right, open symbols) and with quenching (right, filled symbols).

Table 3.2. Nanocapsule size obtained at Reynolds number ~ 1000 in five different samples corresponding to two different MR.

oil $\mu\text{L/ml}$	8	4.8	3.2	15	8
copolymer mg/mL	10	6	4	6	3.2
MR	0.76	0.76	0.76	2.37	2.37
Re ~ 1000 limiting size, nm	224	234	226	241	499

Figure 3.8 shows results for nanocapsules obtained with CIJM-d1 for different initial oil and copolymer concentrations, but at the same relative mass ratio to investigate the role of the total concentration of both copolymer and oil.

The results clearly show that at MR lower than one, the total concentration of polymer and oil is not important, but is their mass ratio that determines the final size, indicating that the copolymer is able to block oily drops growth by surrounding them; at higher mass ratios, results depend on the polymer concentration. In fact, at low copolymer content much larger particles are obtained, even in case of quench; the relative increase observed for non-quenched particles, then, is very relevant.

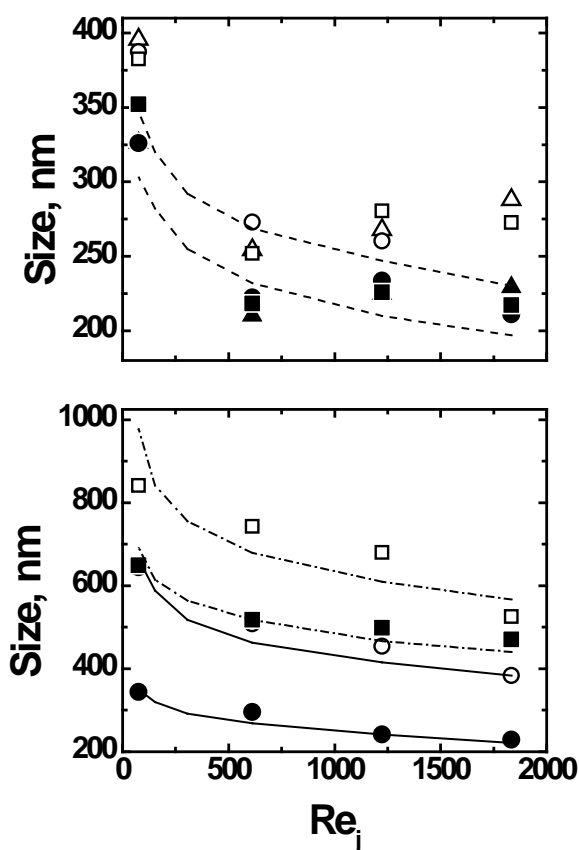


Figure 3.8. Mean particle size versus the jet Reynolds number for nanocapsules obtained with CIJM-d1 without quenching (open symbol) and with quenching (filled symbol) at two different constant oil-to-copolymer mass ratio for different copolymer and oil concentrations; upper graph: MR = 0.76 with 4 mg/ml copolymer and 3.2 μ L/ml oil (\square, \blacksquare), 6 mg/ml copolymer and 4.8 μ L/ml oil (\circ, \bullet), 10 mg/ml copolymer and 8 μ L/ml oil ($\triangle, \blacktriangle$); lower graph: MR = 2.37 with 3.2 mg/ml copolymer and 8 μ L/ml oil (\square, \blacksquare , - - -), 6 mg/ml copolymer and 15 μ L/ml oil (\circ, \bullet , - -).

As it clearly emerges, the main factor in nanocapsule formation is the relative amount between oil and copolymer: while the oil amount acts as a destabilizing factor, the copolymer amount greatly helps in preventing aggregation and coalescence.

To conclude, this second data set shows that increasing the copolymer amount, nanocapsule size decreases and probably copolymer wall thickness increases. Quenching is useful in stabilizing the system, preventing further aggregation especially when the copolymer amount is lower (and probably the copolymer wall is thinner), but below a certain polymer concentration nanocapsules of controlled size cannot be obtained; the limit conditions, that probably depend on residual polymer solubility in the liquid mixture, and on process yields, require further investigation.

3.5.Conclusions

Nanocapsules were prepared for the first time using CIJMs. The results reported in this chapter demonstrate that CIJMs can be successfully used in nanocapsule production and represent possibility route for their continuous production. These devices provide good mixing and were already used for obtaining nanoparticles of different materials. The influence of mixer geometry on nanocapsule formation will be deepen in next Chapter.

Different types of nanoparticles are now reaching the clinical trial level, therefore a continuous route for producing them with reproducible characteristics is highly desirable.

Further investigations on the properties of nanoparticles produced by this way are shown in Chapter 5.

3.6.References

Alvarez-Roman R., Barre G., Guy R.H., Fessi H., 2001, Biodegradable polymer nanocapsules containing a sunscreen agent: preparation and photoprotection. *European Journal of Pharmaceutics and Biopharmaceutics* 52, 191-195.

Ammoury N., Fessi H., Devissaguet J.P., Puisieux F., Benita S., 1990, In vitro release kinetic pattern of indomethacin from poly(D,L-Lactide) nanocapsules. *Journal of Pharmaceutical Sciences* 79, 763-767.

Fessi H., Puisieux F., Devissaguet J.Ph., Ammoury N., Benita S., 1989, Nanocapsule formation by interfacial deposition following solvent-displacement. *International Journal of Pharmaceutics* 55, R1-R4.

Gavi E., Rivautella L., Marchisio D.L., Vanni M., Barresi A.A., Baldi G., 2007, CFD modelling of nano-particle precipitation in confined impinging jet reactors. *Chemical Engineering Research & Design* 85, 735-744.

Gavi E., Marchisio D.L., Barresi A.A., 2008, On the importance of mixing for the production of nanoparticles. *Journal of Dispersion Science and Technology* 29, 548-554.

Gavi E., Marchisio D.L., Barresi A.A., Olsen M.G., Fox R.O., 2010, Turbulent precipitation in micromixers: CFD simulation and flow field validation. *Chemical Engineering Research & Design* 88, 1182-1193.

Horn D., Rieger J., 2001, Organic nanoparticles in the aqueous phase - theory, experiment, and use. *Angewandte Chemie International Editions* 40, 4330-4361.

Johnson B.K., Prud'homme R.K., 2003a, Flash NanoPrecipitation of organic actives and block copolymers using a confined impinging jets mixer. *Australian Journal of Chemistry* 56, 1021-1024.

Johnson B.K., Prud'homme R.K., 2003b, Chemical processing and micromixing in confined impinging jets. *AIChE Journal* 49, 2264-2282.

Lince F., Marchisio D.L., Barresi A.A., 2008, Strategies to control the particle size distribution of poly- ϵ -caprolactone nanoparticles for pharmaceutical applications. *Journal of Colloid and Interface Science* 322, 505-515.

Lince F., Marchisio D.L., Barresi A.A., 2009. Smart mixers and reactors for the production of pharmaceutical nanoparticles: Proof of concept. *Chemical Engineering Research & Design* 87, 543-549.

Lince F., Bolognesi S., Marchisio D.L., Stella B., Dosio F., Barresi A.A., Cattel L., 2011a, Preparation of poly(MePEGCA-co-HDCA) nanoparticles with Confined Impinging Jets Reactor: experimental and modelling study. *Journal of Pharmaceutical Sciences* 100, 2391-2405.

Lince F., Marchisio D.L., Barresi, A.A., 2011b, A comparative study for nanoparticle production with passive mixers via solvent-displacement: use of CFD models for optimization and design. *Chemical Engineering & Processing*, 50, 356-368.

Lince F., Bolognesi S., Stella B., Marchisio D.L., Dosio F., 2011c, Preparation of polymer nanoparticles loaded with doxorubicin for controlled drug delivery. *Chemical Engineering Research and Design* 89, 2410-2419.

Marchisio D.L., Rivautella L., Barresi A.A., 2006, Design and scale-up of chemical reactors for nanoparticle precipitation. *AIChE Journal* 52, 1877-1887.

Peracchia M.T., Desmaele D., Couvreur P., d'Angelo J., 1997, Synthesis of a novel poly(MePEG cyanoacrylate-co-alkyl cyanoacrylate) amphiphilic copolymer for nanoparticle technology. *Macromolecules* 30, 846-851.

Quintanar-Guerrero D., Allemann E., Fessi H., Doelker E., 1998, Preparation techniques and mechanisms of formation of biodegradable nanoparticles from preformed polymers. *Drug Development and Industrial Pharmacy* 24, 1113-1128.

Stella B., Arpicco S., Rocco F., Marsaud V., Renoir J.M., Cattel L., Couvreur P., 2007, Encapsulation of gemcitabine lipophilic derivatives into polycyanoacrylate nanospheres and nanocapsules. *International Journal of Pharmaceutics* 344, 71-77.

Vauthier C., Labarre D., Ponchel G., 2007, Design aspects of poly(alkylcyanoacrylate) nanoparticles for drug delivery. *Journal of Drug Targeting* 15, 641-663.

Zambrano-Zaragoza M. L., et al., 2011, Optimization of nanocapsules preparation by the emulsion-diffusion method for food applications. *LWT - Food Science and Technology* 44, 1362-1368.

4. Production of nanospheres and nanocapsules for pharmaceutical use: process design and scale up

4.1. Introduction

This chapter is focused on the investigation of the main engineering parameters affecting nanocapsule size, through comparison with nanospheres.

It has been shown that nanoparticle diameter depends on operating conditions, mixer characteristics and polymer concentration. Since mixing is important in nanoparticle formation, especially when fast process steps are involved, micromixers and microdevices are extensively used to precipitate nanoparticles, following the initial suggestion by Johnson and Prud'homme (2003a). Tee, Confined Impinging Jets and Vortex mixers have been tested in previous work for the production of both organic and inorganic particles, by means of reactive precipitation, solvent displacement, sol-gel process (Abkulut et al., 2009; Cheng et al., 2009; Gavi et al., 2008; Hussain et al., 2010; Johnson and Prud'homme 2003a, 2003c; Lince et al. 2008, 2009, 2011a, 2011b; Liu et al. 2009; Marchisio et al., 2006, 2008, 2009).

In this chapter, experimental results already shown in previous chapter are studied and compared with results from previous work, in order to understand which parameters affect more significantly final nanocapsule size in CIJMs. Fluid

dynamics plays an important role and the flow field and mixing dynamics have been deeply investigated, both experimentally (Johnson and Prud'homme, 2003b, Gavi et al., 2010) and through Computational Fluid Dynamics (CFD) simulations (Cheng and Fox 2010, Lince et al. 2009, 2011a, 2011b; Icardi et al., 2011; Gavi et al., 2007, 2010; Liu and Fox, 2009), confirming that both the inlet jet diameter and the mixer chamber size can influence the final particle size.

Studying in details poly- ϵ -caprolactone (PCL) nanoparticle production by flash-precipitation, design criteria applicable to polymeric nanosphere production have been defined, showing also that the complex interaction between mixing and polymer concentration can be taken into account by means of the Damkhöler number, defined as the ratio between the characteristic mixing time and the particle formation time (Lince et al., 2011a).

It has been suggested that scale up criteria in CIJMs can be based on the mixing time for both inorganic and polymeric particles and also for homogeneous competitive reactions. In a previous work mixing times in CIJ and Tee mixers of different size have been calculated by CFD (Lince et al. 2011a). A different approach was used by Johnson and Prud'homme (2003b) who studied these mixers using competitive fast reactions as a probe: the dependence of the mixing time on the operating conditions is derived from turbulent mixing theory and is correlated to characteristic geometric parameters, such as the dimensionless inter-nozzle separation ($\Delta=D_c/d_j$, where D_c is the chamber diameter and d_j is the inlet jet diameter).

The Damkhöler number, that comprises both mixing time and the characteristic particle formation time, function of the polymer concentration, gave encouraging results, allowing in particular the deep investigation to describe the performance of different devices, like Tee-mixer and CIJMs (Lince et al., 2009, 2011a). The scatter of the experimental data partially masked the eventual differences between mixers of different size and geometry, evidencing anyway a band where the size of produced nanospheres with different devices was confined; this was already a result of relevant practical interest. A deeper analysis of the data

highlights a stratification of the data obtained in different mixers, similarly to what can be observed also in the selectivity data for homogeneous competitive mixing-sensitive reactions published by Johnson and Prud'homme (2003b) in CIJMs of different size and with different Δ value. This suggests that the Damköhler number takes into account some of the phenomena, but does not describe all those occurring in the mixers. It must be also noted that generally the value of Damköhler number cannot be easily calculated for a system, and thus its use is of limited practical interest for evaluating a new device or a different polymer or reaction, even if it has been proved effective for correlating experimental data. In fact, it requires to know the kinetics of the process of interest, or at least its order; kinetic information are available for a limited number of inorganic precipitation (see Marchisio et al., 2006 for an example), but very rarely these data are known for processes occurring in the precipitation of polymeric particles by solvent-displacement. In addition, it requires the knowledge of the mixing time, that in turns depends on the geometry of the mixer and on the fluid properties. As already mentioned, in Lince et al. (2011a) CFD is used to calculate it, whereas in Johnson and Prud'homme (2003b) it is related to a constant which depends on the geometry. It can be evidenced that the previous authors always refer to the micromixing time (therefore assuming that this is the controlling phenomenon) whereas Liu and Fox (2006) propose to use the sum of micro, meso- and macro-mixing time.

The use of the Reynolds number, that allows to take into consideration size and hydrodynamics of the device has also been considered in some cases (Marchisio et al., 2006; Lince et al., 2011a), but no extensive investigation of its relevance for the production of polymeric nanoparticles has been carried out up to now.

In this chapter the size of particles obtained with different micromixers will be related to the operating conditions, and in particular to the polymer and oil initial concentration, and to the hydrodynamics conditions in the mixer, in order to find how they affect nanoparticle precipitation. Previous experiments (see Chapter 3) will be also compared with experiments carried out at non-equal solvent and anti-solvent flow rates. CIJMs are investigated in this chapter, focusing on the influence

of the scale, for apparatus with the same geometry and on the complex role of the relative size of the inlet jets with respect to the chamber diameter. The phenomena of the CIJMs will be also compared with that of other mixer geometries, in particular the Tee-mixer (TM) and Multi-inlet Vortex Mixer (MIVM), to evidence the influence of the mixing chamber and of the impinging jets. Finally, the relevance of the different dimensionless number of interest in this case will be evaluated, in order to suggest a scale up criterion that allows at least a partial similitude for this very complex process.

4.2. Materials and methods

4.2.1. Materials

Nanocapsule data which are used in this chapter are the same shown in previous chapter. Nanosphere data come from previous work already published (Lince et al., 2011a) and are all quenched. Nanocapsules measurements were performed after solvent evaporation, while nanosphere data were obtained from samples not evaporated.

Nanospheres obtained in MIVM were produced from an acetone solution of 6 mg/ml of copolymer poly(MePEGCA-co-HDCA) with the same procedure described in previous chapter and samples were analysed after solvent evaporation through Dynamic Light Scattering (DLS) with Zetasizer Nanoseries ZS (Malvern).

4.2.2. Mixers

CIJMs with scaled dimensions and different geometrical details were used. Four different mixers with conical heads were used, three scaled with the same geometry and one with larger inlet jets diameter. In the three scaled mixers $\Delta = D_c/d_j$ is 4.8 whereas in CIJM-d2 is 2.4. For comparison purposes Tee-mixer of two different size were used in producing nanospheres. Preliminary texts for the production of nanospheres and nanocapsules on vortex mixer were performed and results are here shown and compared with the performance of CIJMs. Two

geometries of MIVMs were tested: one with two inlet jet (VM-2) and another one with four inlet jets (VM-4). Geometrical details are shown in Figure 4.1 and numerical details are given in Table 4.1.

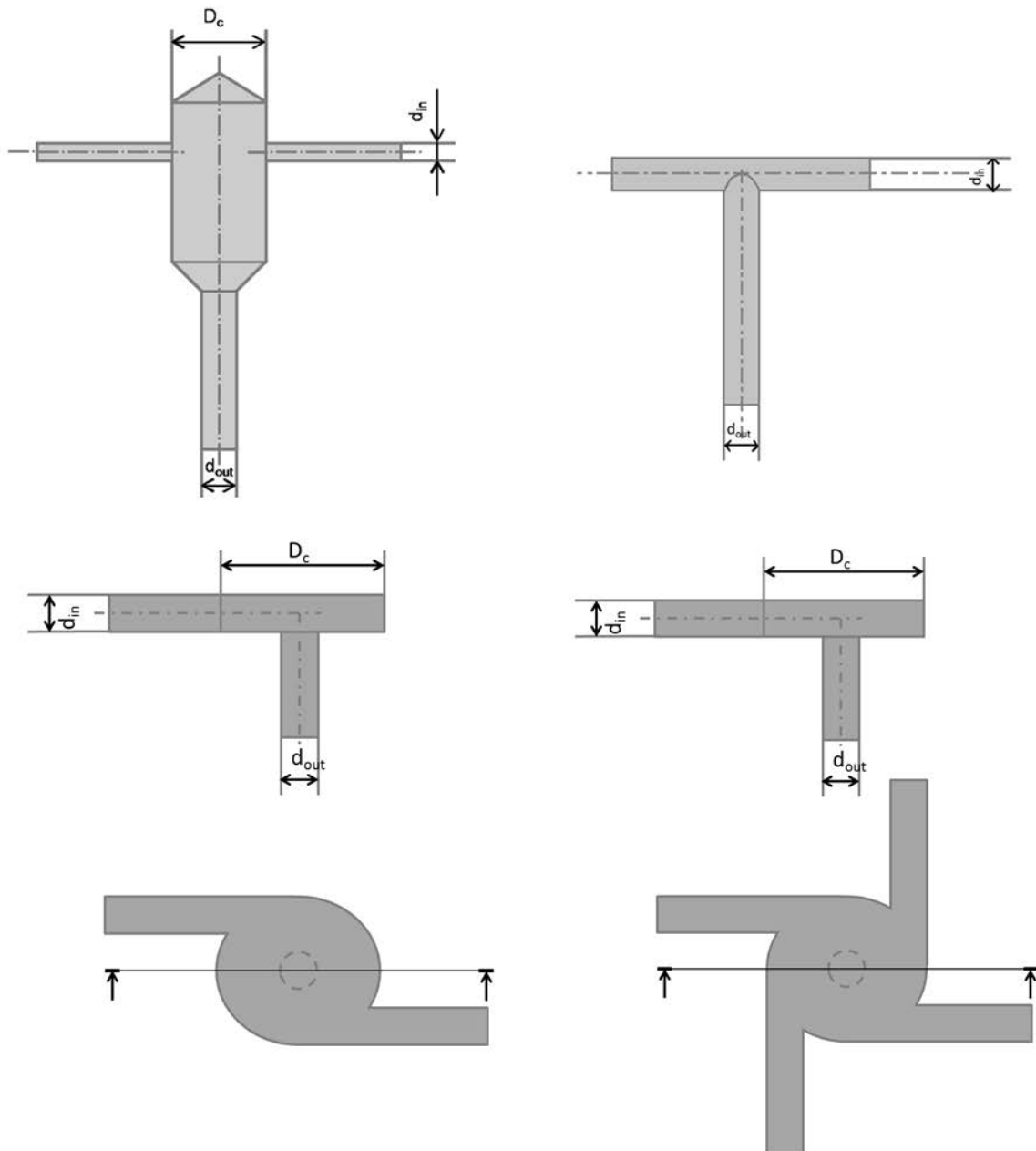


Figure 4.1. Confined Impinging Jets, Tee and Vortex Mixers: section view.

Table 4.1. CIJMs, Tee and Vortex Mixer numerical details. d_{in} is the inlet diameter, d_{out} is the outlet diameter, D_c is the chamber diameter.

Mixer	d_{in} (mm)	d_{out} (mm)	D_c
scale down	0.5	1	2.4
CIJM-d1	1	2	4.8
scale up	2	4	9.8
CIJM-d2	2	2	4.8
TM-d1	1	1	-
TM-d2	2	2	-
VM-2	1	1	4
VM-4	1	2	4

Flow rates in the range between 3 and 120 ml/min were investigated, usually with an equal flow rate of solvent and anti-solvent. A series of experiments with the water/acetone ratio (W/A) varying between 1 and 8 (obtained by reducing the acetone flow rate at constant water flow) were also considered.

4.2.3. Nanoparticle preparation

Nanospheres and nanocapsules were prepared through the solvent-displacement technique as described in previous chapter. Let me remind the way of preparation and some terms which will be used in this chapter.

The poly(MePEGCA-co-HDCA) was dissolved in acetone (solvent) together with the oil (in the case of nanocapsules) and the acetone solution was mixed with water (the antisolvent). The product was collected in an empty beaker (without quenching) or in a volume of 4 ml of water (with quenching). Nanoparticles were prepared at different oil to copolymer mass ratios, MR, corresponding to the following values: $MR = 0$ (nanospheres) and $MR = 0.76, 1.26$ and 2.37 (nanocapsules). These ratios are calculated using the mass in grams of the oil and of

the copolymer, whereas throughout the paper the oil concentration in the acetone solution is generally given $\mu\text{l}/\text{ml}$. The initial copolymer concentration in the solvent ranged from 0.7 mg/ml to 15 mg/ml. In nanocapsule production the MRs were obtained varying the copolymer from 4 mg/ml to 10 mg/ml and oil concentration from 3.2 $\mu\text{l}/\text{ml}$ to 10 $\mu\text{l}/\text{ml}$. Flow rate in the range between 3 and 120 ml/min was used, usually with an equal flow rate between solvent and anti-solvent. A series of experiments were carried out varying the water/acetone ratio (W/A) between 1 and 8, reducing the acetone flow rate.

Quenching allows to dilute the mixture out of the mixer, avoiding possible further aggregation phenomena. Some experiments were carried out without quenching in order to see and eventually determine an effect of quenching.

4.3.Results and discussion

4.3.1. Nanospheres (MR=0) in CIJMs

Figure 4.2 shows an example of the dependence of the final mean particle size on the flow rate (FR) for nanospheres obtained in CIJMs at different W/A ratios. The mean particle size here reported is the Z-average size obtained by DLS. As it is seen increasing the flow rate the mean particle size decreases. The effect of flow rate on polymeric nanospheres was extensively investigated and discussed in previous works (Lince et al. 2008, 2011b); further analysis of available unpublished data confirms that the trend is the same at every concentration and with every mixer. In fact, at higher flow rates the solvent and the antisolvent mix faster resulting in higher supersaturation levels and thus in smaller particles. Figure 4.2 also shows that, as it was already noted in previous works, at least at lower polymer concentration, for a given flow rate, when the antisolvent-to-solvent ratio is increased, the particle size increases, probably as a consequence of the lower mixing efficiency achieved; in fact, it must be reminded that W/A increases because the acetone solution feed is decreased, and thus also the turbulence intensity in the chamber is reduced. The feed flow rate influences not only the turbulence level in

the mixer (which is affected by the inlet jet velocity and thus by the inlet jet diameter) but also the residence time (which in turn is affected by the mixer volume). As it will be cleared out in the next section, the residence time has a minor role in the investigated conditions, with respect to turbulent mixing, thus data will be analysed comparing the performances at equal inlet velocity in order to have comparable turbulent conditions.

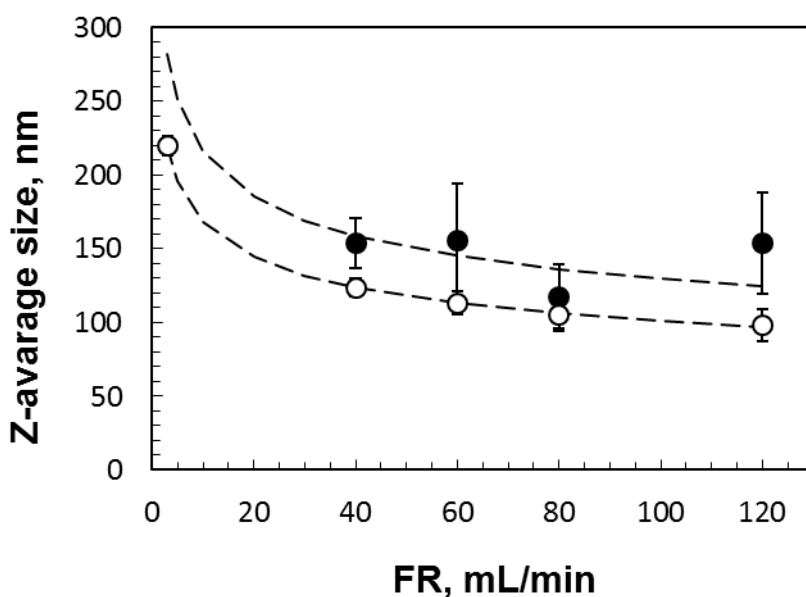


Figure 4.2. Nanosphere size dependence on solvent feed flow rate with CIJM-d1 at two different W/A ratios: ○ W/A = 1, ● W/A = 8. Inlet copolymer concentration: 2.5 mg/ml Quenched, measured after synthesis.

The influence of the inlet jet velocity is shown in Figure 4.3 at different copolymer initial concentrations: the mean size of nanospheres obtained by CIJM-d1 is compared with the average of those obtained by TM-d1; in this case the jet velocity is varied by modifying the flow rate, while the inlet diameter is kept constant (1 mm) for both the mixer geometries compared in the figure.

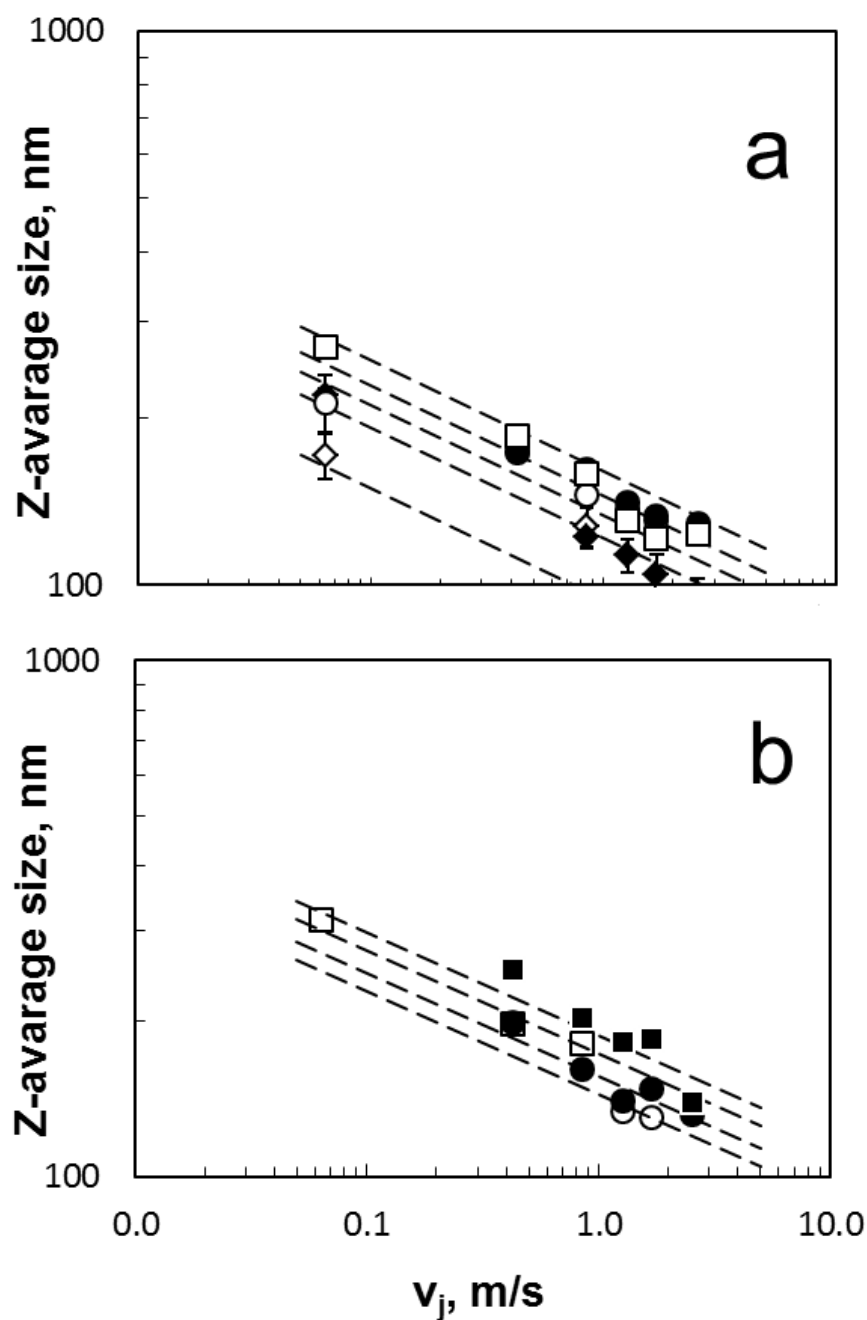


Figure 4.3. Nanosphere size dependence on average inlet jet velocity in CIJM-d1 and TM-d1 mixers at different initial copolymer concentrations. (a) CIJM-d1: 0.7 mg/ml (\diamond), 2.5 mg/ml (\blacklozenge), 4.0 mg/ml (\circ), 6 mg/ml (\bullet), 10.2 mg/ml (\square); (b) T-d1: 4.0 mg/ml (\circ), 6 mg/ml (\bullet), 10 mg/ml (\square), 15 mg/ml (\blacksquare). Quenched, measured after synthesis.

The relationship between the mean nanosphere size (d_p), the inlet jet velocity and the initial copolymer concentration (C_{pol}) seems to be well represented by the

following empirical equation for both geometries (see also Figure 4.4 that shows the dependence of the proportionally terms $A_{vj}=d_p/v_j^{0.2}$, where d_p is in nm and v_j is in m/s):

$$d_p = A_0 (C_{pol})^{0.2} (v_j)^{-0.2} \quad (1)$$

where the parameter A_0 takes the value 101.3 and 109.2 for CIJM-d1 and TM-d1 respectively. As it can be seen CIJM-d1 results to be a little bit more efficient than TM-d1 allowing the production of smaller nanoparticles, thanks to the mixing chamber which allows better mixing, as extensively discussed in Lince et al. (2011a).

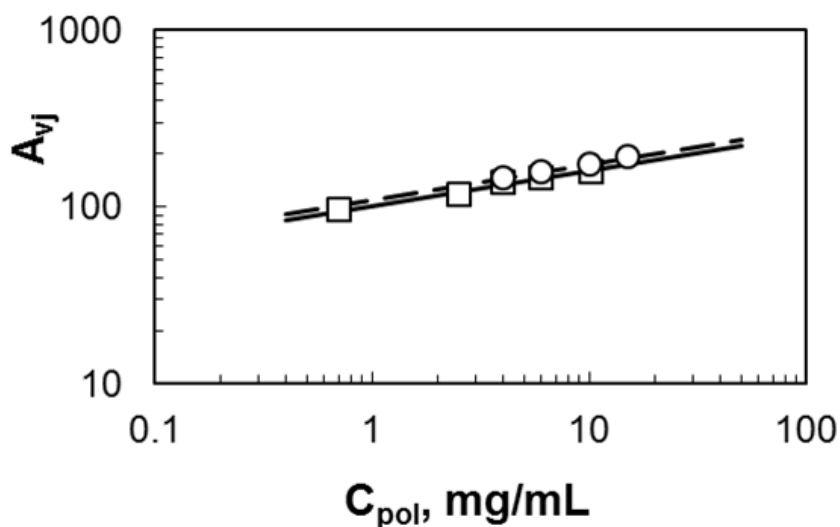


Figure 4.4. Dependence of nanosphere size on copolymer concentration in two different mixers: CIJM-d1 (\square , continuous line) and TM-d1 (\circ , dashed line). Quenched, measured after synthesis. The proportionality constant of the relationship $d_p = A_{vj} v_j^{-0.2}$ is plotted, calculated from the data shown in Figure 4.3.

The effect of the antisolvent-to-solvent ratio, W/A , on mean nanosphere size is reported in Figure 4.5 at $FR = 120$ ml/min. As already shown in Figure 4.2, modifying the relative flow rate of solvent and antisolvent, that is the W/A ratio, affects the particle size, but the trend with respect to the antisolvent (water) flow rate remains the same. It is shown that while at low polymer concentration the particle size increases slightly with W/A , at higher concentration the trend is

reversed. The different behaviour in the two cases can be due to the fact that at high polymer concentration, the attainment of supersaturation conditions is favoured by increasing the relative amount of water, as solvent dilution becomes faster, even if mixing is less effective. At low concentration, when the copolymer is already diluted in the initial solvent solution, the negative effect of increasing the mixing time predominates, reducing nucleation rate and thus causing the particle size to increase as will be discussed in the next section. CFD simulations clearly indicate the reduced mixing efficiency when the W/A ratio increases (Lince et al. 2011b). Thus the dependence of nanoparticle size on the investigated parameters can be described by the following general relationship

$$d_p = F_{pf} A_0 (W/A)^\gamma v_j^\beta C_{pol}^\alpha \quad (2)$$

α and β have already been estimated (see equation 1): $\alpha = 0.2$ and $\beta = -0.2$. A_0 depends on the mixer used and it can be considered as the size obtained at $v_j = 1$ m/s, $W/A = 1$ at a polymer concentration of 1 mg/ml. In the previous cases nanoparticle size has been measured just after synthesis, quenching them to avoid further growth; the final particle size is affected by treatment after synthesis, for example by solvent evaporation, especially if not-quenching is used.

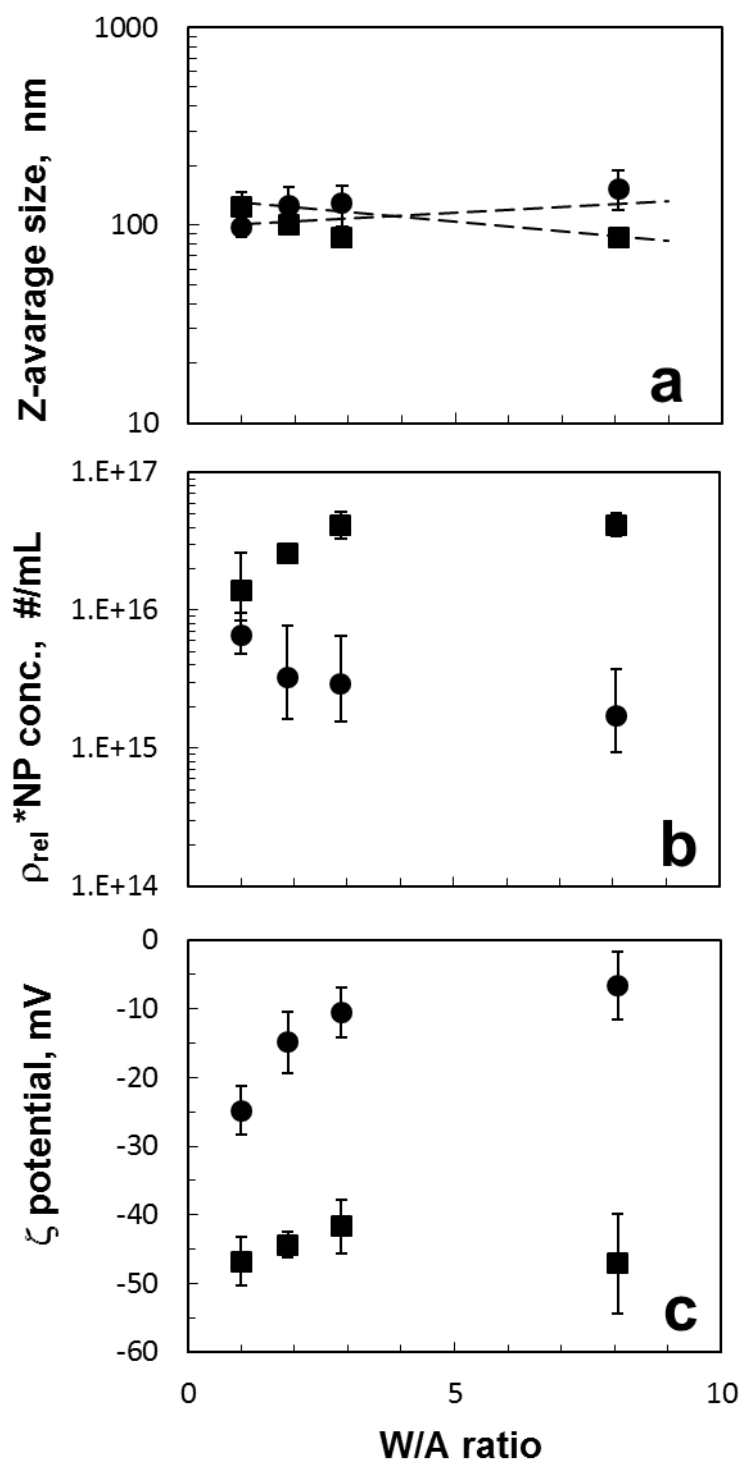


Figure 4.5. Dependence of mean nanosphere size (a), estimated number of particle formed per millilitre of solvent fed (b) and Zeta potential (c) on W/A ratio at two different initial copolymer concentrations: 2.5 mg/ml (●), 10.45 mg/ml (■). Water flow rate = 120 ml/min. Quenched, measured after synthesis.

The factor F_{pf} allows to take into account the effects of post-formation treatments on nanoparticle size, which, as said before, usually bring to an increase in particle size.

$$F_{pf} = f_q * f_{se}$$

where F_{pf} is the post formation size factor, f_q is the no quenching factor and f_{se} is the solvent evaporation size factor.

Increasing the W/A ratio forces the impinging plane to move from the central zone of the mixer, finally leading to lower mixing efficiency. In CIJMs geometries it is important the two fluids have similar momentum in order to avoid that a fraction of fluid leaves the chamber unmixed. Even with equal flow rate the mixing plane moves from the mid plane because the two fluids have different density. This fact has a limited effect; on the contrary, different flow rate causes a strong variation, as shown by previous CFD investigation, and the effect is related to the property of the solvent.

Vortex mixers can overcome CIJM limitations. In these mixers the inlet jets are tangential to a cylindrical chamber: each stream contributes to lead to micromixing in the chamber and so it is possible to operate with an inlet at higher flow rate and another one at lower flow rate. Some preliminary results on this mixers will be presented in chapter 4.3.5.

Comparing the results obtained in this work on the copolymer and previous ones on the PCL nanospheres (Lince 2010, Thesis), it can be observed that in this case the influence of the W/A ratio on final size is stronger, while the effect of the initial concentration is weaker. In principle, this will allow to improve the efficiency of the process, operating at higher concentration, but keeping small the particle size modifying the W/A ratio; for this reason, a modification of the mixing geometry that reduces the penalization caused by higher W/A ratio would be particularly advantageous.

Nanosphere size depends on competing nucleation and growth phenomena: generally an improvement of the mixing efficiency leads to smaller final particles because increases the number of particles that can grow only to a limited extent. In

order to better understand the role of the polymer initial concentration, it is necessary to separate the contributions of the two mechanism: this is difficult, but some indications can be obtained with the help of some simplifying assumptions. The factors determining final particle size are three: number of formed nuclei, available polymer amount and yield. The number of nuclei depends on nucleation velocity, i.e. on supersaturation which is a function of initial concentration and mixing and of the interaction volume where the nucleation takes place, which in turns depends on mixer geometry (the inlet jet relative size can have a role) and hydrodynamics. The total amount of polymer available for growth depends on initial concentration, volume of solvent and antisolvent and solubility limits. Yield, related to the residual supersaturation in the outlet solution, depends on residence time and growth rate (which can be eventually limited by mass transport). The relationship between particle size and described variables is thus the following

$$d_p^3 = 8\eta/\pi^*[c_{pol} V_A - c_{pol,eq} (V_A + V_W)]/(\rho_{pol} NP) \quad (3)$$

where d_p is the particle diameter, η is the yield, c_{pol} is the copolymer inlet concentration, $c_{pol,eq}$ is the equilibrium copolymer concentration in the water-acetone mixture, V_A and V_W are respectively the acetone and the water volume considered, ρ_{pol} is the copolymer density and NP is the number of particles formed.

If the number of particles formed was not influenced by the concentration, this variable would affect only growth, and for unity yield a dependence of size on $c_{pol}^{1/3}$ would be expected. The significantly lower experimental value clearly indicates that nucleation is affected by polymer concentration.

From equation 3 an estimation of the concentration of nuclei formed can be obtained. Yield is assumed to be one and residual solubility to be negligible for sake of simplicity, even though it is not so low, as shown in Chapter 2; of course these values must be regarded just as an indicative number, because are dependent on the assumptions done.

Figure 4.5b shows the influence of the W/A on the estimated nuclei concentration, confirming that at higher concentration the reduction of size is related to the increase in nucleation rate; the opposite occurs for the lower

concentrations. It can be noted that at value $W/A=1$, the nuclei concentration increases with initial polymer concentration. It is also possible to extract a relationship (at $W/A=1$) for the dependence of nuclei concentration on jet velocity and polymer concentration. From equation (3)

$$\frac{NP}{V_A} \propto \frac{c_{pol}}{d_p^3} \quad (4)$$

Plotting data at different initial polymer concentration, as a function of flow rate the dependence on v_j can be estimated: since the slope does not change with the polymer concentration, it can be calculated the dependence from c_{pol} by plotting the intercepts. The following relationship is found:

$$\frac{NP}{V_A} = v_j^{0.60} c_{pol}^{0.40} \quad (5)$$

This dependence is stronger than that observed for PCL, suggesting that the formation of nuclei is slower for the copolymer investigated in this work, thus limiting more severely the rate: an increase of the concentration has therefore a more sensible effect.

4.3.2. Nanocapsules in CIJMs

In the first set of experiments nanocapsules were prepared using three scaled CIJMs ($\Delta = 4.8$) and one at $\Delta = 2.4$ at a fixed copolymer and oil concentration (oil/polymer mass ratio $MR=1.26$ with a copolymer concentration of 6 mg/ml), to investigate the effect of the concentration. Results, as function of the jet velocity for the different mixers, are shown in Figure 4.6. Only quenched particle are taken into consideration in this first step, to highlight the influence of operating parameters. Let us remember that operating with quenching means that the mixture reaction is collected and diluted in water. With quenching nanocapsules are a little smaller and the difference between quench/no quench is influenced even by mixer geometry: the effect is complex, function also of the oil and polymer concentration, and related to more complex phenomena that requires further investigation, as discussed in Chapter 3. In all the cases shown for nanocapsules the size has been measured after

solvent evaporation. The data show that in this case the dependence on the inlet velocity is the same in the four different mixers, and (at least for quenched particles) also for the different MR values investigated: $\alpha = -0.14$.

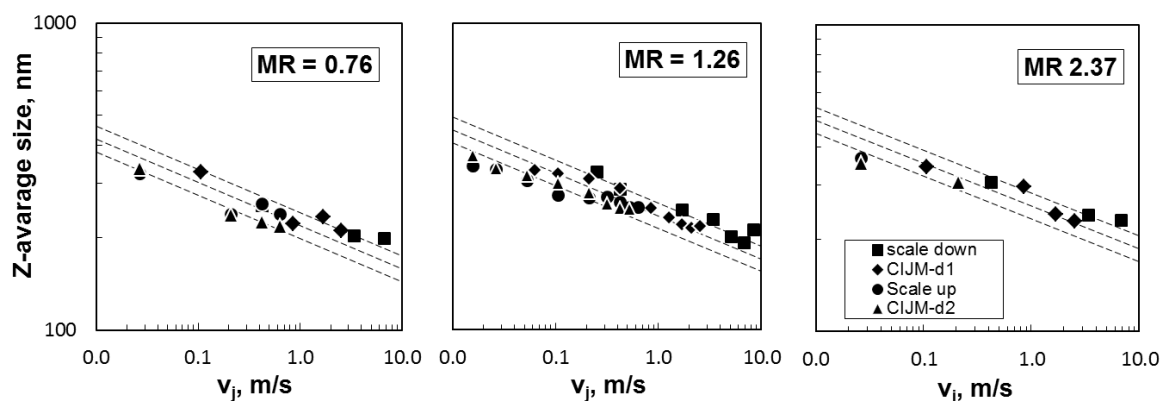


Figure 4.6. Dependence of nanocapsule size on average inlet jet velocity v_j at three different oil to polymer concentration ratio, MR: inlet copolymer concentration = 6 mg/ml, oil concentration variable. Quenched, measured after solvent evaporation. Mixers: scale down (■), CIJM-d1 (◆), scale up (●) and CIJM-d2 (▲).

The graphics show a clear dependence of particle size on mixer size for all the cases. In particular it can be noted that the performance of CIJM-scale up and CIJM-d2, which have the same inlet jet diameter (and thus the same velocity), have similar performances, independently on the chamber size. Much strong is the effect of MR on final particle size, as shown clearly in Figure 4.6. This strong effect has been confirmed also by experiments carried out varying the oil concentration.

These results confirm that, as discussed in Chapter 3, the main parameter to take into account is probably the ratio between the quantity of oil and the quantity of copolymer. It affects the final particle size and slightly also the Zeta potential, as it will be discussed later. As discussed in previous chapter, nanocapsule formation is a more complex process than nanosphere synthesis, because it involves the oily drop formation and the deposition of the polymer wall that should block coalescence phenomena. Polymer works as a stabilizer of the oily drop, and it is necessary that its amount in the solution is sufficient to cover all the oily drops.

4.3.3. Characterization

Zeta Potential

Nanospheres and nanocapsules precipitated from an initial copolymer solution of 6 mg/mL were characterized both in term of size and Zeta potential (as shown in previous chapter). The aim is to compare nanocapsule data (the same of previous chapter) and nanosphere data from previous work. Particles are considered stable if the Zeta potential is in the range between +30 mV and -30 mV: as shown in Figure 4.7 the Zeta potential is in the range -20 mV and -50 mV, but generally below -30 mV. Dashed curves on the graph group together particles at the same MR: as discussed in previous chapter the data show that there is no strong relation between either Zeta potential and size, or between Zeta potential and composition; it must also be evidenced that the scatter of the data is relatively large, even within the same set of experimental results. Figure 4.7 shows the correlation between Zeta potential and particle size for quenched nanospheres and nanocapsules (upper graph) and a comparison between quenched and not-quenched nanospheres and nanocapsules (lower graph, please note that the x-axis scale is larger than before). It can be noted a slight dependence of Zeta potential on particle size, with Zeta potential values closer to zero when particle size is smaller.

In Figure 4.5c it is shown the effect of W/A ratio on Zeta potential in nanospheres, which become bigger and less stable increasing the W/A ratio: it can be noted that more concentrated samples give nanospheres with lower Zeta potential. It can be due to the fact that in smaller nanospheres PEG chains are in the external layers, as it is expected, while increasing nanosphere size some PEG chains can be trapped inside the particle, therefore modifying the surface characteristics of the particle itself.

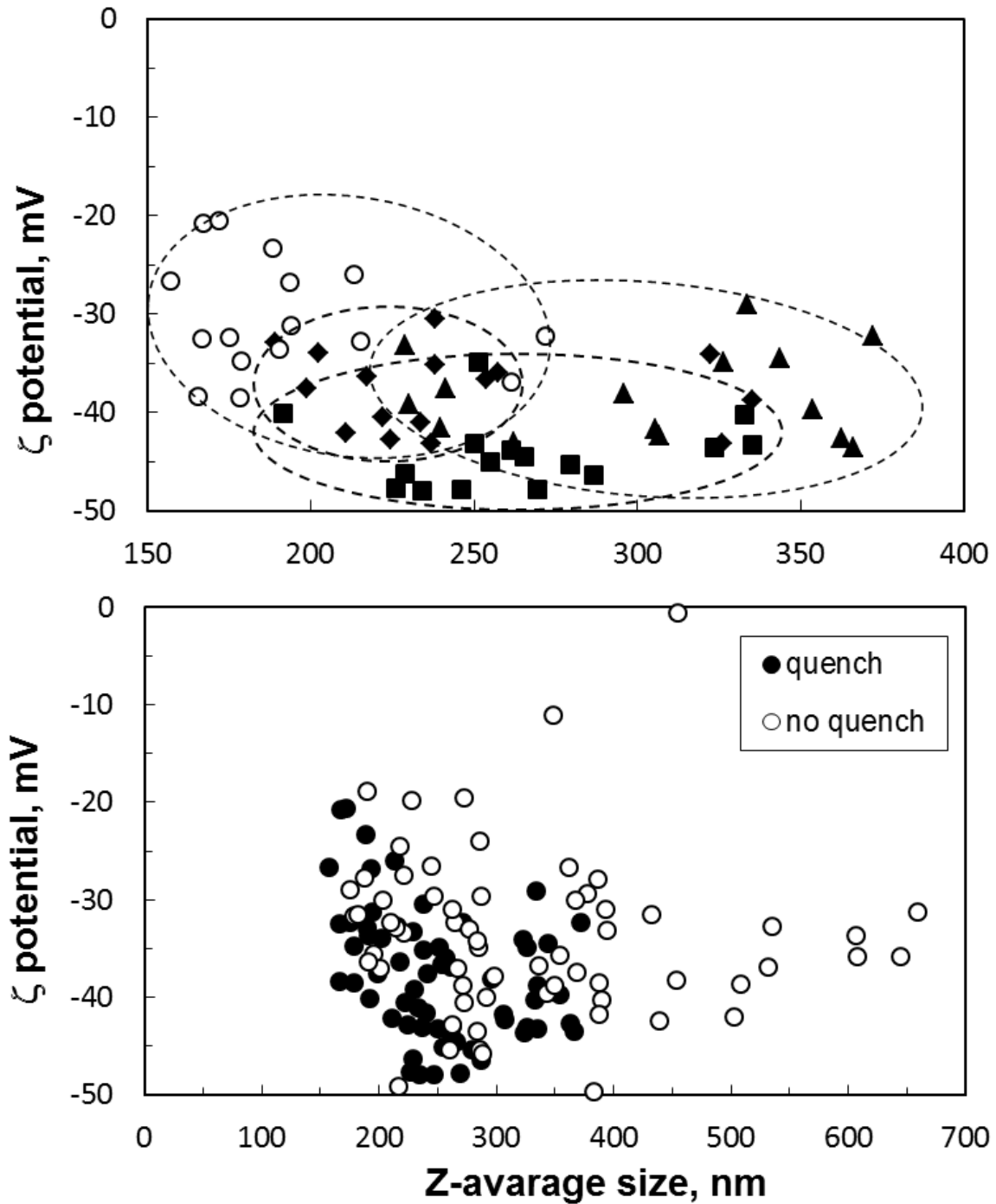


Figure 4.7. Zeta Potential - particle size relationship; data refer to nanocapsule and nanospheres produced in the four CIJ mixers at 4 different FR (5, 40, 80 and 120 ml/min), measured after solvent evaporation. Upper graph: influence of the MR for quenched nanoparticles; ○ for MR 0 (nanospheres), ◆ for MR 0.76, ■ for MR 1.26 and ▲ for MR 2.37. Lower graph: comparison of quenched and non-quenched nanoparticles.

Solvent evaporation and quenching effect

Solvent evaporation and quenching are two processes which were investigated in order to highlight their effect on final particle size. Solvent evaporation is a step required by pharmaceutical application, whereas quenching is a procedure which can help to stabilize the system.

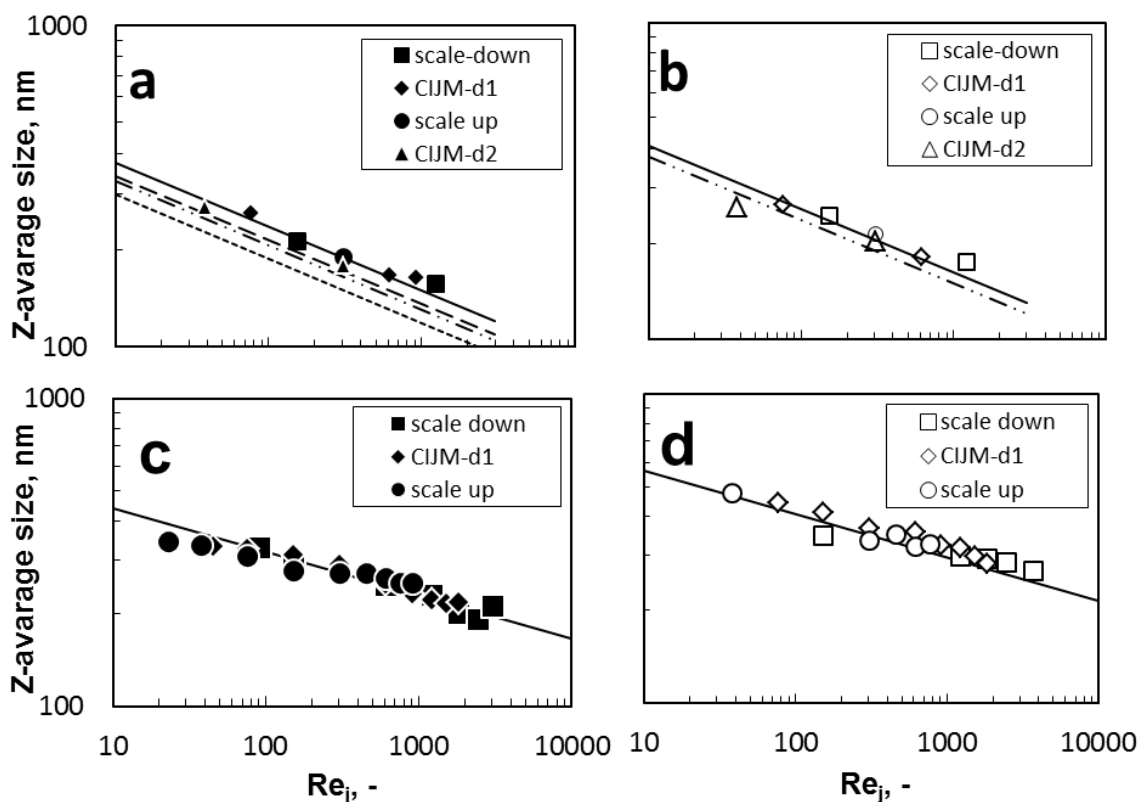


Figure 4.8. Dependence of nanospheres and nanocapsules on mixer dimension. Graph a) Nanospheres at 6 mg/ml for different mixers: line (—) approximation of CIJM-d1 data, line (---) approximation of CIJM-d2 data, line (---) approximation of CIJM-d1 data without solvent evaporation, line (---) approximation of CIJM-d2 data without solvent evaporation. Graph b) Nanospheres at 6 mg/ml for different mixers without quenching: line (—) approximation of CIJM-d1 data, line (---) approximation of CIJM-d2 data. Graph c) Nanocapsules at MR 1.26 with quenching for different mixers. Graph d) Nanocapsules at MR 1.26 without quenching for different mixers.

In Figure 4.8 both nanosphere and nanocapsule results are shown, comparing the results obtained with and without quenching. In graph a) it is also possible to see the effect of evaporation: dashed lines relates to particle size without any evaporation steps (data are not shown for sake of clarity). Nanospheres are slightly larger after solvent evaporation. The F_{pf} described in the nanosphere section is about 1.1. The effect of evaporation in nanocapsules seems to be negligible, as shown in Figure 4.9, where the variation between pre and post evaporation is practically absent.

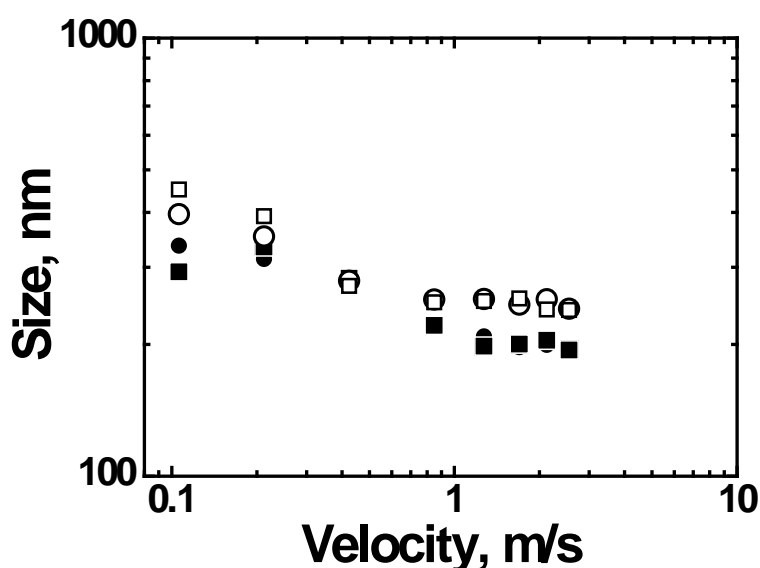


Figure 4.9. Nanoacapsule size at different flow rate, before (circle symbols) and after (square symbols) solvent evaporation. Open symbols are for not-quenched samples and filled symbols for quenched samples.

Graph 4.8b) shows the results of nanospheres obtained without quenching. The two lines show the effect of the Δ parameter on the size. Dashed line refers to CIJM-d2 data, continuous line to CIJM-d1 data. On graph c) and d) data referred to nanocapsules are shown (c) graph with quenching, (d) graph without quenching, in the case of MR=1.26. It can be noted that the slope of nanospheres and nanocapsules are different, indicating a different role of hydrodynamics, probably related to the different formation-controlling mechanism. Nanocapsule formation is a more

complex phenomena than nanospheres precipitation and results show that dependence on fluidodynamic is less strong than in nanospheres. Nanocapsules are a system with two components and their formation depends on the oily drop formation and on polymer deposition, whereas in nanospheres there is just one component and nucleation and growth steps are the two phenomena involved in their synthesis.

4.3.4. Relationships for particle size and scale up

As discussed in the introduction, the Damkhöler number (Da) has been proposed to correlate the size of polymeric nanoparticles obtained by nanoprecipitation. It has been successfully employed also for inorganic reactive precipitation and complex homogeneous reactions. Using the Damkhöler number allows to take into account mixing efficiency and process kinetics, even if it is necessary to previously evaluate the mixing time in the considered apparatus and have sufficient information on the kinetic order of the process involved.

As a first attempt the data concerning the nanospheres (obtained at different initial concentration in different mixers) have been correlated using the Damkhöler number, to verify the validity of this approach and the possibility to use Da as a scale up criterion. For this purpose Damkhöler number has been defined as

$$Da = \tau_{mix} k_p c_{pol}^{\alpha'} \quad (6)$$

assuming an α' kinetic order for the process controlling the particle formation, presumably the nucleation step; τ_{mix} , the mixing time, evaluated as the sum of micro, meso and macromixing time as suggested by Liu and Fox (2006), has been calculated by CFD as discussed in previous work (Lince et al., 2011a).

Unfortunately the value of the k_p constant is not available, but this is not a big problem if the purpose is to correlate data concerning the same polymer, as its value is incorporated in the proportionality constant. In order to keep the quantity dimensionless, the concentration has been divided by a reference concentration,

taken as unit in the same units used for the polymer concentration. Thus in the upper graph of Figure 4.10

$$Da = \tau_{mix} (c_{pol} / c_{pol,ref}) \tag{7}$$

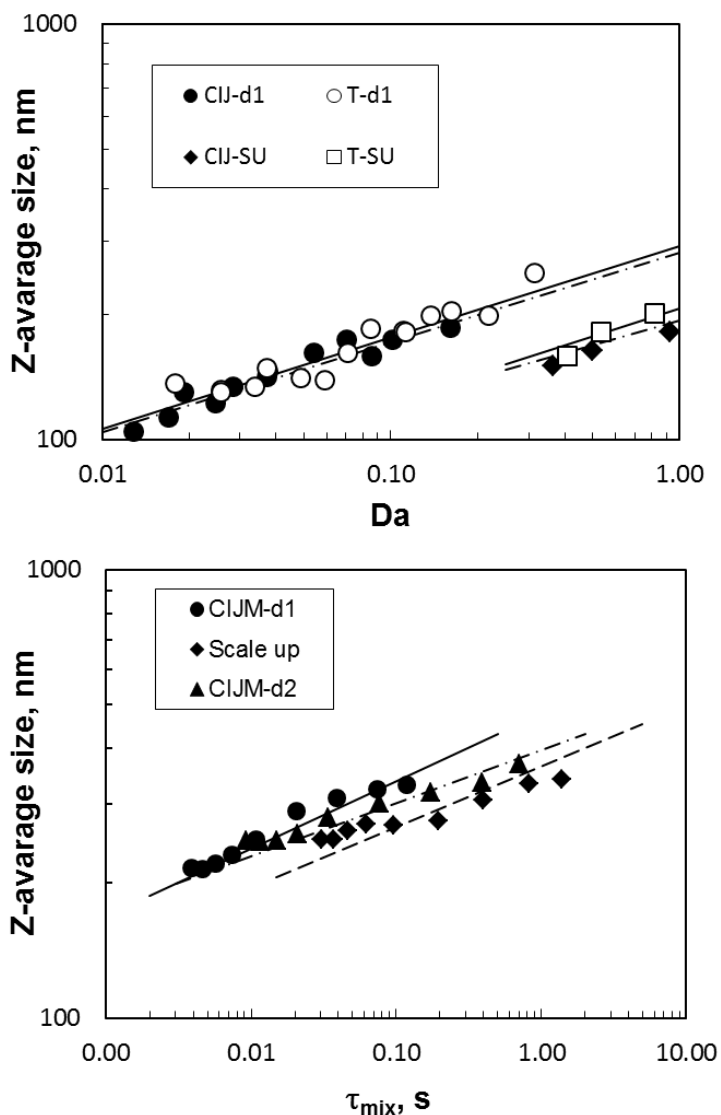


Figure 4.10. Correlation of experimental data using mixing time and Damkholer number in different mixers. Upper graphh: nanospheres, quenched, measured after synthesis, copolymer concentration in the range 2.5 -15 mg/ml (only 10 mg/ml for the scaled up mixers), flow rate in the range 20-120 ml/min. Lower graph: nanocapsules, quenched, measured after solvent evaporation, flow rate in the range 20-120 ml/min; all data at the same concentration: copolymer = 6 mg/ml, oil = 8 mg/ml.

The value of α' has been chosen as the one that gives the best correlation for the data obtained in a single mixer: it resulted to be about 0.9 for both CIJM-d1 and TM-d1. The initial concentration tested ranged from 2.50 to 10 mg/ml for CIJM-d1 and from 4 to 15 mg/ml for TM-d1. It can be noted that the quality of the correlation is quite good for both mixer and their performances are also very similar. This is just a consequence of the fact that at the same flow rate the two mixers have similar mixing time, and, as already shown in Figure 4.4, the sizes of the particles produced by them are close.

Further analysis of the data show that $d_p \propto Da^{0.22}$ for all mixers; considering that $Da \propto c_{pol}^{0.9}$, the same value $d_p \propto c_{pol}^{0.20}$ obtained by the investigation of the dependence on polymer concentration is recovered.

On the other hand it is evident that correlation *vs* Da is dependent on the size of the mixer, as it is not possible to get the different curves to collapse on a single curve even in case of perfectly geometrically similar mixers. On the same figure data referring to the scale up CIJM and Tee-mixer show what said above. For CIJM scale up and Tee-mixer scale up only data at 10 mg/ml are available and this explains the lower range shown.

In case of nanocapsules there is a further difficulty in using Da to correlate the data, because it is not clear which is its kinetic expression. Limits of this approach are shown plotting the data versus the mixing time; data set is at the same copolymer and oil concentration, thus data are comparable and conclusions are valid. In this case three CIJMs are compared, differing for the size or for the relative dimensions of the inlets. Figure 4.10 (lower graph) shows that three different curves are obtained for the three mixers (also the slope is different in this case). Thus it is confirmed that Damkhöler accounts for interaction of hydrodynamics and fast process kinetics, but it is not useful for scale up, and mixing time itself does not allow to account for small differences in the geometry of the mixers.

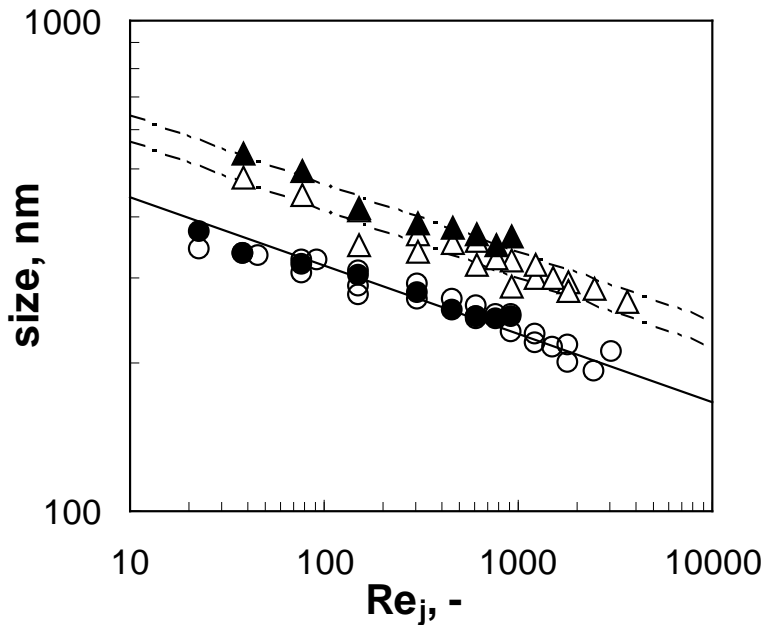


Figure 4.11. Dependence of nanocapsule average diameter on CIJ mixer geometry (chamber to inlet jet diameter ratio); inlet copolymer concentration = 6 mg/ml, MR = 1.26, $D_c/d_j = 4.8$ (open symbols) and $D_c/d_j = 2.4$ (filled symbols) are compared. Circles are for quenched samples and triangles are for non-quenched samples; measured after solvent evaporation.

It can be noted that in the range of operating conditions considered the mixing time, evaluated from CFD simulations, shows a weaker dependence on jet velocity than the one predicted by the correlation proposed by Johnson and Prud'homme. (2003b), who took into account micromixing time. In this case micromixing time gives a smaller contribution to the total mixing time, which in turns shows a dependence on jet velocity close to -1 or slightly higher (but always lower than -3/2); it can be noted that in our case two liquids with different properties are mixed while Johnson and Prud'homme considered aqueous solutions. In any case the conclusions do not change even considering only the micromixing time.

In order to highlight the potentially relevant dimensionless number a dimensional analysis has been carried out. It is clear that as the formation of nanoparticles is very complex, with different mechanisms potentially contributing, it may be necessary to take into account several of them.

In nanosphere formation, two are the main steps involved: nucleation and growth. After nucleation, which depends mainly on the mixing efficiency, growth step depends on the residual supersaturation, on transport resistances and on residence time. In nanocapsule formation there is firstly the oily drop formation, followed by the polymer deposition around it, with eventually successive breakage or coalescence and wall growth.

It is also well known that in reactive systems, or in systems where complex particle formation mechanism occurs, as in this case, a perfect similitude of geometrical, hydrodynamic and kinetic factors is never possible. For reliable scale up, based on what is defined approximate similitude or partial modeling, it is important to find out which are the most important dimensionless numbers. This is just the aim of this work.

In dimensional analysis plays a fundamental role the choice of the variables which are considered influent in the overall process.

For the nanospheres it can be assumed that

$$d_p \propto K d_j^a v_j^b D_c^c \rho^d \mu^e k_p^f c_{pol}^g k_G^h \tau_{mix}^k \quad (8)$$

thus considering relevant the geometric size of inlet jets, d_j , and chamber diameter (as parameter which takes into account the volume of the mixing chamber), D_c , average fluid density, ρ , and viscosity, μ , the polymer inlet concentration, c_{pol} , and the kinetic constant relative to particle formation (nucleation), k_p and particle growth, k_G . The final conclusion does not change if a fractional kinetic order is considered, as before, that is $r_{nucl} = k_p c_{pol}^{\alpha}$, but this adds a parameter that must be known. In addition also a quantity related to the turbulent energy dissipation in the mixer is included; this is essential to take into account the micromixing time. The average energy input could have been considered, for example including the pressure drop in the mixer, but for simplicity the mixing time has been taken into account (alternatively the eddy-break up time, proportional to k_t/ε was a good choice).

The dimensionless numbers that come out are the geometric parameter $\Delta = D_c/d_j$, the Reynolds number $(\rho v_j d_j)/\mu$ (or alternatively Re_c based on D_c), the

Damkhöler number based on nucleation characteristic time ($\tau_{\text{mix}} k_p c_{\text{pol}}^{\omega}$), the ratio of the characteristic time of nucleation and growth, and the group $(k_G c_{\text{pol}})/v_j$ that can be considered a second Damkhöler number based on growth time and residence time (which is inversely proportional to the inlet velocity).

For the nanocapsules also the oil concentration must be considered; this leads to an additional dimensionless number, that is the ratio of the characteristic time of oil drop formation and polymer film formation. In case the kinetic order of two processes is the same, it reduces to concentration ratio (or MR, already discussed).

A similitude analysis leads to the same conclusions.

It has already been shown that for nanospheres the final size depends on v_j and initial polymer concentration. In the following, results shown in Figure 4.8 and Figure 4.11 will confirm that Re_j is the parameters that allows scale up (together with Da , that is related to the concentration); the geometrical ratio D_c/d_j is also relevant. The other Da based on residence time and growth seems to play a minor role in the cases considered.

For nanocapsules, MR comes out to be the other most important parameter (see Figure 4.12), thus suggesting that Re_j and the ratio of the two characteristic time of oil drop and polymer film formation are the most relevant dimensionless numbers. Thus in this case it is the interaction of the two demixing processes to control phenomena, and not the interaction between nucleation and turbulence.

In Figure 4.8a and Figure 4.8b results for nanospheres are shown. Data obtained at the same concentration with different geometrically similar mixers can be related by Reynolds number with a slope -0.2. In the case of CIJM-d2 having a different Δ values, a different curve is obtained. It can be noted that respectively at the same jet velocity, smaller particles are obtained passing progressively from CIJM-d1 to CIJM scale up and to CIJM-d2. Thus a larger interaction zone of the two streams seems favourable. In nanocapsule formation (Figure 4.8c and Figure 4.8d) the slope is lower than in nanospheres, as discussed before.

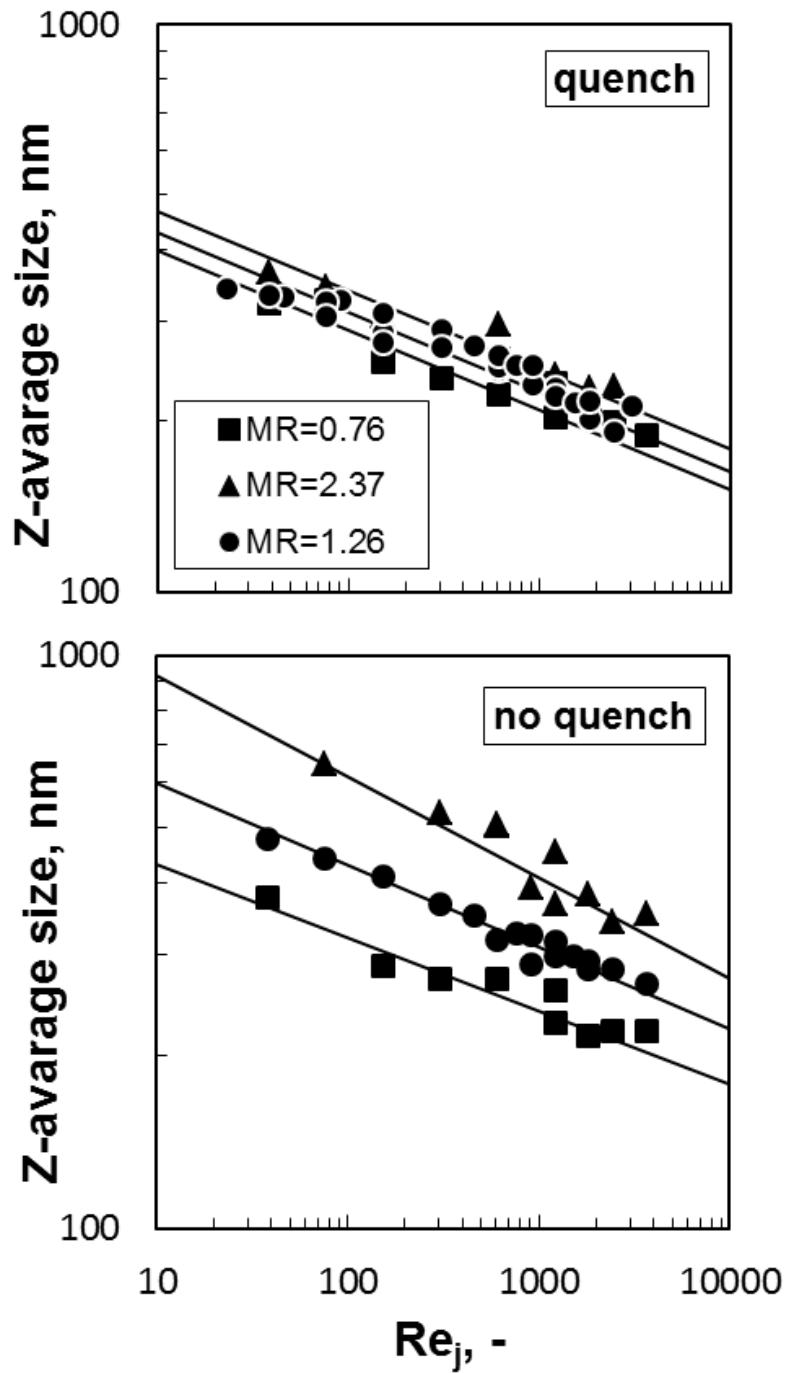


Figure 4.12. Dependence of nanocapsule size on copolymer/oil MR; copolymer concentration hold constant, 6 mg/ml. Upper graph: with quench; the data refer to the four CIJ mixers, including CIJ-d2. Bottom graph without quench: the data refer to the three scaled CIJ mixers only.

In Figure 4.11 all nanocapsule data obtained at MR=1.26 in the different CIJMs are reported as a function of Reynolds number. Nanocapsules obtained without quench are 30% bigger than the quenched ones. The ratio D/d_j influences final size only in case of not quenched nanocapsules. That can be due to the fact that when D/d_j decreases, mixing efficiency decreases as CFD simulations show (Lince et al. 2011a) and reaction volume is no more completely contained in the mixer volume. It is probably that particles continue to grow outside the mixer, when not quenched with water, and data show that these increasing is higher with CIJM-d2, maybe due to less efficient mixing.

The effect of MR is shown in Figure 4.12. The two proposed relationships for nanospheres and for nanocapsules are reported here:

$$(NS) d_p = d_{0NS} \text{Re}^\beta (c_{pol})^\alpha \quad (9)$$

$$(NC) d_p = d_{0NS} \text{Re}^\beta (MR)^\varepsilon \quad (10)$$

where α is 0.20 (as discussed before) and ε is -0.14 for quenched samples (calculated from non-linear regression of experimental data).

In Figure 4.13 the effect of the total concentration in nanocapsule samples is shown. Nanocapsules at MR=0.76 were obtained changing the concentration of copolymer and of oil (values are reported in the caption of the figure). The total concentration does not affect significantly the final size, confirming that what it is important is the MR between the two components, and not the total component amount. This is true if the concentration of the polymer is sufficiently high (that is MR not much higher than 1). Data obtained at MR>2 show that very large increases can occur, but this is probably related to the coalescence of the droplet not considered here.

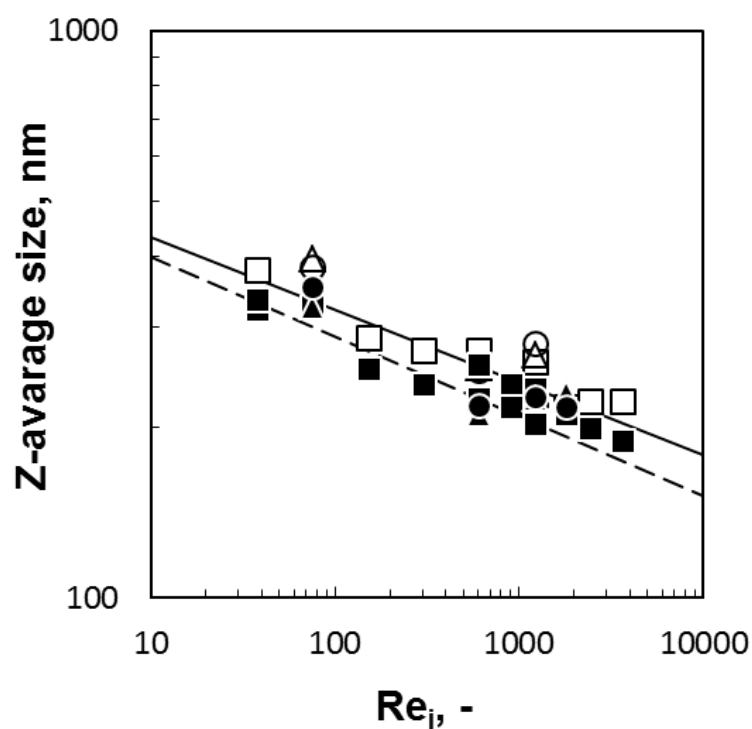


Figure 4.13. Dependence of nanocapsule size on oil and copolymer inlet concentration, at constant concentration ratio ($MR = 0.76$): 6 mg/ml and 4.8 $\mu\text{L/ml}$ (square symbol), 10 mg/ml and 8 $\mu\text{L/ml}$ (triangle symbol), 4 mg/ml and 3.2 $\mu\text{L/ml}$ (circle symbol). Filled symbols, quenched; open symbols, not quenched. CIJ mixers; measured after solvent evaporation.

4.3.5. Vortex mixers

As a final consideration, it can be reminded that, as shown in the nanosphere section, it is possible to operate at different W/A ratio. This possibility can be desirable in case the formulation becomes more complex or need a different feeding of the chemical components in the solutions. What CFD simulations show and what our experimental results confirm, is that in CIJMs a $W/A \neq 1$ affects mixing efficiency, resulting in a worst result. In principle, vortex mixer allows to overcome these limitations, since mixing efficiency does not depends on the two momenta of the fluids, so that it is possible to vary the W/A ratio without affecting mixing efficiency. Preliminary text in a vortex mixer with two and four inlet jets confirms that MIVM can be competitive with CIJMs in nanoprecipitation processes. Nanospheres were produced in VM-2 and VM-4 and results are shown in Figure

4.13a. Different connections have been tested and results show there are no significant differences working with different connections while VM-2 looks to have a better performance than VM-4. In Figure 4.13b nanosphere size obtained in alternated VM-4 at different W/A ratios is shown. Unlike CIJMs, VMs used with W/A ratio >1 gives better results than working at $W/A=1$, as expected from the way the two jets mix in the chamber in the two different systems.

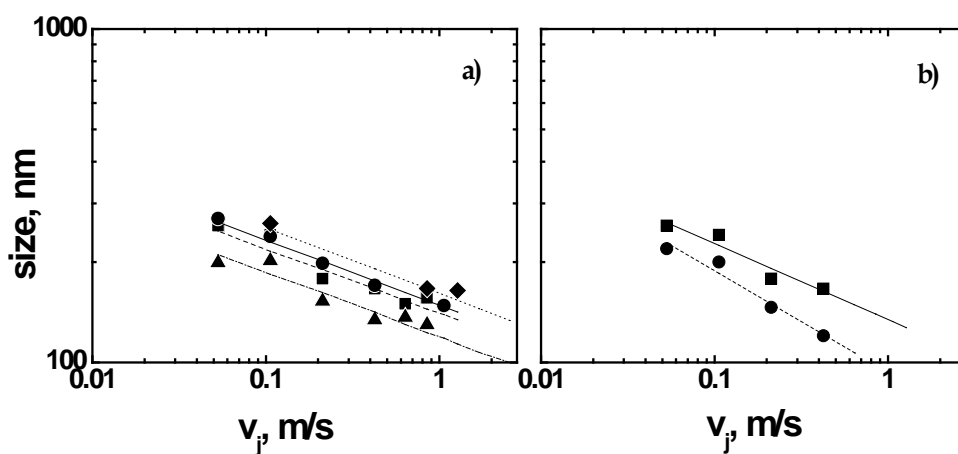


Figure 4.14. Nanospheres from polymer concentration of 6 mg/ml. a) Comparison of CIJM-d1 and Vortex mixer at different inlet feeding for the production of nanospheres: CIJM-d1 (\blacklozenge), VM-2 (\blacktriangle), VM-4 with alternated connexions (\blacksquare) and VM-4 with adjacent connexions (\bullet). Polymer concentration = 6 mg/ml; quenched, measured after solvent evaporation. b) Comparison between alternated VM-4 at $W/A=1$ (\blacksquare) and at $W/A=2$ (\bullet).

4.4. Conclusions

Results obtained in nanospheres and nanocapsules precipitation in CIJMs show that Damkhöler and Reynolds number can be used to relate particle size at different conditions, like initial copolymer concentration and flow rate. The effect of after-synthesis processes has also been investigated, in order to highlight that requested treatments or particular conditions can affect the final nanoparticle size. The use of quenching reduces nanoparticle size and allow to obtain nanospheres and nanocapsules in a reproducible way. Reproducibility is very important in

industry and must be reminded that the use of devices that allow continuous processes is very favourable in this respect.

Data obtained by different mixers can be related through Reynolds number. In nanospheres the dependence on fluidodynamic is stronger than in nanocapsule formation, where phenomena involved are not well understood as in nanosphere precipitation. Mixing chamber and inlet jet diameter influence are here investigated: their effect in nanocapsule formation is still not well completely cleared out, but data show that at the same inlet jet velocity a bigger inlet diameter give better results, while the opposite is true in nanosphere precipitation. Inlet velocity remains an important parameter in affecting final particle size, but in nanocapsules the final result is a combination of different factors.

Preliminary investigation on vortex mixer gives new prospective on the production of nanoparticles through micromixers. Mixing efficiency is reached without an impinging plane and vortex mixer offer more possibilities of combination to mix liquids, providing more interesting prospective in this field of investigation.

The current analysis can be extended to different polymers and solvent, allowing to gather information on relative velocity of the different involved phenomena, allowing to compare kinetics from different polymers.

4.5.References

Akbulut M., Ginart P., Gindy M.E., Theriault C., Chin K.H., Soboyejo W., Prud'homme R.K., 2009. Generic method of preparing multifunctional fluorescent nanoparticles using flash nanoprecipitation, *Advanced Functional Materials* 19, 718-725.

Cheng J.C., Olsen M.G., Fox R.O., 2009. A microscale multi-inlet vortex nanoprecipitation reactor: Turbulence measurement and simulation. *Applied Physics Letters* 94, 204104.

Cheng J.C., Fox R.O., 2010. Kinetic modelling of nanoprecipitation using CFD coupled with a population balance. *Industrial and Engineering Chemistry Research* 49, 10651-10662.

Fessi H., Puisieux F., Devissaguet J.P., 1989. Nanocapsule formation by interfacial polymer deposition following solvent displacement, *International Journal of Pharmaceutics* 55, R1-R4.

Gavi E., Marchisio D.L., Barresi A.A., 2007, CFD modeling and scale up of Confined Impinging Jets Reactor, *Chemical Engineering Science* 62, 2228-2241.

Gavi E., Marchisio D.L., Barresi A.A., 2008, On the importance of mixing for the production of nanoparticles, *Journal of Dispersion Science and Technology* 29 (4), 548-554.

Gavi E., Marchisio D.L., Barresi A.A., Olsen M.G., Fox R.O., 2010, Turbulent precipitation in micromixers: CFD simulation and flow field validation, *Chemical Engineering Research & Design* 88, 1182-1193.

Gradl J., Schwarzer H.C., Schwertfirm F., Manhart M., Peukert W., 2006. Precipitation of nanoparticles in a T-mixer: Coupling the particle population dynamics with hydrodynamics through direct numerical simulation. *Chemical Engineering and Processes* 45, 908–916.

Hussain M., Ceccarelli R., Marchisio D.L., Fino D., Russo N., Geobaldo F., 2010, Synthesis, characterization, and photocatalytic application of novel TiO₂ nanoparticles, *Chemical Engineering Journal* Vol. 157(1), 45-51.

Icardi M., Gavi E., Marchisio D.L., Barresi A.A., Olsen M.G., Fox R.O., Lakehal D., 2011, Investigation of the flow field in a three dimensional Confined Impinging Jets Reactor by means of microPIV and DNS, *Chemical Engineering Journal* 166, 294-305.

Johnson B.K., Prud'homme R.K., 2003a. Flash NanoPrecipitation of organic actives and block copolymers using a confined impinging jets mixer. *Australian Journal of Chemistry* 56, 1021-1024.

Johnson B.K., Prud'homme R.K., 2003b. Chemical processing and micromixing in confined impinging jets. *AIChE Journal* 49, 2264-2282.

Johnson B.K., Prud'homme R.K., 2003c, Mechanism for rapid self-assembly of block copolymer nanoparticles, *Physical Review Letters* 91 1183021.

Lince F., Marchisio D.L., Barresi A.A., 2008, Strategies to control the particle size distribution of poly-ε-Caprolactone nanoparticles for pharmaceutical applications, *Journal of Colloid and Interface Science* 332 (2), 505-515.

Lince F., Marchisio D.L., Barresi A.A., 2009. Smart mixers and reactors for the production of pharmaceutical nanoparticles: Proof of concept. *Chemical Engineering Research & Design* 87, 543-549.

Lince F., 2010. Preparation and characterization of polymeric nanoparticles for pharmaceutical applications. PhD Thesis.

Lince F., Marchisio D.L., Barresi A.A. 2011a. A comparative study for nanoparticle production with passive mixers via solvent-displacement: Use of CFD models for optimization and design. *Chemical Engineering and Processing* 50, 356-368.

Lince F., Bolognesi S., Marchisio D.L., Stella B., Dosio F., Barresi A.A., Cattel L., 2011b. Preparation of poly(MePEGCA-co-HDCA) nanoparticles with Confined Impinging Jets Reactor: experimental and modeling study. *Journal of Pharmaceutical Science* 100, 2391-2405.

Liu Y. and Fox R.O., 2006, CFD predictions for chemical processing in a Confined Impinging-Jets Reactor. *AICHE Journal* 52, 1877-1887.

Liu Y., Olsen M.G., Fox R.O., 2009. Turbulence in a microscale planar confined impinging-jets reactor. *Lab on a Chip* 9, 1110-1118.

Marchisio D.L., Rivautella L., Barresi A.A., 2006, Design and scale-up of chemical reactors for nanoparticle precipitation., *AICHE Journal* 52 (5), 1877- 1887.

Marchisio D.L., Omegna F., Barresi A.A., Bowen P., 2008, Effect of mixing and other operating parameters in sol-gel processes, *Industrial & Engineering Chemistry Research* 47 (19), 7202-7210.

Marchisio D.L, Omega F., Barresi A.A., 2009, Production of TiO₂ nanoparticles with controlled characteristics by means of a Vortex Reactor, *Chemical Engineering Journal* 146 (3), 456-465.

Peracchia M.T., Vauthier C., Desmaele D., Gulik A., Dedieu J.C., Demoy M., d'Angelo J., Couvreur P. 1998. Pegylated nanoparticles from a novel methoxypolyethylene glycol cyanoacrylate hexadecyl cyanoacrylate amphiphilic copolymer. *Pharmaceutical Research* 15, 550-556.

Vauthier C., Labarre D., Ponchel G. 2007. Design aspects of poly(alkylcyanoacrylate) nanoparticles for drug delivery. *Journal of Drug Targeting* 15, 641-663.

5. Nanoparticle advanced characterization

5.1. Introduction

Nanospheres and nanocapsules were characterized in terms of their morphological aspects. Transmission electron microscopy (TEM) is a common technique used for this purpose for the high resolution it can reach. TEM uses a beam of electrons which pass through an ultra thin specimen and returns back an image formed from the interaction of the electrons with the specimen. The high resolution is due to the small de Broglie wavelength of electrons, which enables to detect fine details. TEM investigations were performed to confirm particle formation, as well as their size and their shape, and in order to gain more information about our product, such as surface morphology and copolymer behaviour in nanoprecipitation process. Scanning electron microscopy (SEM) was also used in a first attempt to characterize both nanospheres and nanocapsules, but it was successful only with nanospheres.

X-ray photoelectron spectroscopy (XPS) is a quantitative technique which measures elemental composition of a material. It irradiates the sample with a beam of X-rays while simultaneously measuring the kinetic energy and number of electrons escaping from the sample.

It has been known for a long time that the XPS analysis provides semi-quantitative information about the atomic percentage of elements in close

proximity to the surface, and that the chemical bonds between the elements of a polymeric material compound can be studied thoroughly.

The purpose of the characterization by XPS was to investigate the effectiveness of angle resolved XPS analyses, as well in depth profiles, for the estimation of the thickness of the nanocapsule walls.

5.2. Materials and methods

5.2.1. Materials and operating conditions

Nanospheres were prepared from an acetone solution of copolymer with an initial concentration of 6 mg/ml by using CIJM-d1. Only not quenched nanospheres were analysed with XPS, whereas quenched and not quenched ones were observed by TEM and SEM.

Nanocapsules were produced from an acetone solution of copolymer with an initial concentration of 6 mg/ml and with 8 μ l/ml (MR = 1.26) by CIJM-d1 with and without quenching. In order to study wall characteristics of nanocapsules, also nanocapsules at MR 0.76 (6 mg/ml and 4.8 μ l/ml) and 2.37 (6 mg/ml and 15 μ l/ml) were produced. The procedure is the one described in Chapter 3.3.

All the samples characterized by XPS and TEM were produced using a flow rate of 120 ml/min.

5.2.2. Preparation for XPS analysis

A drop of polymeric nanosphere and nanocapsule suspension was deposited on a Silicon substrate for the XPS analyses.

One can suppose safely that the substrate do not affect the investigations of the nanospheres and nanocapsules since the Silicon peaks have different binding energies with respect to those of the polymer elements.

The drop of polymeric material, deposited on Silicon substrate, was dried for one day in an dryer and, after this procedure, it remained for 12 hours in the XPS

pre-chamber, under vacuum conditions, in order to outgas all the volatile components of the polymer before XPS analyses were undertaken.

Initially, a SXI (secondary X-ray generated image) in situ analysis was performed, in order to have an overview of the sample surface and to carry out the analysis on a homogeneous area.

5.2.3. Preparation for TEM analysis

TEM observations were performed according to two different preparation methods. The first one consisted on a negative fixation which allows the imaging of thinly spread particulate material by surrounding it with a heavy metal-containing salt solution. The differential electron scattering by the heavy metal stain versus the lower atomic mass content of the polymeric material generates reverse-contrast negative electron images (e.g. nanospheres/nanocapsules should appear as white particles surrounded by dark areas). Specifically for the negative staining, a phosphotungstid acid (PTA) solution 4% was prepared with 4 g of PTA and 96 g of milliQ water (solution A). Staining solution was prepared by diluting solution A with ethanol 100% in a proportion 1 to 4 and added to the aqueous nanosphere/nanocapsule suspension. A drop of the final mixture was deposited on a copper grid covered by a carbon film and dried at ambient temperature before observation.

“Positive” images (e.g. nanocapsules appear dark and the surroundings are bright) were obtained from the second preparation method. In this case, a drop of the particulate suspension was directly deposited on the film grid and observed after drying. The contrast is lower than in the negativated samples, but the specimen thickness becomes smaller and consequently more details become visible. Shadowing with Pt/C at an angle of 15° was in some cases performed in order to observe surface details and to get information on thickness of the specimen. A schematic representation of this sample preparation is shown in Figure 5.1.

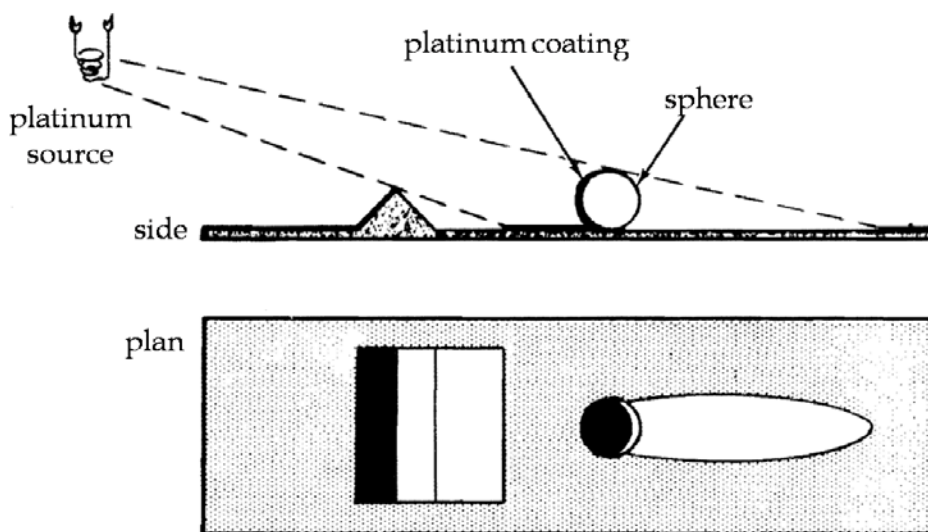


Figure 5.1. Schematic representation of shadowing with platinum. According to the angle the metal hits the surface, there will be an area not covered close to the particle, forming the “shadow” of the particle.

5.2.4. Characterization

X-ray Photoelectron Spectroscopy

The X-ray Photoelectron Spectroscopy is a VersaProbe5000 (Physical Electronics) Scanning ESCA Microprobe, with a monochromatic X-ray beam, Al source (1486.6 eV). The instrument calibration is performed by matching the literature binding energy values of Au 4f_{7/2}, Cu 2p_{3/2} and Ag 3d_{5/2} peaks (Powell, 1995).

Data (counts of photoelectrons emitted for second, versus energy binding) were acquired with the Summit 1.3.6 software and the fitting calculations were carried out with the Mulipak software version 9.2.

A 100 mm X-ray diameter spot size, with a power of 25.6 W, on a rectangular area of 100 mm × 800 mm, was employed in order to avoid corruption of the polymer characteristics.

During the data acquisition a double neutralization system was employed in order to avoid charging effects on the non conductive polymeric surface. The neutralization system consists in an Argon ion gun combined with an electron gun.

The energy resolution achieved, with VersaProbe, on polymeric materials, is 0.85 eV.

Transmission electron microscopy

Morphologic observations of nanoparticles and nanocapsules were carried out with a Philips TECNAI 10 transmission electron microscope (TEM) at an accelerating voltage of 80 kV and a Focus Ion Beam Zeiss Neon 40 instrument for scanning micrographs. Carbon coating was accomplished by using a Mitec K950 Sputter Coater (endowed with a film thickness monitor k150x).

Scanning electron microscopy

Nanospheres characterization was carried out also with a column scanning electron microscopy with field emission Shottky, 4pA-20nA, 0.1-30 kV, resolution 1.1 nm.

5.3.XPS results

Survey scans on nanosphere and nanocapsule samples were acquired from 0 eV to 1200 eV, as the main spectral features of the elements in polymeric materials under investigation fall within this energy range. The results show the typical spectra of polymeric materials with O1s, C1s and N1s main peaks, as clarified in the survey scans reported in Figure 5.2:

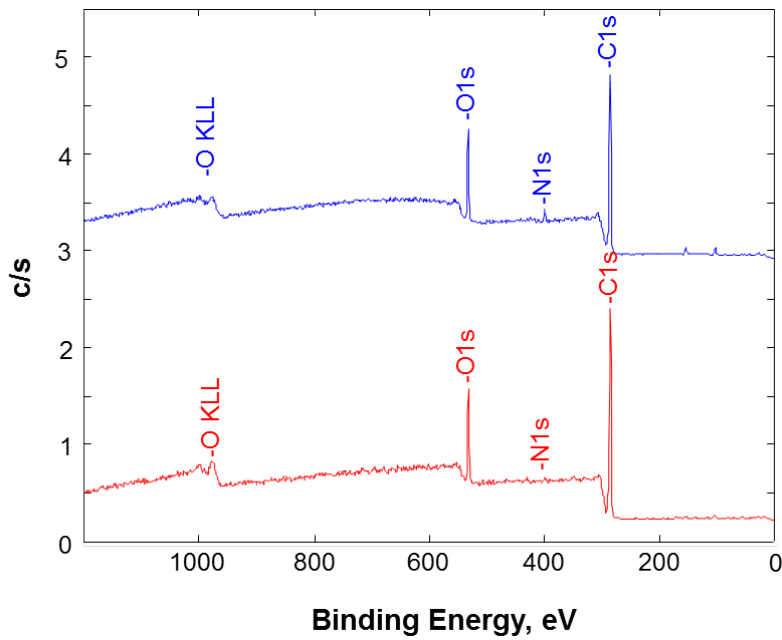


Figure 5.2. Survey scan of nanoparticles surfaces: nanospheres (blue) and nanocapsules (red).

The blue survey scans refers to nanosphere sample and the red scan to nanocapsule sample and both report typical XPS spectra of polymeric materials, with a huge amounts of carbon signal at 284.8 eV combined with oxygen peak at 532.3 eV.

The presence of the oxygen peak is confirmed by the OKLL Auger peak, at higher energy binding (980 eV). The intensity of the Auger peaks is strictly related to the intensity of O1s signals. It is present a nitrogen peak, with lower intensities, as we expected, from the chemical composition of the polymer. Standard procedure for the atomic % calculation is used in order to have a semi-quantitative information of each element.

The formula adopted is reported in Equation 1

$$atomic\% = \frac{I_c f_c}{\sum_i I_i f_i} \quad (1)$$

where I is the area under the curve (the subscript indicates the element, C stands for carbon, for example) and f is the sensitivity factor of the element, which allows to

keep into account the sensitivity of each elements to the radiation. Element sensitivity depends basically on the atomic weight (lower atomic weight elements have lower sensitivity) but also on other variables, like the incident angle of the radiation.

The semi-quantitative information about surface composition of non quenched samples is reported in the table below:

Elements	Nanospheres (%)	Nanocapsules (%)
N1s	3.5	1.6
O1s	16.2	16.9
C1s	80.3	81.4

It can be noted that the ratio between the atomic percentage of C1s and O1s peak is the same in nanocapsule and nanosphere samples while a higher amount of N1s signal in the nanosphere material (3.5%) compared to the nanocapsules sample (1.6%).

The high resolution scans, acquired with a pass energy of 23.5 eV, in limited range of energy, were carried out on C1s, O1s and N1s in order to study the chemical bonds between these atoms located on the surface layer. On nanospheres and nanocapsules there is evidence of the C1s region which comprises three components: 1) direct C-C bound, 2) C-O and C≡N bound and 3) O-C=O. Energy binding at 286 eV may correspond to a single bond C-O as well as to a triple bond CN. After the fitting procedure, it is possible to have an estimation of the percentage of each bond. According to Peracchia et al. (1998), the C-O bond is assigned to PEG. There is a larger amount of C-O and CN bound (27.9%) in the nanosphere samples compared to the amount (18.7%) in the nanocapsule samples and 4.7% of O-C=O in the nanosphere sample compared to 9.7% in the nanocapsule sample. As reference also the pure polymer was analyzed: a drop of a polymer solution was dried and analyzed at XPS (see Figure 5.3). Its results represent a random distribution of chains, where polymer chains does not arrange in a “frozen” state like in nanospheres and nanocapsules.

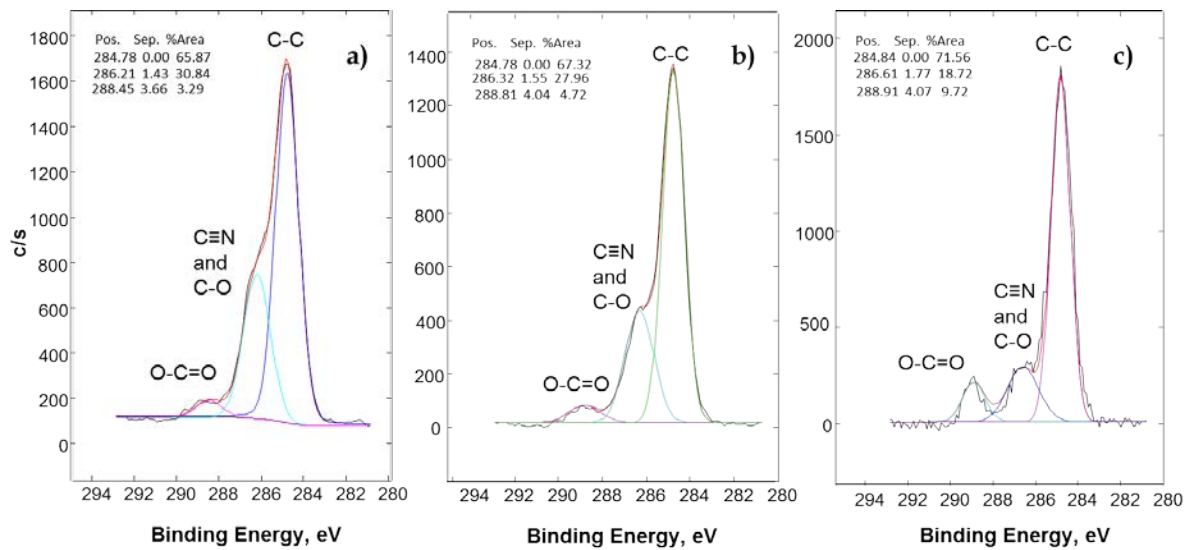


Figure 5.3. Surface analysis of carbon region in: a) pure polymer, b) nanospheres and c) nanocapsules. Relative atomic percentage of carbon bonds are reported on the figure. Samples are not quenched.

It has to be noted the C-O bond and CN bond have the same energy binding: in Peracchia et al. (1998) that peak is attributed just to C-O bond of PEG, without considering the contribution of CN bond. The C-O bond is surely predominant in polymer structure, but comparing nitrogen spectra with carbon spectra of both samples (nanospheres and nanocapsules) it can be said, without any doubt, that also CN bond contribution is present in that peak (see Figure 5.4). Attribution is confirmed by the behavior of the intensity peak of nitrogen, which decreases proportionally like carbon shoulder (286 eV).

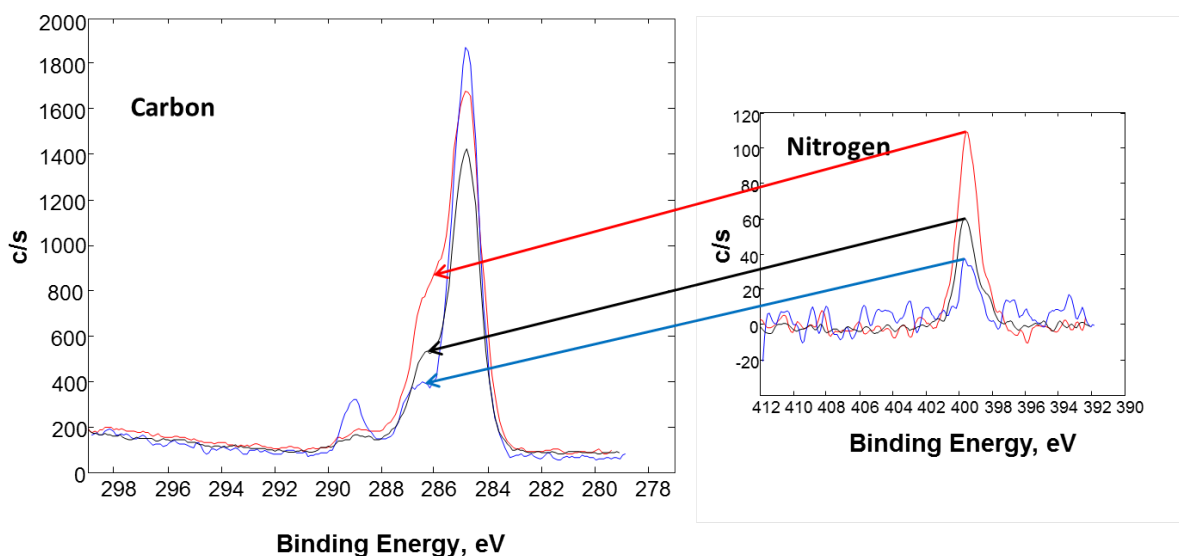


Figure 5.4. Carbon and nitrogen spectra of pure polymer, nanospheres and nanocapsules. Red spectrum is pure polymer, black spectrum is nanosphere sample, blue spectrum is nanocapsule sample.

The angle resolved XPS analysis provide information about the first 8.5 nm in non-destructive mode, tilting the sample from 10° degree to 90° degree with a 10° degree step. A constant behaviour of carboxylic groups is obtained in the outer layer (8.5 nm thick) for both samples (nanospheres and nanocapsules), as reported in the following layout.

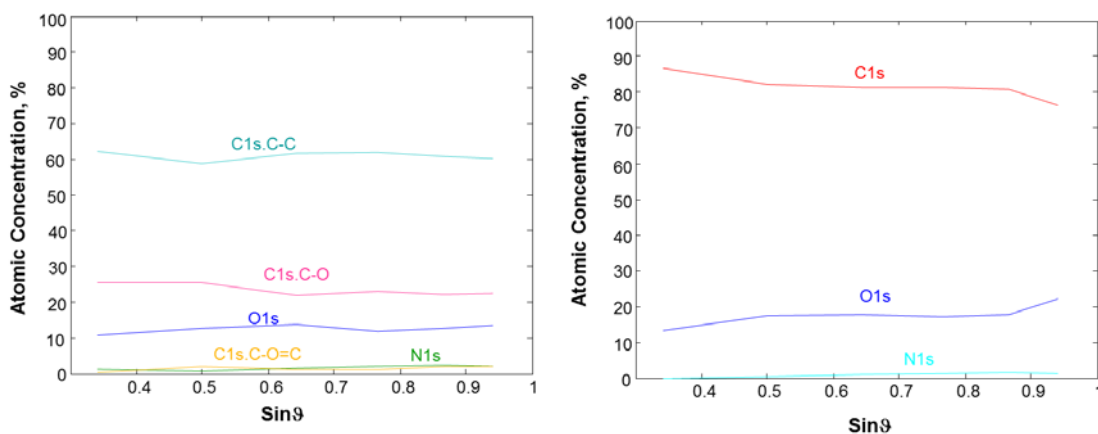


Figure 5.5. Angle resolved analysis of nanospheres (left) and nanocapsules (right). Atomic concentration versus sin theta. Theta is the angle of the sample with respect to the analyzer.

Figure 5.5 (Angle Resolved nanospheres and nanocapules) reports the atomic percentage information of single bond corresponding to the thickness where the information come out. The atomic percentage values are in agreement with the values obtained with the standard surface and the depth profiles analysis.

During the depth profiles analysis a C60 gun is employed in order to have an information regarding the behaviour of the bonds versus depth. During this analysis a C60 gun bombards the surface removing layer of material, giving us an information about the internal part of the polymer (3.5 nm/min etch rate). In nanosphere samples it can be noted a strong decrease of the C-C bond and a relative increase of the C-O signal. In the nanocapsules there is a different behavior: an instantaneous increment of both C-C and C-O signal versus an asymptotic constant behavior.

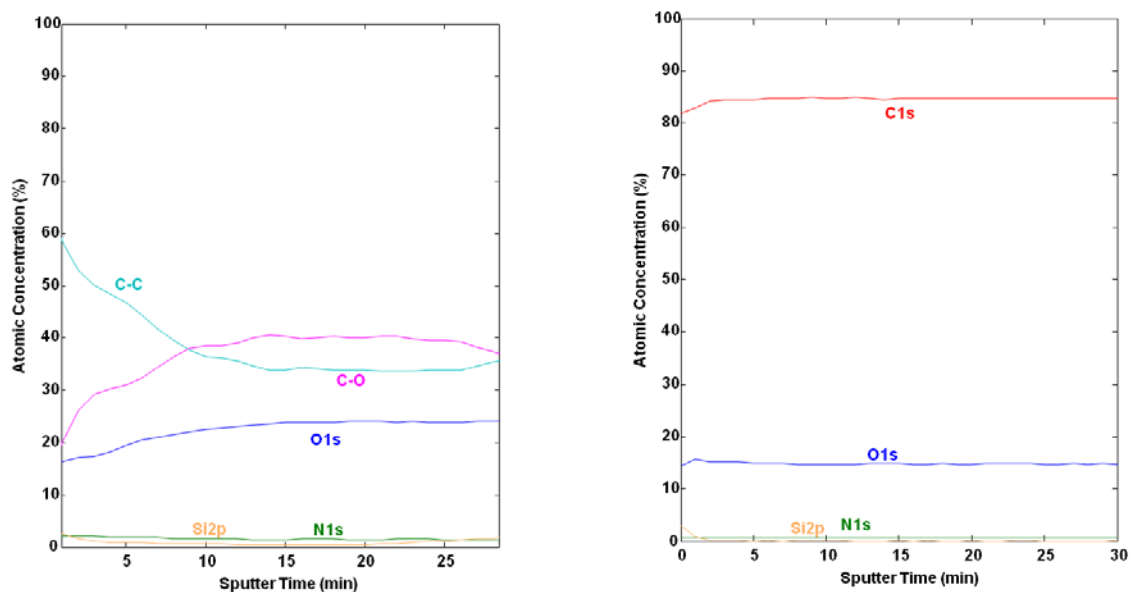


Figure 5.6. Depth profile using C60 gun. Sputter time is the time of C60 on the sample.

On the contrary, with Argon gun, adopted during the preliminary investigation, in depth profiles mode, it was noted the break C-O polymeric chains,

due to the interaction with small dimension of the Argon ion, and consequently a distortion of the information relative to these investigations.

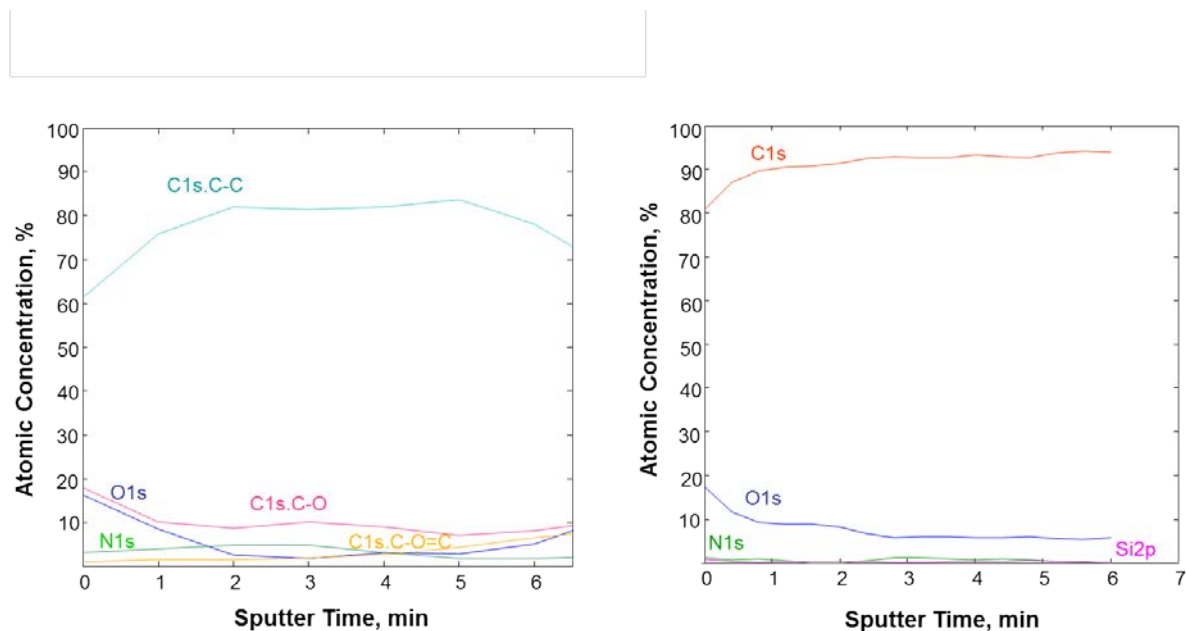


Figure 5.7. Depth profile using Argon gun: nanospheres (left) and nanocapsules (right).

In the following part, we will focus our attention on nanocapsules.

Nanocapsules have a liquid core, surrounded by a polymeric layer. As core we use Miglyol® 812N, which is a mixture of fatty acids and glycerol. In nanocapsules with PEG the hexadecyl chains are in contact with the hydrophobic core, whereas the PEG chains stretch out.

The XPS angle resolved analysis is more sensitive to the surface and it is possible to obtain chemical information from the surface to a thickness of 8.5 nm, in a non-destructive mode.

Starting from the Oxygen peak, it is visible a different behaviour between nanosphere samples and nanocapsule samples. Nanocapsule samples presented a higher shoulder at higher energy binding, than nanosphere samples.

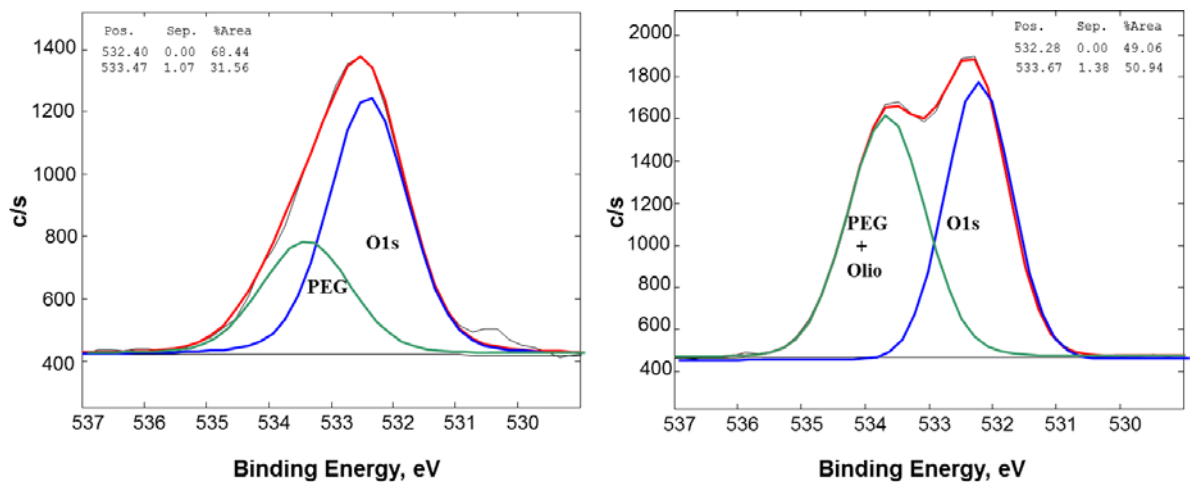


Figure 5.8. Oxygen spectra of nanospheres (left graph) and nanocapsules (right graph) with the relative deconvolution process and the attribution to each bond. Nanospheres were obtained from 6 mg/ml solution and nanocapsules from 6 mg/ml and 8 μ L/ml. Not quenched samples.

In nanosphere spectra signal deconvolution shows two different contributions: the main peak (532,4 eV) related to the Oxygen signal of the material, and the left shoulder (533.6 eV), at higher energy binding, related to PEG signal.

In nanocapsule signals the main O1s peak (532.3 eV) is attributed to the oxygen signal of the material, but the shoulder at higher energy binding (533.6 eV) could be related not only to PEG but also to oil signal. This result could be attributed to the oil signal coming from the core of the nanocapsules, that has the same energy binding value as the PEG signal. Consequently, it was tried to analyze the thickness of the nanocapsule shells studying the behaviour of the intensities related to the shoulder at higher energy binding. Furthermore there was evidence of a significant change in oxygen profile and this change occurs at different depth according to the MR value investigated.

The tilted condition of the samples respect to the analyzer ranged from 10 to 90 degrees. In Figure 5.9 the right-hand column shows the quenched and the left-hand column shows the unquenched nanocapsules. In each panel the first spectra was acquired at 10° and the following spectra were recorded to 90° with a 10° tilting step respect to the analyzer. This step was gradually increased to 90°. These lines are plotted from the bottom of the picture and shifted in the z direction towards the top.

The big variation of the shoulder intensities ratio changes proportionally with the nanocapsule oil to polymer mass ratio (MR) from radent surface to bulk (8.5 nm). According to Leber and Ratner (2009) the information depth on PEG ranges until 8.5 nm.

The intensity difference between main O1s peak and shoulder, at higher energy binding, changed proportionally to the MR. When the signals comes from the topmost layer ($\theta=10^\circ$) there is always the same intensity of two O1s peaks at 532.5 eV and 533.7 eV.

When θ increases and consequently the information come from deeper layer, the left shoulder at 533.7 eV decreases, and this could be related to the end point of the nanocapsule wall. In quenched nanocapules, this O1s left shoulder intensity reduction happens in deeper layer, this indicating thicker nanocapsule wall. According to the literature, the angle resolved information gives chemical information until 8.5 nm on PEG based materials. It can be calculated the depth where this variation of left O1s peak intensity start to decrease and calculate the depth where this information come out and consequently the nanocapsule wall thickness. The formula used is:

$$\text{thickness (nm)}=8.5*\sin\theta$$

Whenever the intensity of the shoulder is comparable with the O1s one we do expect that the record signal is due walls nanoparticles. On the contrary when the shoulder intensities start to decrease it means that no more signal comes from the wall nanoparticles, but only form the oil internal part.

In the quenched nanocapsules with MR=2.37 there is the same intensity in the shoulder at (533.7 eV) and the main O1s peak until $3/9$ angle acquisition (4.25 nm).

In the intermediate MR value this variation of intensities starts form $9/9$ (8.5 nm) and in MR=0.76 there is always the same intensities. In the last case it is possible to assume that the wall thickness is, surely, thicker than 8.5 nm.

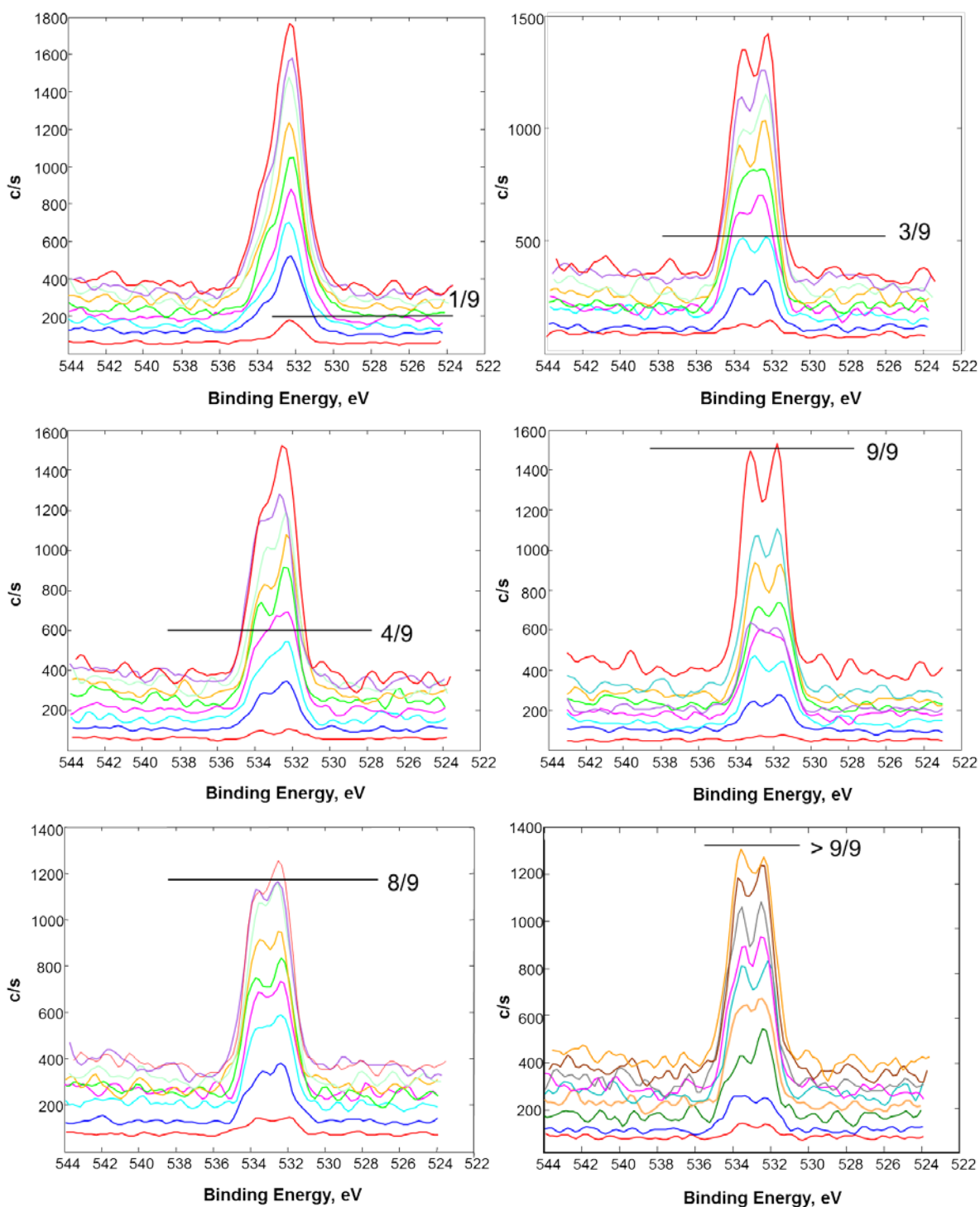


Figure 5.9. XPS analysis at different angles (from 10° to 90°) of nanocapsules at different MR without quenching (left column) and with quenching (right column). From the top: nanocapsules at MR 2.37, at MR 1.26 and at MR 0.76. In each graph are reported nine oxygen peaks obtained at different angle, from the bottom to the top: 10° , 20° , 30° , 40° , 50° , 60° , 70° , 80° and 90° . A line highlights where the oxygen profile changes, indicating a change in chemical composition.

In the non-quenched nanocapsules, where the average of the wall thickness is lower, we obtain the same trend: the same shoulder intensities until 1/9 (1,44 nm), for nanocapsules at MR=2.37, 4/9 (5,44 nm) for MR=1.26 and 8/9 (8,33 nm) for MR=0.76 one. All these values are reported in Table 5.1:

Table 5.1. Estimated value of polymer wall at different MR values with and without quenching.

	Non quenched, nm	Quenched, nm
MR 2.37	1.44	4.25
MR 1.26	5.44	8,5
MR 0.76	8.33	>8.5

The quenched nanocapsules shows thicker walls respect to the non-quenched nanocapsules. That can be explained as that, diluting by water, medium composition changes having a bigger fraction of water that results in reduced polymer solubility which precipitates around nanocapsules, but this will be discussed in more details in the discussion.

5.4.TEM results

Figure 5.10 shows nanocapsule photos both “positive” (a, c) and “negative” (b, d). TEM analysis confirmed spherical shape of the nanocapsules and their size dimensions. Two MR were analysed by TEM: 1.26 and 0.76. The bigger amount of oil in MR=2.37 was considered dangerous for the equipment, due to the higher oil quantity, and no samples were analysed.

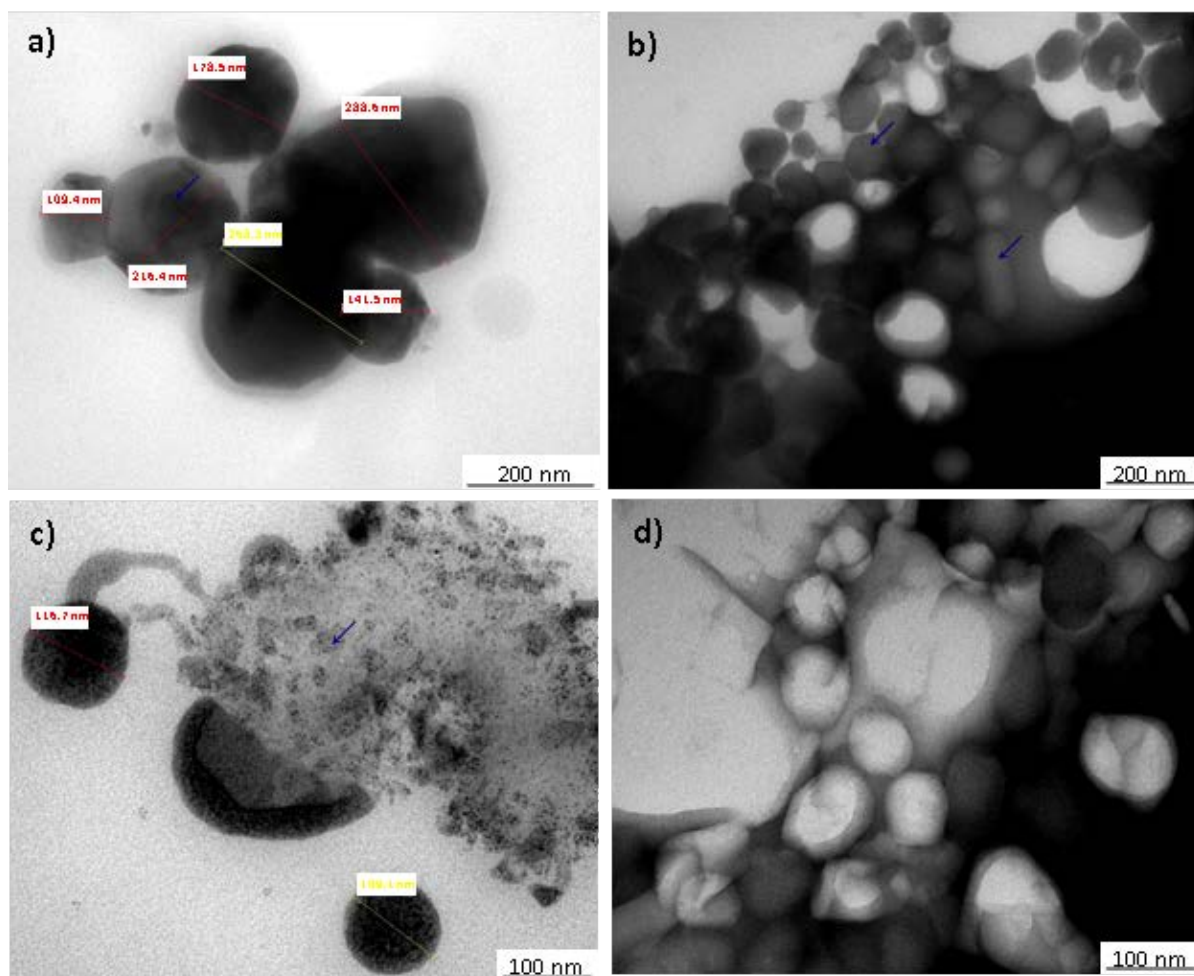


Figure 5.10. Positive (a, c) and negative (b, d) TEM micrographs taken at different magnifications of poly(MePEGCA-co-HDCA) nanocapsules containing Miglyol 812. Samples were prepared with MR = 1.26, FR = 120 ml/min and initial copolymer and oil concentrations of 6 mg/ml and 8 μ L/ml, respectively. Blue arrows point out the pseudoregular geometries that can be observed inside the capsules, probably as a consequence of a regular arrangement of some oil molecules.

Nanocapsules show a spherical shape with some regular geometries inside (blue arrows in the photos), which can be due to oil molecules, because, as it will be shown later nanospheres have a different shape. Acquisition of photos with TEM, under high vacuum conditions, was quite hard, due to the fact that the polymer was easily burnt by electrons and nanocapsules could break. An interesting image is shown in Figure 5.10c, where a nanocapsule clearly “exploded” leaving the oil outside. In many samples most of the nanocapsules showed an halo (see for

example Figure 5.11a) around the particle, which is due to the oil leakage. Figure 5.11c and d were acquired while the electron radiation was burning the sample: in Figure 5.11c it is shown the fracture in the polymer wall, whereas in Figure 5.11d the polymer film is burnt on the surface letting see the internal structure which has pseudoregular geometries. Nanocapsule breakage and spilling out of the oil is common with nanocapsule structure (Guinebrieter et al., 2002).

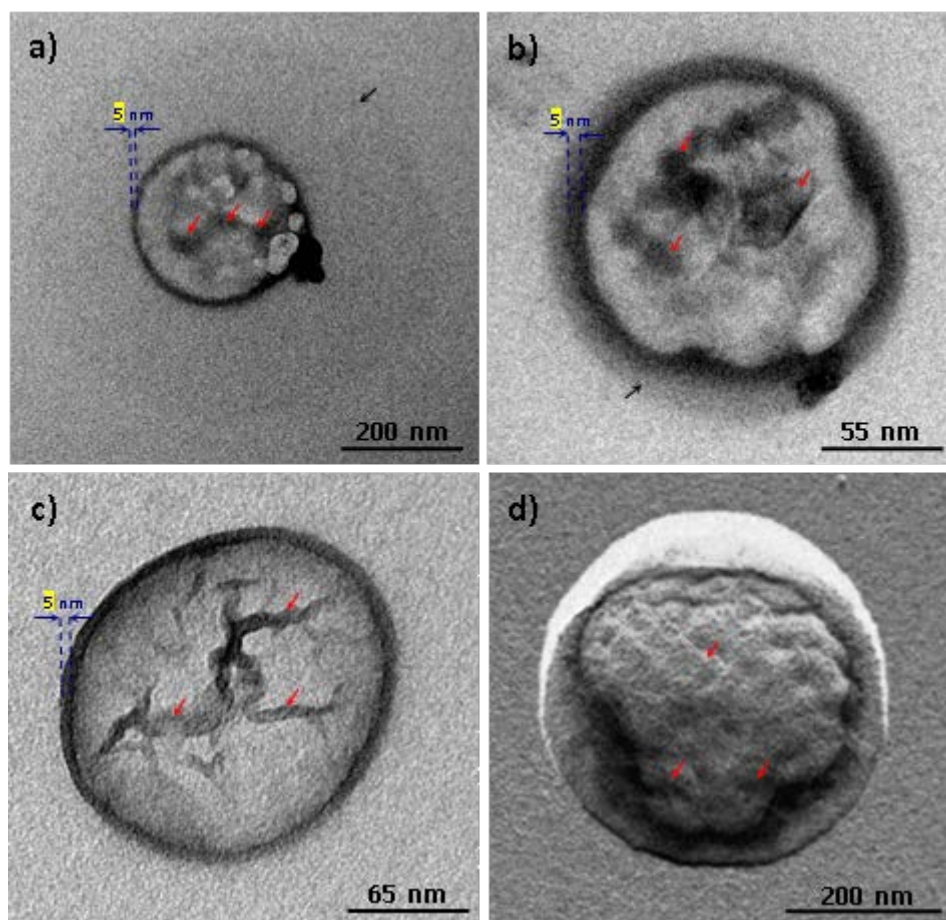


Figure 5.11. TEM micrographs taken at different magnifications of poly(MePEGCA-co-HDCA) nanocapsules containing Miglyol 812. Samples were prepared with MR = 0.76, FR = 120 ml/min and initial copolymer and oil concentrations of 6 mg/ml and 8 μ L/ml, respectively. Sample (d) was shadowed with Pt/C. Red and black arrows point out pseudoregular geometries inside nanocapsules and spilled oil outside nanocapsules, respectively. Wall thickness of nanocapsules is indicated by the blue asides.

5.4.1. Nanosphere photos

Nanospheres are constituted just by the polymer and are a monolytic structure. Differently from nanocapsules, they can be analyzed quite easily by SEM. Photo in Figure 5.12 shows nanospheres seen with SEM. Some of them are measured, confirming the size measured by dynamic light scattering. In the picture are also visible smaller nanospheres, highlighting there is a size distribution in the sample.

Nanospheres photos show spherical nanoparticles. Some of them were measured by SEM, and average size of the measured ones is around 150 nm. Smaller nanospheres are present. In Figure 5.12b) size distribution measured by dynamic light scattering (DLS) is shown, both number distribution (solid line) and volume distribution (dashed lines) are reported.

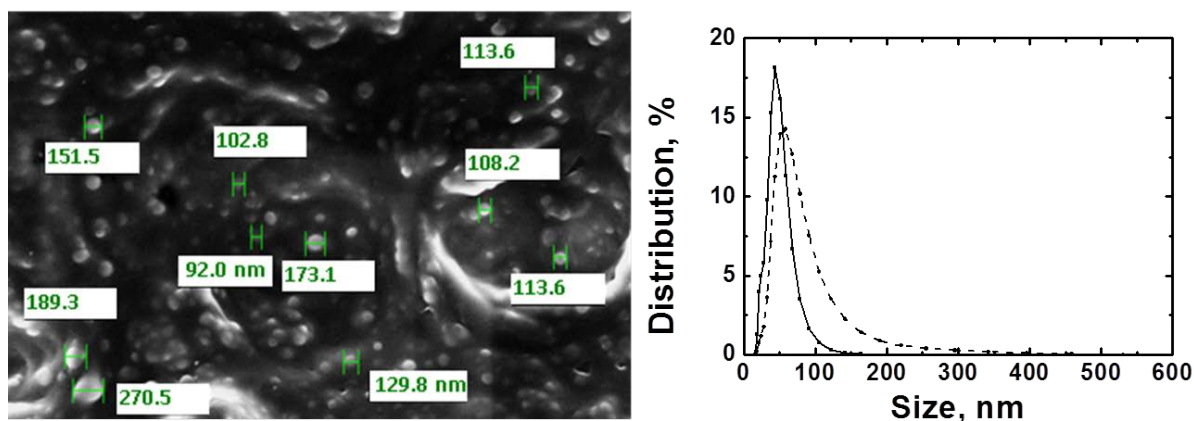


Figure 5.12. a) Nanosphere picture obtained with SEM. b) Particle size distribution of the sample measured by DLS: number distribution (—) and volume distribution (---).

Nanospheres shadowed by Pt/C and seen at TEM are shown in Figure 5.13. The typical “shadow” of the technique is present, revealing the spherical shape of nanospheres.

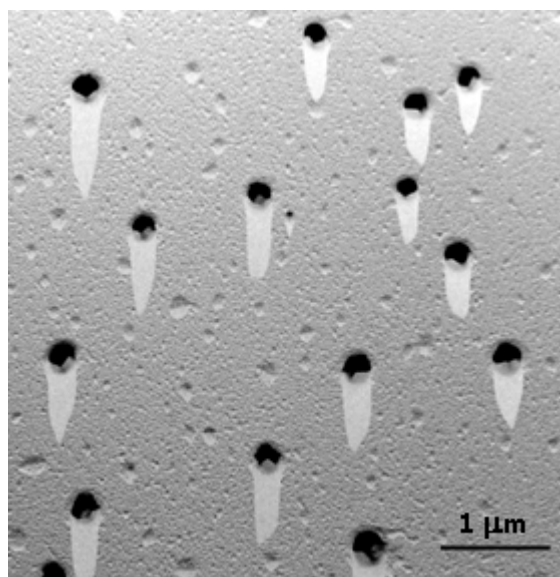


Figure 5.13. Nanospheres covered with Pt. The large shadow indicate spherical shape of the sample.

Positive and negative nanosphere samples are shown in Figure 5.14. It is noticeable that positive image reveals a particular morphology, like the nanosphere is constituted by many smaller aggregates. This morphology is not evident in the negative image. It indicates that the surface is fragmented and the surface might be rough.

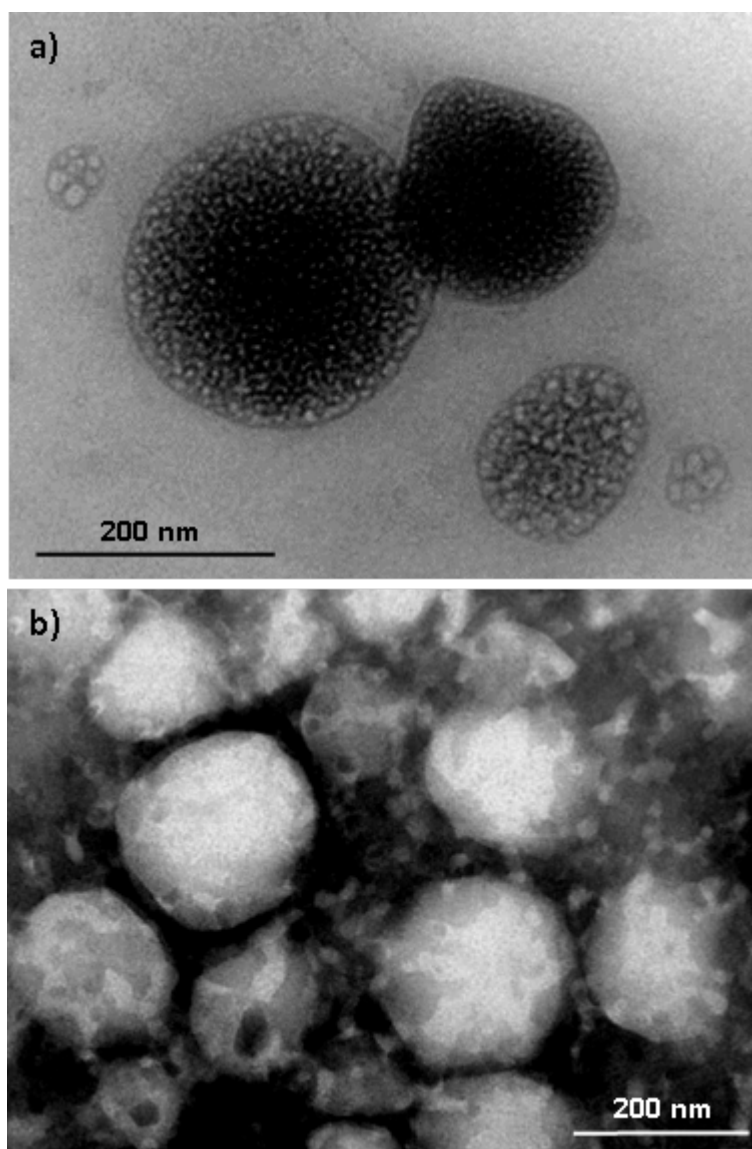


Figure 5.14. a) positive nanosphere sample; b) negative staining nanocapsule staining.

5.5.Discussion

Nanocapsules obtained at different MR oil/polymer were analyzed by XPS at variable angle in order to study the composition of the external layer and estimate polymer wall thickness. Nanospheres and nanocapsules analyzed in this work by XPS and TEM were all produced at 120 ml/min as flow rate, which is a value that ensures good mixing performance and reduces experimental variability.

XPS results suggest that increasing oil to polymer concentration (i.e. from MR 2.37 to MR 0.76) nanocapsule thickness decreases in both the cases analyzed, with and without quenching. Without quenching polymer wall was estimated to vary from 1.44 nm (MR 2.37) to 8.33 nm (MR 0.76), while with quenching from 4.25 nm (MR 2.37) to over 8.5 nm (MR 0.76). In a solution at high MR there is less polymer in comparison to oil amount and polymer amount increases as MR decreases. In nanocapsules obtained from MR 2.37 polymer amount is very low with respect to the oil amount, so polymer wall will be thinner. On the contrary, when a high polymer quantity is available, polymer wall will be thicker. This conclusion is in agreement with what other authors reported (Cauchetier et al., 2003, Romero-Cano and Vincent, 2002)

At the same time quenching nanocapsules resulted to be more thicker of the corresponding non quenched samples. Some solubility tests of the polymer at different water fraction were performed in order to highlight if a bigger percentage of water could modify residual solubility of the polymer (chapter 2). Test were performed at 30 °C and solution at 50%, 66% and 90% water were investigated. Non quenched samples correspond to a 50% water fraction, while quenched sample to 66% water fraction. Starting from acetone solution of the polymer, water was added and it was observed if precipitation happened. Results are shown in Figure 5.15. They show that solubility of the polymer is lower in 66% than in 50% mixture. It is possible that operating with quenching more polymer precipitates at the outlet of the mixture when diluting with water. Polymer tends to precipitate over nanocapsules already formed giving a thicker polymer wall.

Nanocapsule samples at MR 1.26 (Figure 5.10) and 0.76 (Figure 5.11) with quenching were analyzed also by TEM. From images shown in Figure 5.11, polymer wall thickness was estimated. It is around 5 nm (for nanocapsules obtained at MR=0.76), while wall thickness estimation by XPS was >8.5 nm at the same conditions. The fact that it is >8.5 is due to that radiation was not able to go deeper than this thickness. In comparing the two results it is necessary to take into account that both the methods have some limitations. In TEM analysis the limit of the

measure is due to the easy error of the manual measurements. Moreover, the image quality was not perfect and some doubts on the real end of the wall are justifiable. Regarding the method used in XPS analysis, the limitations is that data about the depth reached at 90° is not available for the P(MePEGCA-co-HDCA) and the value used in this work (8.5 nm) is the one reported on literature about PEG based materials.

5.6.References

Cauchetier E., Deniau M., Fessi H., Astier A., Paul M., 2003. Atovaquone-loaded nanocapsules: influence of the nature of the polymer on their in vitro characteristics. *International Journal of Pharmaceutics* 250, 273-281.

Guinebretière S., Briancon S., Fessi H., Teodorescu V.S., Blanchin M.G., 2002, Nanocapsules of biodegradable polymers: preparation and characterization by direct high resolution electron microscopy. *Materials Science and Engineering C* 21, 137-142

Leber E. R., Ratner B.D., 2009, Introduction of carboxyl functional groups onto platinum by RF lasma deposition. *Plasma Processes and Polymers* 6, 219-227.

Peracchia M.T., Vauthier C., Desmaele D., Gulik A., Dedieu J.C., Demoy M., d'Angelo J., Couvreur P., 1998, Pegylated nanoparticles from a novel methoxypolyethylene glycol cyanoacrylate hexadecyl cyanoacrylate amphiphilic copolymer. *Pharmaceutical Research* 15, 550-556.

Powell C.J., 1995, Elemental binding energies for X-ray photoelectron spectroscopy. *Applied Surface Science* 89, 141-149.

Romero-Cano M.S., Vincent, B., 2002. Controlled release of 4-nitroanisole from poly(lactic acid) nanoparticles. *Journal of Controlled Release* 82, 127-135.

6. Drug loading and drug release

6.1. Introduction

Nanospheres and nanocapsules are pharmaceutical carriers for drug release. Thanks to their nanometric size they allow to reach target organs or tissues and accumulate there. Once in the target organs they release the drug. Drug release is an interaction of different mechanisms which depend on the matrix and in drug characteristics. Nanospheres are monolytic structure where the drug is dispersed in the polymeric matrix, while in nanocapsules the drug is dissolved in the inner liquid. In the first case drug release is an interaction of two main mechanisms: diffusion of the drug through the polymer and degradation of polymer matrix. In nanocapsules drug release depends mainly on the partition coefficient between the inner liquid and the outer medium.

To understand the complex mechanism of drug release is quite difficult. Different mechanisms occur simultaneously. In pharmaceutical field empirical and semiempirical models are usually used to describe drug release:

- Zero-order kinetic
- First order kinetic
- Higuchi Equation
- Hixson-Crowell equation

These models are, as said, empirical or semi-empirical, so that they allow to have a good approximation of experimental data obtained in the usual range of operating conditions.

A detailed study of release should be performed in order to evaluate the mechanisms involved, but it is not part of this work. The interest of this chapter is to show results about loaded nanospheres and nanocapsules, in order to highlight the behavior of the system in loading and release and to provide a direct comparison between the two systems obtained in the same conditions.

In order to provide a good kinetic model it should be possible to quantify drug amount in every single particle, but this is quite difficult to determine experimentally. This is why usually drug release is modelled by using empirical and semiempirical approaches like the ones cited above. Higuchi model and first order model provided a discrete fitting of experimental data and results will be shown in this chapter. Mechanism release from microencapsulated drugs was mathematically modelled in detailed in the past. These systems considered drug microparticles surrounded by a polymeric wall (Manca and Rovaglio, 2003, Petitti et al., 2008). The system here presented is different. The drug used as model drug is Triclosan, a little lipophilic drug, with great affinity for the organic oil of the inner core of nanocapsules, while it is supposed triclosan precipitates simultaneously with the polymer in nanospheres synthesis, in order to be dispersed in the polymer matrix.

6.2. Materials and method

6.2.1. Materials

Acetone Chromasolv® by Sigma Aldrich and ultrapure water produced by Millipore® were used as solvent and antisolvent for nanosphere and nanocapsules production. Triclosan by Sigma Aldrich was used as model drug.

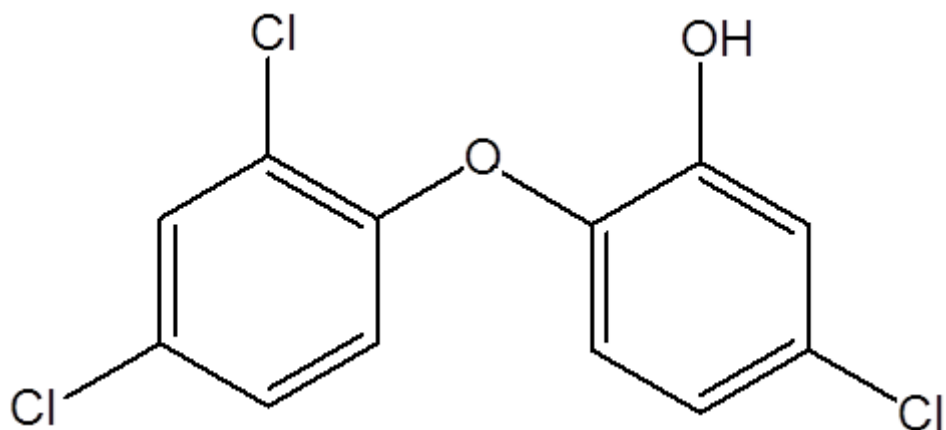


Figure 6.1. Chemical structure of Triclosan.

6.2.2. Preparation of loaded nanoparticles

Nanospheres and nanocapsules of poly(MePEGCA-co-HDCA) containing triclosan were prepared by the solvent displacement method using CIJM-d1. Nanospheres at 6 mg/ml and nanocapsules at MR 1.26 (6 mg /ml polymer concentration and 8 μ L/ml oil concentration) were loaded with triclosan. Triclosan was added to acetone solution in order to have 0.3% (w/v) of triclosan (3 mg/ml). 25 ml of this solution were injected into the mixer together with 25 ml of water and quenched in 25 ml of water kept in magnetic stirring at the out of the mixer. Two flow rates were investigated: 120 ml/min and 10 ml/min. Finally, the acetone was rotaevaporated (30 minutes at room temperature) to get an aqueous suspension of nanospheres.

Nanocapsules were prepared following the same methodology after adding 8 μ L/ml of Miglyol 812 to the initial organic solution of the copolymer in order to form the inner oily cavity.

Nanoparticle and nanocapsule suspensions were extensively dialyzed (Spectra/Por® 3500 MWCO dialysis membrane, Spectrum, Huston, TX) during 4 hours against a Sørensen solution supplemented with 10% (v/v) of ethanol in order to remove all non loaded triclosan. Aliquots of 200 μ L of the sample suspension after dialysis were sonicated and extracted with 1 ml of 70% ethanol to quantify

triclosan by UV analysis. From this value it was measured the total amount of triclosan that was incorporated in nanospheres and nanocapsules. Drug incorporation percentage ($\%TCS_{INC}$) is calculated from equation 1:

$$\%TCS_{INC} = \frac{mgTriclosan_{INC}}{mgTriclosan_{TOT}} \quad (1)$$

Drug loading was calculated as the drug incorporation percentage over the total amount mass amount:

$$\%DL_{NS} = \frac{mgTriclosan_{INC}}{mgPolymer + mgTriclosan_{INC}} \quad (2)$$

$$\%DL_{NC} = \frac{mgTriclosan_{INC}}{mgPolymer + mgOil + mgTriclosan_{INC}} \quad (3)$$

An UV-3600 spectrophotometer controlled by the UVProbe v2.31 software (Shimadzu, Tokyo, Japan) was employed. Calibration curves were obtained by plotting the absorbance measured at 281 nm against triclosan concentration.

In the same conditions (of concentrations and flow rate), precipitations of nanospheres and nanocapsules were carried out and particle size was measured by DLS after solvent evaporation and an average value is reported in the following section.

6.2.3. Drug release

10 ml of the aqueous suspension containing triclosan-loaded nanoparticles or nanocapsules (3 mg/ml of triclosan) were confined in a dialysis bag, which was introduced in a vessel provided of magnetic stirring and containing 20 ml of the selected release medium. This consisted on a mixture (3/7 v/v) of Sørensen medium (pH 7.4) and ethanol. Aliquots (1 ml) were drawn at predetermined intervals to determine the amount of released triclosan by UV spectroscopy. The volume of the release medium was kept constant by addition of 1 ml of fresh medium after removal of each aliquot. All drug release tests were carried out using five replicates to control the homogeneity of the release and to average the results. The triclosan remaining in the samples was determined again by UV analysis. In

this case, aliquots (200 μ l) of the dialysis bag sample were sonicated and extracted with 1 ml of 70% ethanol which ensures complete dissolution of triclosan.

Higuchi model and first order model were used to fit data. Higuchi equation is

$$Q = K_H t^{1/2} \quad (4)$$

where Q is the total drug amount released, K_H is the Higuchi constant and t is time in hours. Data are plotted as the cumulative percentage of drug released versus the square root of time in hours.

First order equation in drug release is expressed as follows

$$\text{Log}C = \text{Log}C_0 - Kt/2.303 \quad (5)$$

where C is drug concentration in the release medium at time t, C_0 is the initial concentration of drug in the dosage form, K is the kinetic constant and t is time in hours. The data obtained are plotted as log cumulative percentage of drug remaining vs. time which would yield a straight line with a slope of $-K/2.303$.

6.2.4. Antibacterial activity

The in-vitro antibacterial activity of nanoparticles and nanocapsules loaded with triclosan was evaluated using the Gram-positive *Micrococcus luteus* (M. luteus) (CECT 245, Spanish Collection of Type Culture, Valencia, Spain) and Gram-negative *Escherichia coli* (E. coli) (CECT 101, Spanish Collection of Type Culture, Valencia, Spain) microorganisms.

Briefly, 7 ml of Luria-Bertani (LB) broth containing 105 CFU/ml was mixed into sterile tubes with 1 ml of the nanoparticle or nanocapsule aqueous suspension. Tubes were inverted 4-6 times to assure mixing and incubated for 24 h and 48 h in a shaking incubator at 100 rpm and a temperature of 37 °C. Cultures of LB broth without and with bacteria were performed as the negative and the maximum bacterial growth controls, respectively. Culture of pure LB broth was the negative control, and pure LB broth with nanoparticles or nanocapsules were also tested as blank of turbidity.

The bacterial growth was determined by measuring the turbidity at 600 nm by UV spectroscopy. The surviving number of bacteria was determined according to the relative growth rate (percentage) calculated from turbidity changes after 24 h and 48 h of incubation. Activities were evaluated using six replicates, in each case the corresponding average value and standard deviation being determined. Two samples were considered statistically significantly different when ANOVA and χ^2 -test gave $p \leq 0.05$.

The antibacterial effect in manner doses-response was also determined for nanocapsules loaded with triclosan. For it, different dilutions of the sample were evaluated and the relative growth evaluated as noted above. The dose-response effect was analyzed according to a logistic model using OriginPro v8 software (Origin Microcal Corp., USA).

6.3.Results

6.3.1. Size

Loaded nanospheres and nanocapsules were produced in quintuplicate at each conditions used in release experiments, in order to measure final particle size. Results are shown in Table 6.1. These data shows that loading with triclosan there is not a significant increase in particle size, if compared with results obtained with unloaded nanocapsules and nanospheres shown in Chapter 3. Nanospheres look to increase their size with respect to their trend in unloaded samples and this can be explained with the fact that in nanospheres the drug is not dissolved but dispersed in the polymeric matrix. As reported in Johnson and Prud'homme (2003), drug nucleation occurs simultaneously with polymeric nucleation, so that polymer can act as stabilizer for drug nuclei. The presence of drug nuclei could explain the bigger dimensions found in loaded nanospheres in comparison to the trend obtained with unloaded nanospheres. According to nucleation theory, drug should nucleate faster than polymer. It is difficult to see the structure of the nanospheres, but it is possible they have a solid core made of drug and a polymer layer around it.

In nanocapsules this deviation from the size trend is not present and size data from loaded nanocapsules are in agreement with the data obtained with unloaded nanocapsules (see Chapter 3). It has to be noted that Triclosan is highly lipophilic, being its water solubility $<10^{-6}$ g/ml (Grove et al., 2003) and so its affinity for inner oil is great.

Table 6.1. Mean particle size of nanospheres and nanocapsules loaded with triclosan.

Nanocapsules			Nanospheres		
FR	Size (nm)	Std dev.	FR	Size (nm)	Std dev.
120	234.13	8.40	120	161.14	12.35
10	377.89	23.10	10	246.57	7.10

6.3.2. Drug incorporation

Drug amount is measured by UV from the sample after dialysis. Quantity found to be in nanoparticles are reported in Table 6.2. No significant differences can be found between drug incorporation in nanospheres and in nanocapsules. Just nanocapsules obtained at 10 ml/min have a lower triclosan incorporation.

Drug loading is measured as the drug contribution to the total weight amount of the product. In this way it is straightforward that drug loading is always lower in nanocapsules than in nanospheres. It has to be noticed that the drug amount used is high (3 mg/ml), being drug mass 50% of the polymer mass used. For this reason drug loading also is high.

Drug release from nanospheres and nanocapsules is shown in Figure 6.2. Release from nanospheres does not change from the ones obtained at lower flow rate and the ones obtained at higher flow rate. Release profile is the same. In nanocapsule sample the results are quite different between the two sample. As reported previously, nanocapsules obtained at 10 ml/min had a lower drug incorporation than the other samples, so it is difficult to compare the two results.

Table 6.2. Drug loading and drug incorporation of triclosan in nanospheres and nanocapsules.

	Flow Rate (ml/min)	mg incorporated	drug incorporation %	drug loading %
Nanospheres	10	61.01	86.54	30.20
Nanospheres	120	64.82	91.94	31.49
Nanocapsules	10	41.06	57.03	11.17
Nanocapsules	120	65.42	90.86	16.70

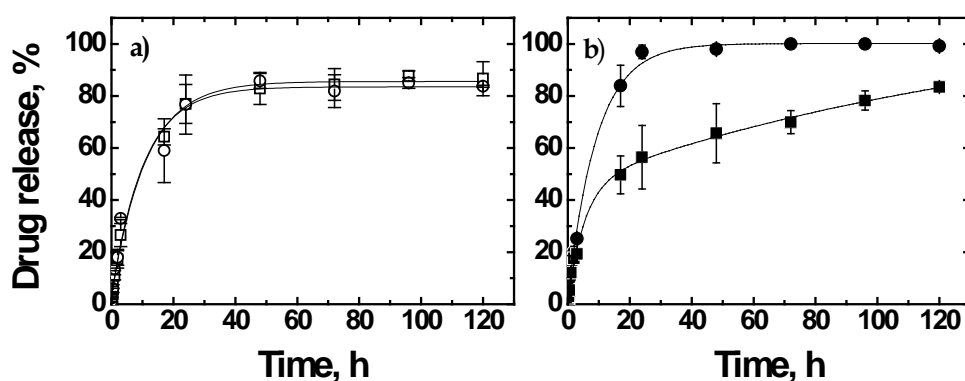


Figure 6.2. Drug release from a) nanospheres, obtained at flow rate = 10 ml/min (○) and 120 ml/min (□). b) nanocapsules, obtained at flow rate 10 ml/min (●) and 120 ml/min (■).

If the total amount of drug released is considered, the release curves as function of time appear like in Figure 6.3. The amount of drug released from nanospheres and nanocapsules is quite the same. It has to be taken into account that the volume precipitated was divided into 5 dialysis bags, and release data reported in Figure 6.3 are shown as milligrams released per millilitres of particle suspension. Drug release velocity was reported as mg/ml h during fixed intervals between following sampling, except in the first interval where it is the velocity in the first hour. In red are reported samples obtained at 10 ml/min and in black the ones at 120 ml/min.

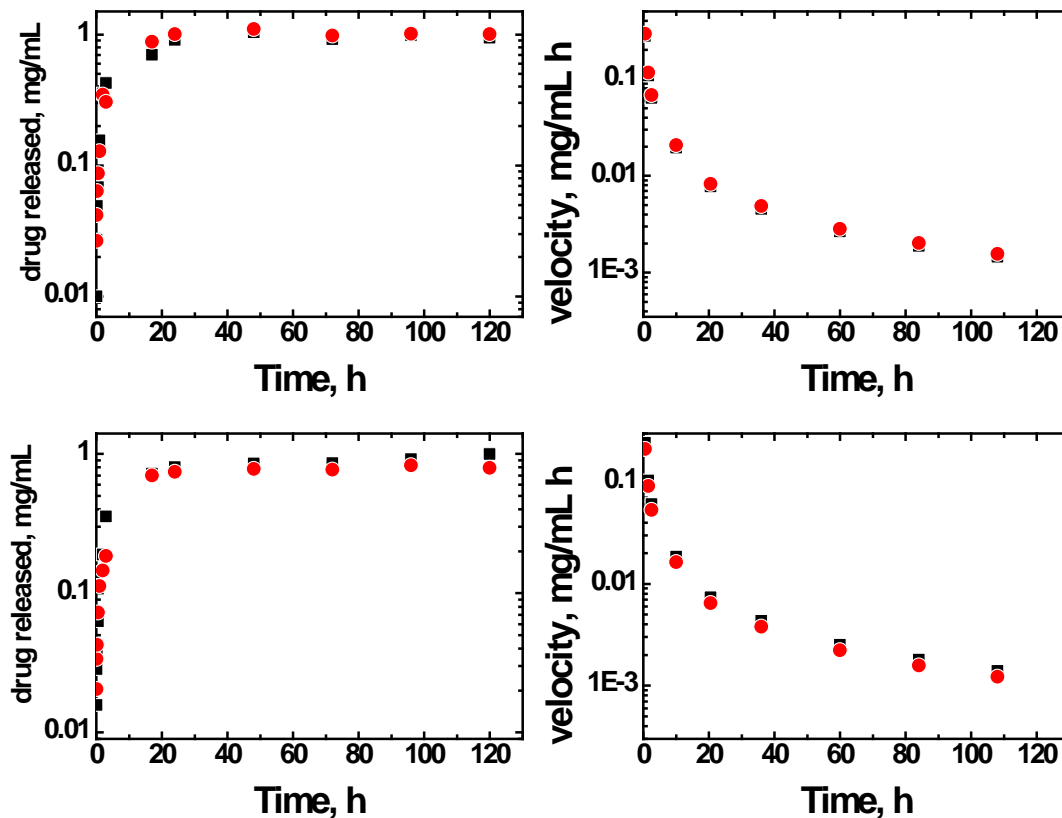


Figure 6.3. Drug released in mg/ml of suspension for nanospheres (upper graph) and for nanocapsules (lower graph): particle obtained at 10 ml/min (red) and at 120 ml/min (black). On right graph velocity of release is reported, as mg/h released in the different time interval.

Drug release increases until 24 hours and then stabilizes to a constant value of release. As graphs of velocity (right column of Figure 6.3) show, velocity of release decreases until 120 hours, the last time of the experiment. Total drug amount is almost the same in all the sample, but in nanocapsules obtained at 10 ml/min (see Table 6.2). The quantity released is however the same in all the samples, meaning in case of nanocapsules obtained at 10 ml/min the depletion is almost 100% (as shown in Figure 6.2). Nanocapsules have a release profile slightly more sustained than nanospheres. It is necessary to remember always that drugs in nanospheres are in solid state in the matrix while in nanocapsules the drug is dissolved. The mechanism the drug gets out the nanosphere includes diffusion through the matrix, eventually through pores present in the matrix, while in nanocapsules it depends

mainly on the partition coefficient between the two liquids on the two sides of the polymer membrane. The slower release from nanocapsules can be explained as a greater affinity toward the inner core of the nanocapsules in comparison to the one of nanospheres.

In order to highlight if there is any preponderant mechanism in the release, data were analyzed by the common methods used in pharmaceutical field. The best fitting is given by dividing the release curve into two parts in order to have linear dependence. In the first part of the curve the best fitting is given by Higuchi model, while in the second part first order method seems to give the best results (see Figure 6.4). As shown previously, velocity of drug released increases until 17 hours and then decreases. At that point, over 50% of drug was released. Higuchi model gives a good fitting of this data set. In this first part of release some of the conditions of the model are, in fact, present: initial drug concentration in the matrix is much higher than drug solubility, matrix swelling and dissolution are negligible and perfect sink conditions are present. With time, concentration of drug in the release medium increases, avoiding the attaining of sink conditions and the concentration in the matrix decreases, becoming closer to the drug solubility. In our samples, as shown in Figure 6.5, particle degradation does not occur in a significant way, i.e. both nanospheres and nanocapsules are still present after release experiments. That means that in the time of release no significant degradation occurs, and this is a condition in Higuchi model, differently from the Hixson Crowell model which requires that particle volume and surface change with time due to erosion.

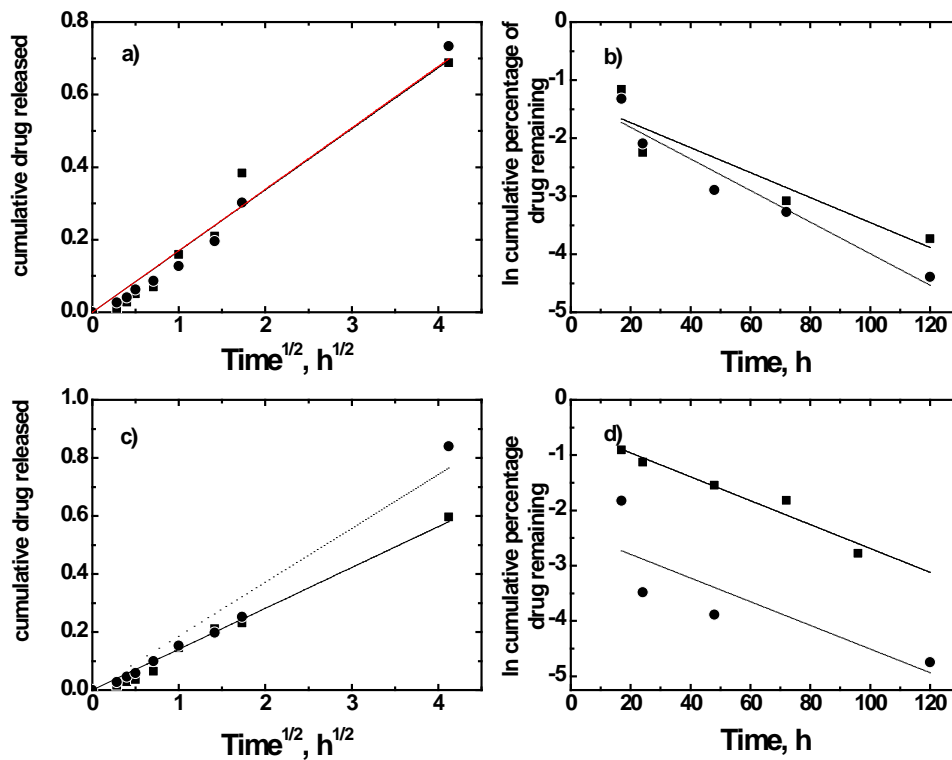


Figure 6.4. Release data fitted by Higuchi model and first order model. a) nanospheres data fitted by Higuchi model in the interval time 0-17 hours: nanospheres obtained at 10 ml/min (●, red fitting curve) and 120 ml/min (■, black fitting curve). b) nanospheres data fitted by first order model in the interval time 17-120 hours: nanospheres obtained at 10 ml/min (●, dashed fitting curve) and 120 ml/min (■, solid fitting curve) ; c) nanocapsules data fitted by Higuchi model in the interval time 0-17 hours: nanocapsules obtained at 10 ml/min (●, dashed fitting curve) and 120 ml/min (■, solid fitting curve). d) nanocapsules data fitted by first order model in the interval time 17-120 hours: nanocapsules obtained at 10 ml/min (●, dashed fitting curve) and 120 ml/min (■, solid fitting curve).

In the second part of drug release, when the release profile starts to be asymptotic, the model which best fits data is the first order model. The mechanism described by this model is quite difficult to conceptualize, but it is commonly used to describe dissolution of drugs in dosage forms. As it can be seen in Figure 6.4, nanocapsule data are fitted better than nanosphere data by first order model, confirming its application in the field of dissolved drugs.

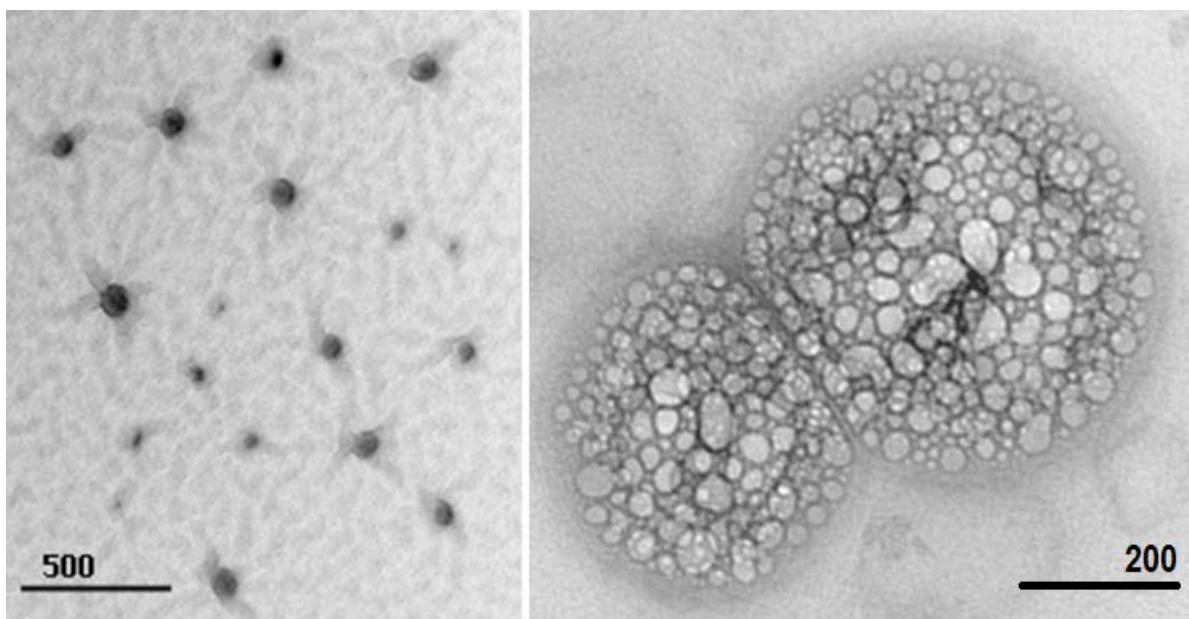


Figure 6.5. Nanospheres (left) and nanocapsules (right) after release experiment.

On these basis, a comparison of the release kinetics of triclosan from nanospheres and nanocapsules are shown in Figure 6.6. To compare the two system samples obtained at 120 ml/min are used.

The maximum release of triclosan from the nanospheres and nanocapsules was near of 80% of the drug loaded, and it is achieved more quickly by the nanospheres, occurring approximately at 50 hours of the release. In the case of the nanocapsules, the maximum release was achieved after 120 hours of release.

On the other hand, about 40% of the loaded drug was released quickly, before of the first 24 hours of release, being more rapid the drug release from nanospheres. In this initial release, the kinetic constants by Higuchi model were $0.1408 \text{ h}^{-1/2}$ (± 0.02) and 0.1686 h^{-1} (± 0.03) for the nanocapsules and nanospheres, respectively. The following final phase (40-100% of drug release) occurred with kinetic constants (by first order model) of 0.0216 h^{-1} (± 0.13) and 0.0215 h^{-1} (± 0.43) for nanocapsules and nanospheres, respectively. These constants are increased when the drug affinity for the release medium increases, and this happens in the case of the nanospheres. The drug loaded in the nanospheres must be deposited in both the surface and

matrix, which explains why the drug release is faster in both the initial and final stage, and it must involve diffusion from the polymer matrix to the release medium.

In contrast, the kinetic constants are lower for the nanocapsules, and this indicates that the drug affinity by the nanocapsules matrix is increased; this case is a logical consideration because the nanocapsule matrix is glycerol, and the affinity of the triclosan-glycerol system is greater than the triclosan-ethanol system.

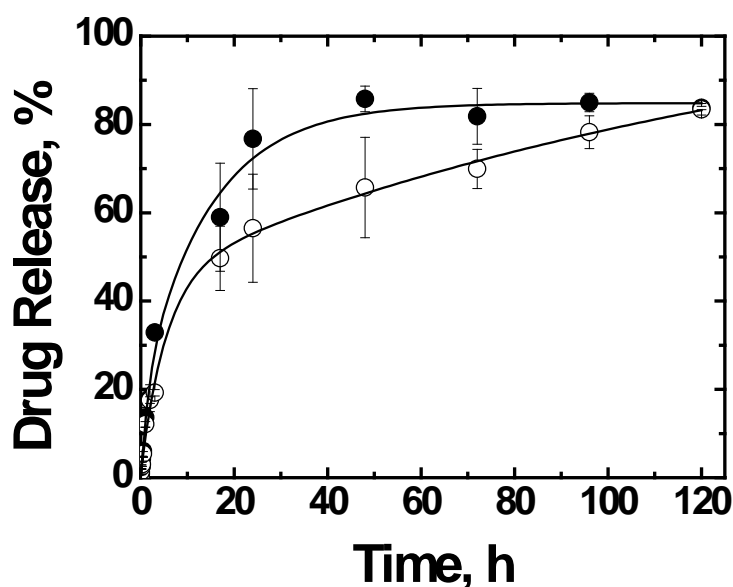


Figure 6.6. Drug release from nanospheres (●) obtained from 6 mg/ml and FR=120 ml/min, and from nanocapsules (○) obtained from 6 mg/ml (polymer) and 8 μ L/ml (oil) at FR=120 ml/min.

6.3.3. Antibacterial activity

The antibacterial activity of the nanocapsules and nanospheres was tested by direct contact with microorganisms. The Figure 6.7 shows the relative growth of *E.coli* (Gram negative bacterium) and *M.luteus* (Gram positive bacterium) for 24 and 48 hours of culture in presence of nanoparticles and nanocapsules.

In the case of *E. coli*, the bacterium is especially sensitive to the antibacterial action of triclosan. At 24 hours of culture, the inhibition of bacterial growth was about 80%, and occurs with both nanospheres and nanocapsules. This antibacterial effect occurs when about 50% and 80% of triclosan was released from the

nanocapsules and nanospheres, respectively. The triclosan released ensures that at 48 hours of culture, the inhibition of bacterial growth remains around 80%.

The *M. luteus* bacterium shows greater resistance to triclosan, thus inhibiting its growth was only about 20% and 10% at 24 hours of culture for nanospheres and nanocapsules, respectively. However, a significant increase in bacterial growth inhibition between 24 hours and 48 hours of culture was observed, and the nanospheres caused 40% of growth inhibition, and for the nanocapsules was of 20%; i.e., the relative inhibition of bacterial growth was doubled as the drug release is increased. In this way, it is possible to expect that with progressive release of the triclosan from nanospheres and nanocapsules, an increase of the antibacterial effect occurs.

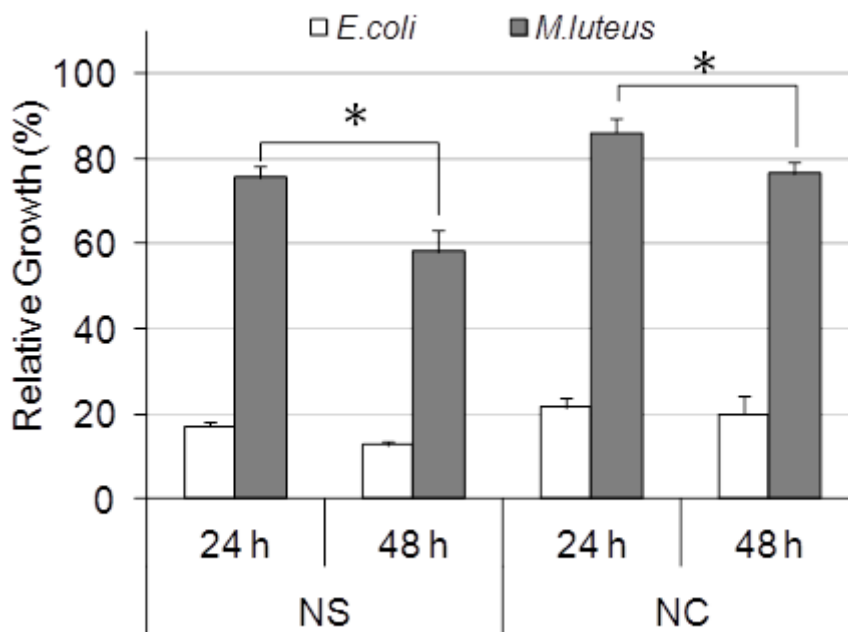


Figure 6.7. Relative growth (%) of bacteria gram negative (white bars) and gram positive (grey bars) in presence of nanospheres and nanocapsules loaded with triclosan.

Figure 6.8 shows the antimicrobial effect of the nanospheres and nanocapsules in relation to quantity of material (it has been handled by dilution). Logically, there is a direct linear relationship between the antibacterial effect and the amount of nanospheres and nanocapsules loaded with triclosan, with R^2 of 0.987 and 0.999, respectively.

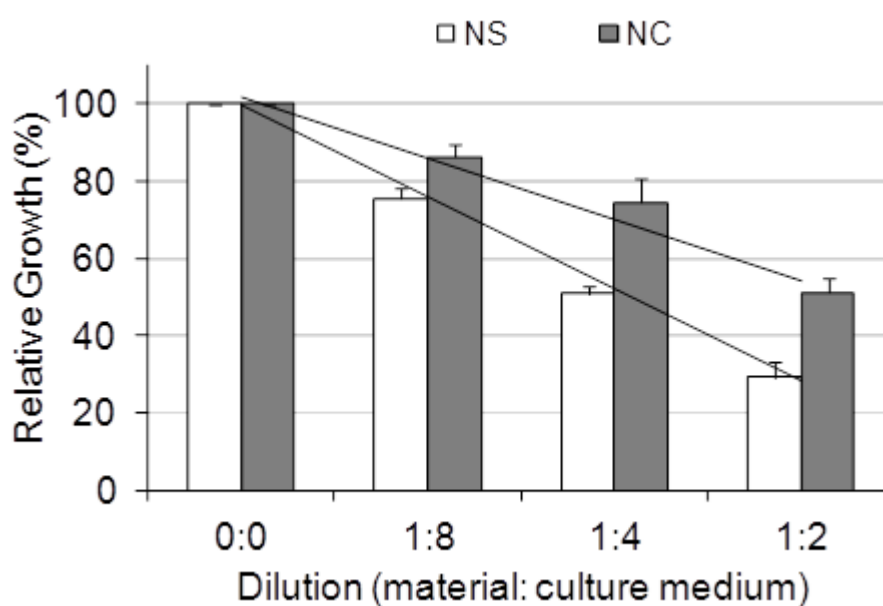


Figure 6.8. Effect on relative growth of nanospheres (white bars) and nanocapsules (grey bars) according to the dilution ratio between nanoparticle suspension (material) and the bacteria suspension (culture medium).

6.4.References

Dash S., Murthy P. N., Nath L., Chowdhury P., 2010, Kinetic modeling on drug release from controlled drug delivery systems. *Acta Poloniae Pharmaceutica - Drug Research* 67 pp. 217-223.

Grove C., Liebenberg W., Du Preez J.L., Yang W., Dev Illiers M.M., 2003, Improving the aqueous solubility of triclosan by solubilization, complexation and in situ salt formation. *Journal of Cosmetic Science* 54, 537-550

Higuchi T., 1963, Mechanism of sustained action-medication. Theoretical analysis of rate of release of solid drugs dispersed in solid matrices. *Journal of Pharmaceutical Science* 52, 1145-1149.

Johnson B.K., Prud'homme R.K., 2003, Mechanism for rapid self-assembly of block copolymer nanoparticles. *Physical Review Letters* 91 1183021.

Manca D., Rovaglio M., 2003, Modeling the controlled release of microencapsulated drugs: theory and experimental validation. *Chemical Engineering Science* 58, 1337-1351.

Petitti M., Vanni M., Barresi A.A., 2008, Controlled release of drug encapsulated as a solid core: theoretical model and sensitivity analysis. *Chemical Engineering Research and Design* 86, 1294-1300.

7. Conclusions

This thesis is focused on a multidiscipline study of a new system to produce nanocapsules for pharmaceutical application. The system under investigation comprises a new amphiphilic polymer from polyalkylcyanoacrylates family, modified with polyethylene glycol chains, named poly(methoxypolyethylene glycol cyanoacrylate-co-hexadecylcyanoacrylate), and micromixers used in nanosphere and nanocapsule production.

The polymer, that should be better referred to as a copolymer, is not a commercial product: it is synthesized in laboratory and it is here characterized from the physicochemical point of view. This characterization showed the copolymer have a particular behaviour due to the presence of the two domains. The low fusion point and rapid degradability in water explains the difficulties in its manipulation and highlights its technological characteristics.

Nanocapsules were produced by confined impinging jets mixers (CIJMs) and results were compared with nanospheres. CIJMs have been already studied in nanosphere production. Here they are used for nanocapsule production and results are compared with previous investigation on nanospheres. CIJMs were successfully used in nanocapsule production: main parameters are investigated and evaluated

and, finally, compared with the previous results on nanospheres. Nanocapsules have a more complicated mechanism of formation and more parameters have to be taken into account for their precipitation in CIJMs. Different geometries were investigated and scale up criteria have been proposed.

Nanocapsules and nanospheres have been characterized using advanced techniques, such as X-ray photoelectron microscopy (XPS) and transmission electron microscopy (TEM). XPS results showed some differences in surface chemical composition between nanospheres and nanocapsules. Measurements at variable angles have been performed in order to investigate the composition of the external layers and estimate polymer wall thickness. TEM analysis have been carried out in order to see the products and investigate the two structures. TEM investigation confirmed the oil is inside the nanocapsules.

Nanospheres and nanocapsules were loaded with a lipophilic drug as model drug. Drug loading and incorporation were very high in both the systems. Drug release experiments highlighted a slower release from nanocapsules, due to the great affinity of the lipophilic drug to the inner core. Antibacterial activity tests confirmed the activity of the drug and the maintaining of the antibacterial activity of the drug even after the encapsulation.

If we assume a formulation with 10 mg/ml of polymer and a concentration in active principle of 1 mg/ml (10% of polymer amount) with an injection pump which can reach a flow rate of 300 ml/min the total productivity it will be around 0.2 kg/h. It should be possible also to use many mixers in parallel: hypothesizing to use 10 mixer in parallel the productivity becomes 2 kg/h, whit 10% of active principle. These numbers match with the usual amount of pharmaceutical industry.

To conclude this system is suitable to produce both nanospheres and nanocapsules. Main problems are related to the manipulation of the polymer and to

its chemical characteristics. More investigation about its residual solubility and the effective PEG amount on the surface are necessary in order to optimize the process. Most of these remaining questions are due the mass quantification of the polymer available for the precipitation and, in particular in case of nanospheres, the determination of the real structure of the loaded particle.

Lists of Figures

Figure 1.1. Blood vessels and lymphatic drainage in a normal tissue and in a diseased tissue: red squares represent the particles, which accumulate more in the diseased tissue.	8
Figure 1.2. Representation of a nanospheres and of a nanocapsules made of an amphiphilic copolymer: blue part is the hydrophobic part, green part is the hydrophilic one.....	10
Figure 1.3. Poly(methoxypolyethyleneglycole cyanoacrylate-co-hexadecyl cyanoacrylate) formula.....	12
Figure 1.4. Section view of some kind of passive mixing devices used in this thesis: a) T-mixer, b)CIJM (front view), c) MIVM with 2 inlet jets (above view) and d) MIVM with 4 inlet jets (above view).....	15
Figure 2.1. Synthesis of MePEGCA.	21
Figure 2.2. Synthesis of HDCA.....	21
Figure 2.3. Polymerization reaction.....	22
Figure 2.4. Precipitation texts of the polymer at different water fraction (K_w): ■ polymer precipitates, ▲ polymer is soluble. Dashed lines indicates solubility curve.	24
Figure 2.5. DSC scans performed on poly(MePEGCA-co-HDCA) (a), poly(HDCA) (b) and PEG samples (c). Scans, from bottom to top, correspond to the heating run of the as-synthesized (a,c) or the commercial sample (c), the cooling run from the melt state (a, b, c), the heating run of a hot crystallized sample (a, b, c) and the heating run of a sample quenched from the melt state (a).....	26
Figure 2.6. Polarizing optical micrographs of poly(MePEGCA-co-HDCA) isothermally crystallized at 4 °C (a, b, c) and -24 °C (d). Micrographs were taken at room temperature (a, d), at 34 °C (b) and at room temperature after heating the crystallized sample to 34 °C. A first-order red tint plate was used for micrograph d). The inset of d) shows a magnification of the dashed area where small and flat microcrystals could be envisaged. Arrows points out crystalline microdomains constituted by poly(HDCA).	28

Figure 2.7. a) Powder X-ray diffraction profiles of poly(MePEGCA-co-HDCA) (blue) and poly(cyano hexadecylacrylate) (brown). b) Down the chain axis projection of the PEG structure showing the packing arrangement of the four 7/2 helices. c) Simulated powder X-ray diffraction profile of PEG and corresponding diffraction pattern (inset).	30
Figure 2.8. a) Plot of the remaining weight of a poly(MePEGCA-co-HDCA) disk sample versus exposure time in distilled water at 18 °C (▲) and 4 °C (□). b) Electron micrograph of PEG lamellar crystals recovered from the release medium. The inset shows the corresponding electron diffraction pattern.	32
Figure 2.9. a) 1H-NMR spectra of the as-synthesized poly(MePEGCA-co-HDCA) sample and chemical scheme showing the assignment of signals (inset). b) 1H-NMR spectra of the solubilized fraction of a poly(MePEGCA-co-HDCA) sample after 8 h of exposure to water at 18 °C. c) 1H-NMR spectra of a poly(MePEGCA-co-HDCA) sample after 8 h of exposure to water at 18 °C.	34
Figure 2.10. H-NMR spectra of polymer after extraction: polymer solubilized in water (top) and polymer solubilized in trichloromethane.	35
Figure 3.1. Sketch of the CIJMs used in this work.	45
Figure 3.2. Zeta potential (top) and mean particle size (bottom) versus the flow rate for nanocapsules obtained without quenching water (left, open symbols) and with quenching water (right, filled symbols) for different mixers: scale down (△,▲), CIJM-d1 (□,■) and scale up (◇,◆). Experiments at constant polymer (6 mg/ml) and oil (8 μL/ml) concentration (MR=1.26).	50
Figure 3.3. Mean particle size versus the inlet stream velocity for nanocapsules obtained with different CIJMs: scale down mixer (▲), CIJM-d1 mixer (■), scale up mixer (◆), CIJM-d2 mixer (●). Experiments at constant polymer (6 mg/ml) and oil (8 μL/ml) concentration (MR=1.26).	52
Figure 3.4. Mean particle size versus the jet Reynolds number for nanocapsules obtained without quenching water (left, open symbols) and with quenching water (right, filled symbols) for CIJMs characterized by different inlet pipes and same	

mixing chamber: CIJM-d1 (□,■), CIJM-d2 (○,●). Experiments at constant polymer (6 mg/ml) and oil (8 μL/ml) concentration (MR=1.26)..... 54

Figure 3.5. Mean particle size versus the jet Reynolds number (a) and versus flow rate (b) for nanocapsules and nanospheres obtained at four different oil-to-copolymer mass ratios, MR = 0 (◇,◆), MR = 0.76 (□,■), MR = 1.26 (○,●) and MR = 2.37 (△,▲) without quenching (left, open symbols) and with quenching (right, filled symbols) for (from top to bottom) scale down, CIJM-d1, scale up and CIJM-d2. Constant polymer concentration (6 mg/ml). 56

Figure 3.6. Zeta potential (mV) as a function of particle size (nm) obtained with different mixers: scale down (triangle), CIJM-d1 (square) and scale up (rhomb). Top graph: particles without quenching. Bottom graph: particles with quenching. Both nanospheres and nanocapsules are present: nanospheres (black), nanocapsules at MR = 0.76 (half black), nanocapsules at MR = 1.26 (light grey) and nanocapsules at MR = 2.37 (white). 58

Figure 3.7. Mean particle size versus the jet Reynolds number for nanocapsules obtained at constant oil concentration (8 μL/ml) and at copolymer concentration of 10 mg/ml (MR = 0.76, □,■), 6 mg/ml (MR = 1.26, ○,●) and 3.2 mg/ml (MR = 2.37, ◇,◆) in CIJM-d1 without quenching (right, open symbols) and with quenching (right, filled symbols)..... 59

Figure 3.8. Mean particle size versus the jet Reynolds number for nanocapsules obtained with CIJM-d1 without quenching (open symbol) and with quenching (filled symbol) at two different constant oil-to-copolymer mass ratio for different copolymer and oil concentrations; upper graph: MR = 0.76 with 4 mg/ml copolymer and 3.2 μL/ml oil (□,■), 6 mg/ml copolymer and 4.8 μL/ml oil (○,●), 10 mg/ml copolymer and 8 μL/ml oil (△,▲).; lower graph: MR = 2.37 with 3.2 mg/ml copolymer and 8 μL/ml oil (□,■, - - -), 6 mg/ml copolymer and 15 μL/ml oil (○,●, - -). 60

Figure 4.1. Confined Impinging Jets, Tee and Vortex Mixers: section view. 69

Figure 4.2. Nanosphere size dependence on solvent feed flow rate with CIJM-d1 at two different W/A ratios: ○ W/A = 1, ● W/A = 8. Inlet copolymer concentration: 2.5 mg/ml Quenched, measured after synthesis. 72

Figure 4.3. Nanosphere size dependence on average inlet jet velocity in CIJM-d1 and TM-d1 mixers at different initial copolymer concentrations. (a) CIJM-d1: 0.7 mg/ml (◇), 2.5 mg/ml (◆), 4.0 mg/ml (○), 6 mg/ml (●), 10.2 mg/ml (□); (b) T-d1: 4.0 mg/ml (○), 6 mg/ml (●), 10 mg/ml (□), 15 mg/ml (■). Quenched, measured after synthesis. 73

Figure 4.4. Dependence of nanosphere size on copolymer concentration in two different mixers: CIJM-d1 (□, continuous line) and TM-d1 (○, dashed line). Quenched, measured after synthesis. The proportionality constant of the relationship $d_p = A v_j^{-0.2}$ is plotted, calculated from the data shown in Figure 4.3. 74

Figure 4.5. Dependence of mean nanosphere size (a), estimated number of particles formed per millilitre of solvent fed (b) and Zeta potential (c) on W/A ratio at two different initial copolymer concentrations: 2.5 mg/ml (●), 10.45 mg/ml (■). Water flow rate = 120 ml/min. Quenched, measured after synthesis. 76

Figure 4.6. Dependence of nanocapsule size on average inlet jet velocity v_j at three different oil to polymer concentration ratio, MR: inlet copolymer concentration = 6 mg/ml, oil concentration variable. Quenched, measured after solvent evaporation. Mixers: scale down (■), CIJM-d1 (◆), scale up (●) and CIJM-d2 (▲). 80

Figure 4.7. Zeta Potential - particle size relationship; data refer to nanocapsules and nanospheres produced in the four CIJ mixers at 4 different FR (5, 40, 80 and 120 ml/min), measured after solvent evaporation. Upper graph: influence of the MR for quenched nanoparticles; ○ for MR 0 (nanospheres), ◆ for MR 0.76, ■ for MR 1.26 and ▲ for MR 2.37. Lower graph: comparison of quenched and non-quenched nanoparticles. 82

Figure 4.8. Dependence of nanospheres and nanocapsules on mixer dimension. Graph a) Nanospheres at 6 mg/ml for different mixers: line (—) approximation of CIJM-d1 data, line (----) approximation of CIJM-d2 data, line (---) approximation of CIJM-d1 data without solvent-evaporation, line (---) approximation of CIJM-d2 data

without solvent-evaporation. Graph b) Nanospheres at 6 mg/ml for different mixers without quenching: line (—) approximation of CIJM-d1 data, line (....) approximation of CIJM-d2 data. Graph c) Nanocapsules at MR 1.26 with quenching for different mixers. Graph d) Nanocapsules at MR 1.26 without quenching for different mixers. 83

Figure 4.9. Nanoacapsule size at different flow rate, before (circle symbols) and after (square symbols) solvent evaporation. Open symbols are for not-quenched samples and filled symbols for quenched samples. 84

Figure 4.10. Correlation of experimental data using mixing time and Damkholer number in different mixers. Upper graphh: nanospheres, quenched, measured after synthesis, copolymer concentration in the range 2.5 -15 mg/ml (only 10 mg/ml for the scaled up mixers), flow rate in the range 20-120 ml/min. Lower graph: nanocapsules, quenched, measured after solvent evaporation, flow rate in the range 20-120 ml/min; all data at the same concentration: copolymer = 6 mg/ml, oil = 8 mg/ml. 86

Figure 4.11. Dependence of nanocapsule average diameter on CIJ mixer geometry (chamber to inlet jet diameter ratio); inlet copolymer concentration = 6 mg/ml, MR = 1.26, $D_c/d_j = 4.8$ (open symbols) and $D_c/d_j = 2.4$ (filled symbols) are compared. Circles are for quenched samples and triangles are for non-quenched samples; measured after solvent evaporation. 88

Figure 4.12. Dependence of nanocapsule size on copolymer/oil MR; copolymer concentration hold constant, 6 mg/ml. Upper graph: with quench; the data refer to the four CIJ mixers, including CIJ-d2. Bottom graph without quench: the data refer to the three scaled CIJ mixers only. 91

Figure 4.13. Dependence of nanocapsule size on oil and copolymer inlet concentration, at constant concentration ratio (MR = 0.76): 6 mg/ml and 4.8 μ L/ml (square symbol), 10 mg /ml and 8 μ L/ml (triangle symbol), 4 mg/ml and 3.2 μ L/ml (circle symbol). Filled symbols, quenched; open symbols, not quenched . CIJ mixers; measured after solvent evaporation. 93

Figure 4.15. Nanospheres from polymer concentration of 6 mg/ml. a) Comparison of CIJM-d1 and Vortex mixer at different inlet feeding for the production of nanospheres: CIJM-d1 (◆), VM-2 (▲), VM-4 with alternated connexions (■) and VM-4 with adjacent connections (●). Polymer concentration = 6 mg/ml; quenched, measured after solvent evaporation. b) Comparison between alternated VM-4 at W/A=1 (■) and at W/A=2 (●).....	94
Figure 5.1. Schematic representation of shadowing with platinum. According to the angle the metal hits the surface, there will be an area not covered close to the particle, forming the “shadow” of the particle.....	103
Figure 5.2. Survey scan of nanoparticles surfaces: nanospheres (blue) and nanocapsules (red).....	105
Figure 5.3. Surface analysis of carbon region in: a) pure polymer, b) nanospheres and c) nanocapsules. Relative atomic percentage of carbon bonds are reported on the figure. Samples are not quenched.....	107
Figure 5.4. Carbon and nitrogen spectra of pure polymer, nanospheres and nanocapsules. Red spectrum is pure polymer, black spectrum is nanosphere sample, blue spectrum is nanocapsule sample.	108
Figure 5.5. Angle resolved analysis of nanospheres (left) and nanocapsules (right). Atomic concentration versus sin theta. Theta is the angle of the sample with respect to the analyzer.....	108
Figure 5.6. Depth profile using C60 gun. Sputter time is the etching time of C60 on the sample.....	109
Figure 5.7. Depth profile using Argon gun: nanospheres (left) and nanocapsules (right).....	110
Figure 5.8. Oxygen spectra of nanospheres (left graph) and nanocapsules (right graph) with the relative deconvolution process and the attribution to each bond. Nanospheres were obtained from 6 mg/ml solution and nanocapsules from 6 mg/ml and 8 µL/ml. Not quenched samples.....	111
Figure 5.9. XPS analysis at different angles (from 10° to 90°) of nanocapsules at different MR without quenching (left column) and with quenching (right column).	

From the top: nanocapsules at MR 2.37, at MR 1.26 and at MR 0.76. In each graph are reported nine oxygen peaks obtained at different angle, from the bottom to the top: 10°, 20°, 30°, 40°, 50°, 60°, 70°, 80° and 90°. A line highlights where the oxygen profile changes, indicating a change in chemical composition. 113

Figure 5.10. Positive (a, c) and negative (b, d) TEM micrographs taken at different magnifications of poly(MePEGCA-co-HDCA) nanocapsules containing Miglyol 812. Samples were prepared with MR = 1.26, FR = 120 ml/min and initial copolymer and oil concentrations of 6 mg/ml and 8 µL/ml, respectively. Blue arrows point out the pseudoregular geometries that can be observed inside the capsules, probably as a consequence of a regular arrangement of some oil molecules. 115

Figure 5.11. TEM micrographs taken at different magnifications of poly(MePEGCA-co-HDCA) nanocapsules containing Miglyol 812. Samples were prepared with MR = 0.76, FR = 120 ml/min and initial copolymer and oil concentrations of 6 mg/ml and 8 µL/ml, respectively. Sample (d) was shadowed with Pt/C. Red and black arrows point out pseudoregular geometries inside nanocapsules and spilled oil outside nanocapsules, respectively. Wall thickness of nanocapsules is indicated by the blue asides. 116

Figure 5.12. a) Nanosphere picture obtained with SEM. b) Particle size distribution of the sample measured by DLS: number distribution (—) and volume distribution (---). 117

Figure 5.13. Nanospheres covered with Pt. The large shadow indicate spherical shape of the sample. 118

Figure 5.14. a) positive nanosphere sample; b) negative staining nanocapsule staining. 119

Figure 6.1. Chemical structure of Triclosan. 125

Figure 6.2. Drug release from a) nanospheres, obtained at flow rate = 10 ml/min (○) and 120 ml/min (□). b) nanocapsules, obtained at flow rate 10 ml/min (●) and 120 ml/min (■). 130

Figure 6.3. Drug released in mg/ml of suspension for nanospheres (upper graph) and for nanocapsules (lower graph): particle obtained at 10 ml/min (red) and at 120 ml/min (black). On right graph velocity of release is reported, as mg/h released in the different time interval.....	131
Figure 6.4. Release data fitted by Higuchi model and first order model. a) nanospheres data fitted by Higuchi model in the interval time 0-17 hours: nanospheres obtained at 10 ml/min (●, red fitting curve) and 120 ml/min (■, black fitting curve). b) nanospheres data fitted by first order model in the interval time 17-120 hours: nanospheres obtained at 10 ml/min (●, dashed fitting curve) and 120 ml/min (■, solid fitting curve) ; c) nanocapsules data fitted by Higuchi model in the interval time 0-17 hours: nanocapsules obtained at 10 ml/min (●, dashed fitting curve) and 120 ml/min (■, solid fitting curve). d) nanocapsules data fitted by first order model in the interval time 17-120 hours: nanocapsules obtained at 10 ml/min (●, dashed fitting curve) and 120 ml/min (■, solid fitting curve).	133
Figure 6.5. Nanospheres (left) and nanocapsules (right) after release experiment..	134
Figure 6.6. Drug release from nanospheres (●) obtained from 6 mg/ml and FR=120 ml/min, and from nanocapsules (○) obtained from 6 mg/ml (polymer) and 8 μL/ml (oil) at FR=120 ml/min.	135
Figure 6.7. Relative growth (%) of bacteria gram negative (white bars) and gram positive (grey bars) in presence of nanospheres and nanocapsules loaded with triclosan.....	136
Figure 6.8. Effect on relative growth of nanospheres (white bars) and nanocapsules (grey bars) according to the dilution ratio between nanoparticle suspension (material) and the bacteria suspension (culture medium).	137